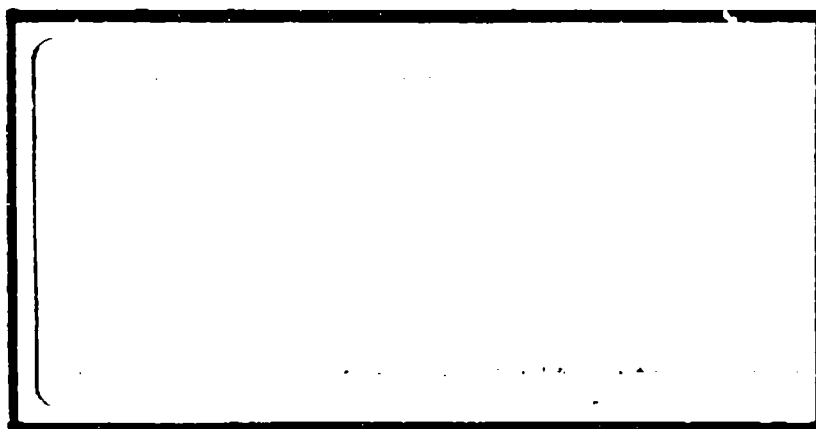AD-A189 845

DTIC
TE
S MAR 0 7 1988
H
D

DEPARTMENT OF THE AIR FORCE

AIR UNIVERSITY

AIR FORCE INSTITUTE OF TECHNOLOGY

Wright-Patterson Air Force Base, Ohio

88 3 01 110

AFIT/GAE/AA/87D-22

EXPERIMENTAL INVESTIGATION OF
TWO-DIMENSIONAL CONFINED JET
THRUST VECTOR CONTROL

THESIS

Timothy A. Talda
Second Lieutenant, USAF

AFIT/GAE/AA/87D-22

DTIC

MAR 0 7 1988

EXPERIMENTAL INVESTIGATION OF

TWO-DIMENSIONAL CONFINED JET

THRUST VECTOR CONTROL

THESIS

Presented to the Faculty of the School of Engineering

of the Air Force Institute of Technology

Air University

In Partial Fulfillment of the

Requirements for the Degree of

Master of Science in Aeronautical Engineering

Timothy A. Talda, B.S.

Second Lieutenant, USAF

December, 1987

Preface

In this thesis, comparison of confined jet thrust vector control was made to other thrust vector control systems, motivating the research. A new nozzle geometry suitable for two-dimensional confined jet thrust vector control was designed and constructed. Effects of several changes in the nozzle design parameters and in the inputs to the nozzle have been analyzed. Still photos and movies of the flow in both axial and vectored conditions have been produced.

This effort would not have been possible without the help of many people. I would like to thank Dr. M. E. Franke for his help, understanding, and patience in the direction of this effort. Thanks also go to Dr. W. Elrod, for his help with the schlieran photography set-up. The construction of the nozzle and all the changes subsequently made to make everything work are due John "the Wizard" Brohaus, and simple thanks is not enough for his effort. The support from the AFIT technicians, particularly Messrs. Nick Yardich, Jay Anderson, Leroy Cannon was outstanding. And thanks to Maj. Ryan, for his insight and ingenuity. Finally, thanks to Marci, without whose support and patience this report would not have been completed nearly as well.

- Timothy A. Talda

ii

Table of Contents

List of Figures

vi

List of Tables

List of Symbols

Symbol	Description	Units
AR	Area Ratio - Exit Area to Throat Area	
As	Secondary Injection Area	in²
At	Area of Throat	in²
δ	Divergence Half-Angle	deg
L	Length of Nozzle (measured from throat to exit)	in
$\dot{m}_p$	Primary Mass Flow	lbm/s
$\dot{m}_s$	Secondary Mass Flow	lbm/s
N-D	Non-Dimensional	
Pp	Primary Pressure	psia
Ps	Secondary Pressure	psia
Pw	Wall Pressure	psia
Ta	Axial Thrust	lbf
Ts	Side Thrust	lbf
Tt	Total Thrust - Vector Sum of Axial and Side Forces	lbf
θ	Exit Angle	deg
We	Width of Exit	in
Wm	Maximum Width of Nozzle	in
Wt	Width of Throat	in
x_s	Distance from Throat to Secondary Injection Location	in

Axisymmetric Nozzle: Expansion in a cone
(Fitzgerald and Kampe, Brown, Lambert, Ryan studies)

Two-Dimensional Nozzle: Expansion in one dimension
(Cates, Talda studies)

AF1T/GAE/AA/87D-22

Abstract

Different types of thrust vector control systems are described, and a comparison of present systems is presented. Confined jet thrust vector control is shown to be an effective alternative. A two-dimensional nozzle that operates as a confined jet thrust vector control nozzle is experimentally demonstrated. Effects of changing geometric variables and inputs on ease of vectoring and performance of vectored thrust are analyzed. Schlieren photographs and movies show flow characteristics. Predictions of performance of operable nozzles are made based on results found in the experiments. Recommendations for further study are made.

EXPERIMENTAL INVESTIGATION OF
TWO-DIMENSIONAL CONFINED JET
THRUST VECTOR CONTROL

I. Introduction and Design Approach

Background

Thrust Vector Control (TVC) is applied in rocket nozzles as a method of controlling thrust direction. Instead of fins, TVC might be employed on a rocket motor to provide changes in direction. One complex method of TVC is nozzle gimballing, in which the thrust is directed using a rotating nozzle. Another simpler type of TVC uses angled thrust from an overexpanded nozzle. The flow through the nozzle is directed off center line using a secondary flow, and this re-direction produces the angled thrust. Several types of this TVC have been researched.

Boundary Layer Thrust Vector Control

One type of TVC is Boundary Layer Thrust Vector Control (BLTVC), Fig 1. This method relies on ambient air to enter the separation region of the overexpanded nozzle, and the pressure difference between this region and the jet forces the jet off-center (4:2). The ambient pressure must be greater than the separation region for operation, which limits BLTVC to low altitudes. Because of this restriction, another type of TVC not limited by altitude is desirable.

1
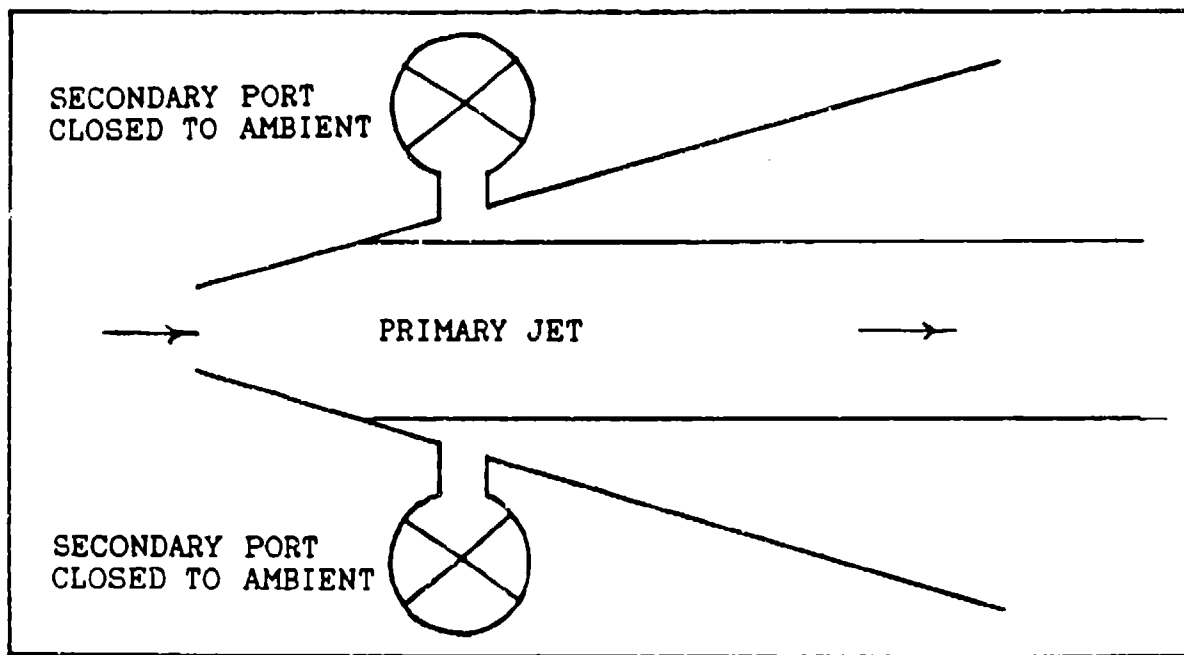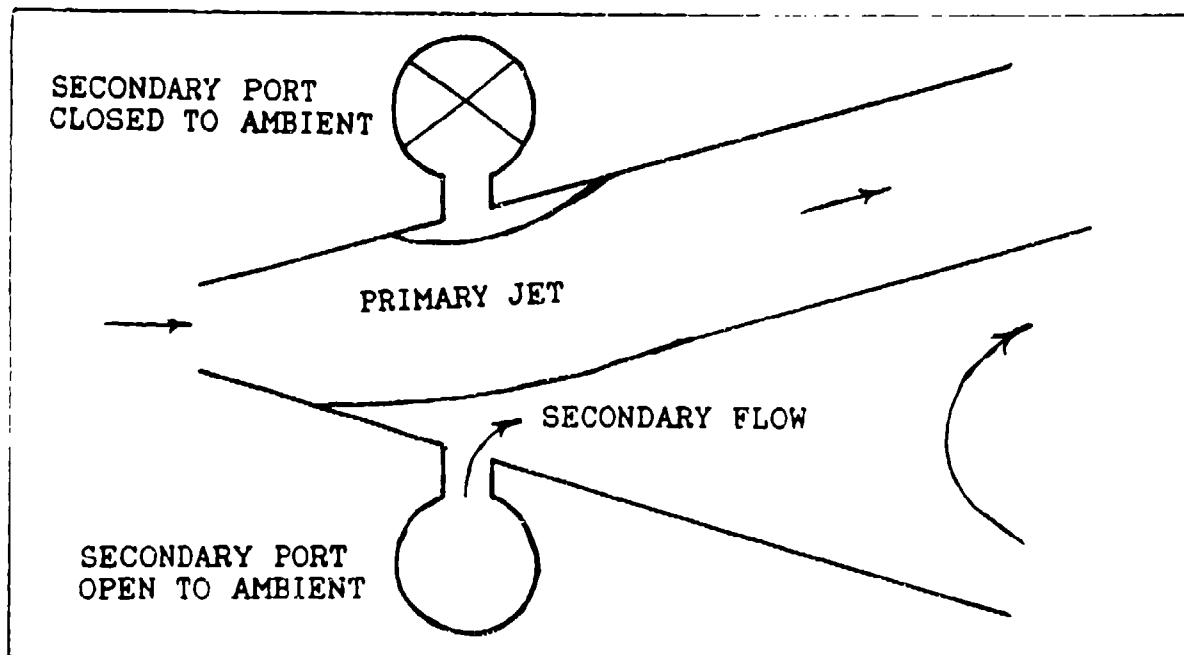
Axial

Vectored

Fig 1. Axial, Vectored Boundary Layer Thrust Vector Control

2

Hot Gas Valve Thrust Vector Control

Hot Gas Valve Thrust Vector Control (HGVTVC) is not limited by altitude. A conventionally expanded nozzle is used, with secondary injection about halfway between the throat and exit. The secondary injection, bled directly from the combustion chamber, causes an oblique shock wave in the supersonic flow, which gives rise to uneven pressure distributions (10:2). The effect of the injection is to slightly angle the thrust, which gives thrust vectoring.

Confined Jet Thrust Vector Control

Confined Jet Thrust Vector Control (CJTVC) is also a type of TVC that is not limited by low-altitude operation. CJTVC is similar to BLTVC, but it uses a reconvergent section downstream of the divergent section, as shown in Fig 2. The reconvergent section contains the separated region inside the nozzle cavity, which tends to insulate the region from ambient pressure. This insulation of the separation region should make CJTVC independent of ambient pressure, and therefore independent of altitude of operation. Instead of using ambient air for secondary injection as in BLTVC, an independent supply of air is injected to vector the flow.

Comparison of CJTVC to Other TVC Systems

The comparison among thrust vector control systems must take several factors into account. These include the system complexity, the thrust angle obtained, the amount of input

3
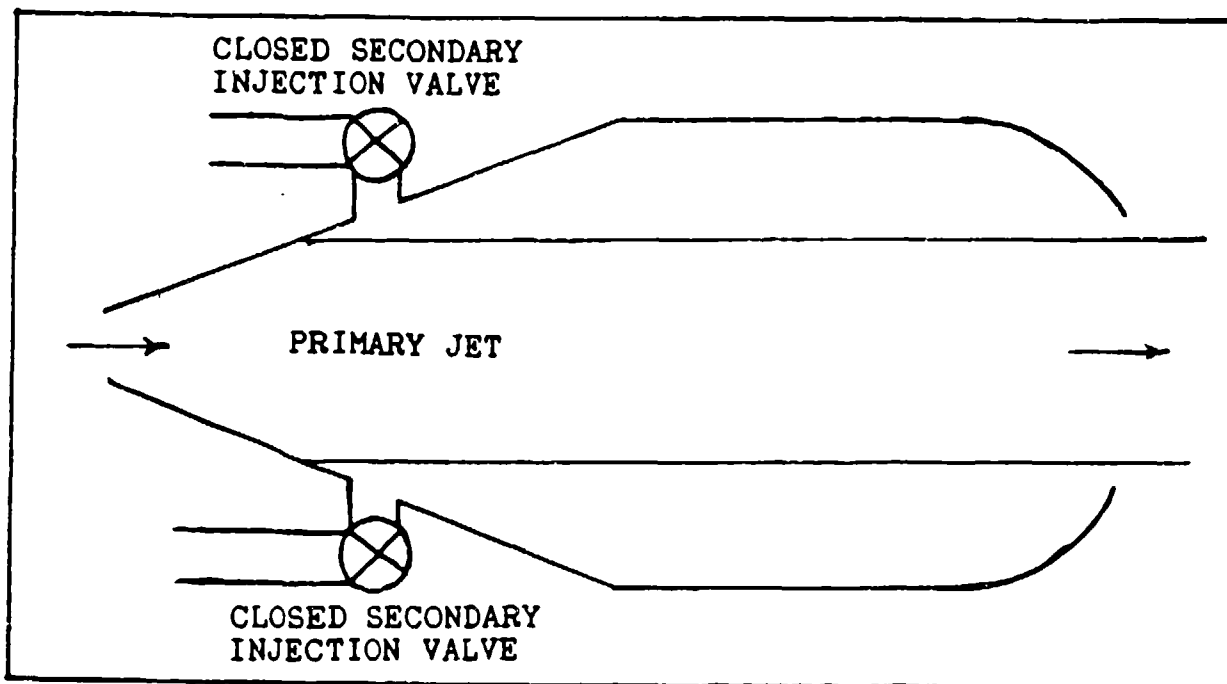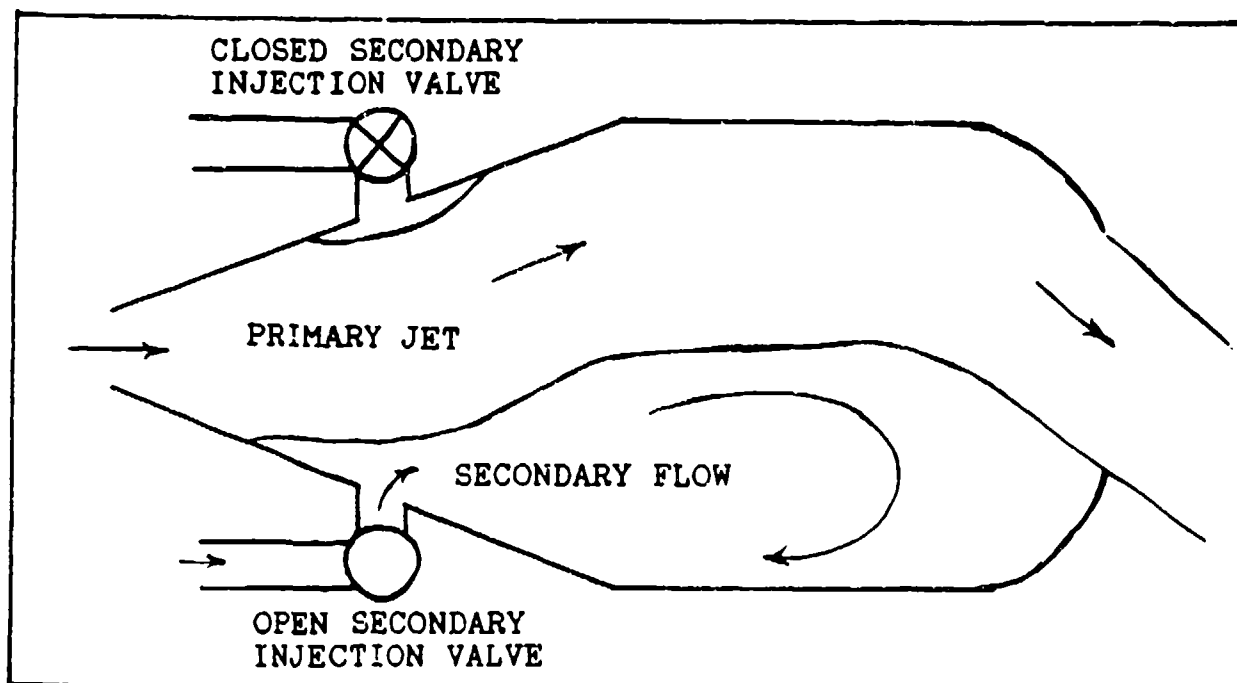
Axial

Vectored

Fig 2. Axial, Vectored Confined Jet Thrust Vector Control

4

required to vector, the system response, and the losses involved in the axial condition. Each system has advantages and disadvantages, and CJTVC overall compares well to gimballing, BLTVC, and HGVTVC as a TVC system.

Gimballing uses a flexible mounting attached to the nozzle, which is moved via actuators to the angle desired (10:2). A practical system gives thrust deflection angles in the range of ±15 degrees, but actuation torques required are high (10:2). Because the nozzle can be moved, it can be designed for the best expansion for the application. Therefore, axial losses are at a minimum, and efficiencies in both the vectored and axial cases are high. The response of the system is limited by the force exerted by the actuators. Also, the mechanism of the actuators and the flexible housing result in a complex system.

BLTVC uses ambient air as a secondary fluid. By opening or closing the secondary ports, the jet can be angled or axial inside an overexpanded nozzle, as shown in Fig 1. BLTVC has been tested extensively, using cold and hot gas firings. Thrust angles of ±20 degrees can be achieved, and response times of the jet are approximately 10 msec (8:10). The mechanism of vectoring is relatively simple, as valves just need to open or close. And because the system uses the ambient air, there is no bleed from the combustion chamber or is an independent secondary supply required for operation. Because the nozzle is overexpanded, it is larger in area than a conventional nozzle, so the drag of the nozzle is higher.

5

Also, the larger shape is heavier than the optimally designed nozzle. The efficiency in the axial case is reduced somewhat due to the overexpanded nozzle. The system is limited in altitude due to the reliance on ambient air pressure to vector the jet.

HGVTVC uses gases bled from the combustion chamber to inject into a conventionally expanded nozzle to set up an oblique shock wave, causing jet deflection (10:3). Thrust deflections of ±12 degrees are obtainable (10:4), and the response time is dependent only on the time required for the hot gas valve to open and close. The axial thrust is not affected, since the nozzle can be optimally expanded. Vectored thrust is somewhat affected, since some of the combustion gases are bled off the main chamber. The complexity of the system lies in the design of the hot gas valves. Because the secondary gases are at the temperature of the combustion chamber, exotic materials have to be used in the valve construction (10:4).

CJTVC was shown to have thrust angles between 20 and 35 degrees (2:46), and a response time of 10 msec with cold flow (9:52). The secondary mass flow to primary mass flow has been shown to be around one percent (9:52). The system is simple in design, as it could use an independent secondary flow, so the design of the valves does not have to be complex. However, compared to the other methods, the nozzle is longer, due to the reconvergent section. This means that the nozzle is also heavier than in the other methods. And

6

the efficiency might be slightly reduced due the recirculation of the jet inside the cavity. But this method seems to be independent of ambient pressure, so there might not be an altitude limitation.

In choosing a TVC system for a specific application, obviously the application will dictate what systems cannot be used because of cost, thrust angle requirements, etc. The fluid injection TVC's are limited in thrust angles to three angles (zero and the ± maximum angle). Therefore, a more complex control system is required to switch the jet the required amount of time for a certain force in some direction. But they are also the mechanically simplest TVC, and therefore probably the least expensive. Of the three types discussed here, each has its limits on application. BLTVC could give excellent thrust angles quickly, if the penalty of the overexpanded nozzle was acceptable and operation was at a low altitude. HGTVC would be an obvious choice if the smaller angles produced by the system are sufficient for the application, since the losses caused by the vectoring are minimal. But CJTVC, with its performance seemingly unlimited by altitude, could be used where the extreme thrust angles were required, and the response of the system needs to be quick. However, the penalty of the extra nozzle weight would have to be considered. The advantages of CJTVC could, in some applications, outweigh the disadvantages and this shows that research on the system is needed to determine the exact advantages.

Development of CJTVC

CJTVC was studied initially by Fitzgerald and Kampe, of Chandler Evans Control Systems, in an effort to overcome the shortcomings of BLTVC (Ref 5). The initial theory was proven in two-dimensional flows, and then applied to axisymmetric nozzles. The primary concern was optimum geometric variables, including secondary injection location, exit area to throat area, and length between exit and throat. Porzio (Ref 11) studied the effects of varying secondary and primary pressure and secondary area on side force, axial force, and other parameters. Brown (Ref 2) further studied axisymmetric CJTVC by varying the length between exit and throat, the exit area to throat area, and the flow exit angle. Cates (Ref 3) studied two-dimensional nozzles at the same time, using the geometry depicted in Fig 3. Furtherwork was conducted by Lambert (Ref 9) and Ryan (Ref 13) on axisymmetric CJTVC, with emphasis on predicting performance.

Purpose

The purpose of this study was to expand knowledge of two-dimensional CJTVC. The characteristics of vectoring, including when nozzles would vector and how much secondary flow was required, were investigated. By using a controllable two-dimensional nozzle, the effects of varying primary pressure, secondary pressure, length, exit area to throat area, and secondary injection area could be

Fixed
Geometry

Wt = 0.25 in

θ_e = 45 deg

δ = 20 deg

As = 0.0275 in^2

Wm = 12 Wt

Variable
Geometry

x_s = 2.5, 4 Wt

1 = 0, 0.5, 1.0 in

AR = 3, 4, 5

Variable
Inputs

Ps = 34.4, 44.4, 54.4,
64.4, 74.4, 84.4,
94.4 psia

Pp = 114.4, 164.4,
214.4 psia
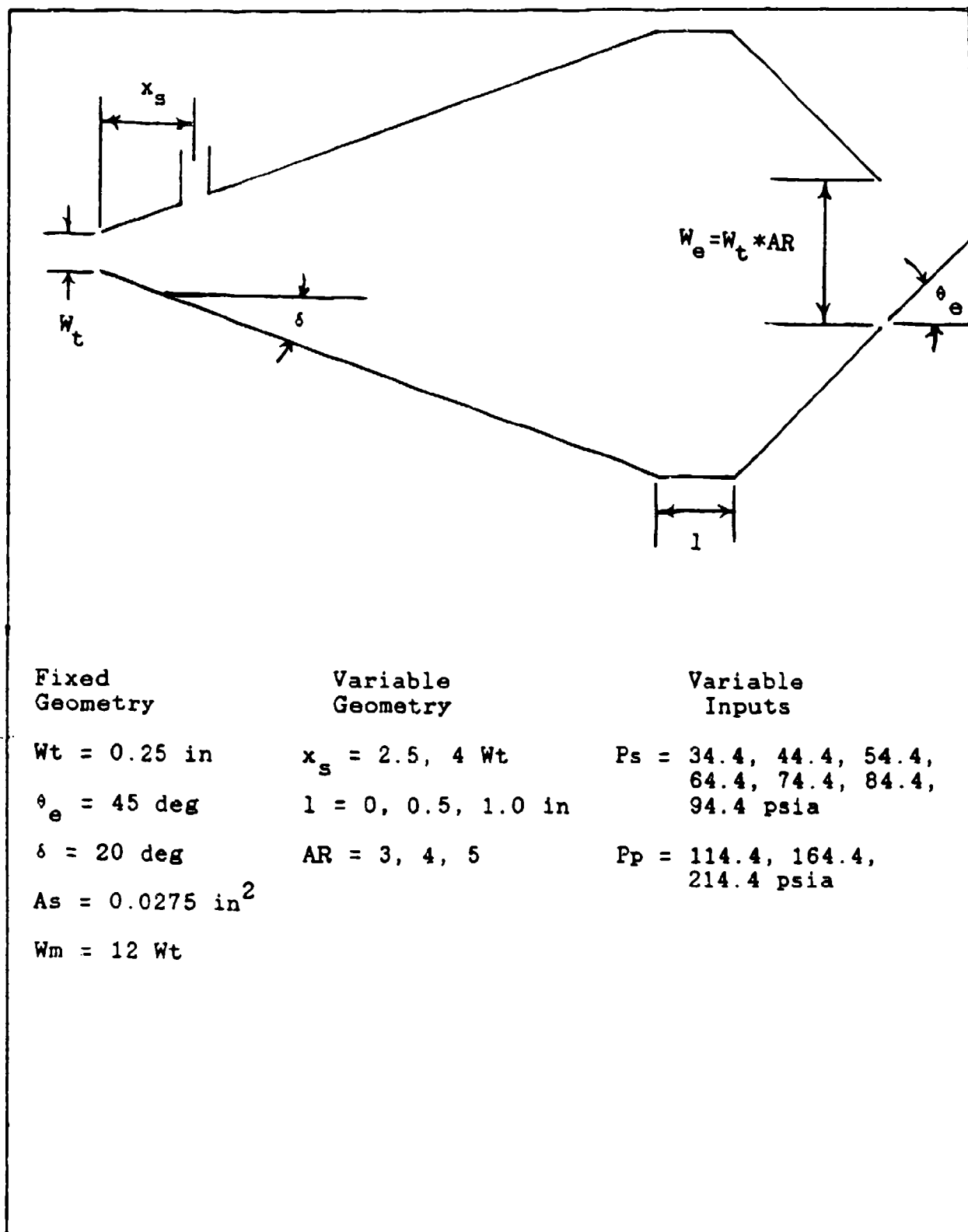
Fig 3.   Geometry of Cates' Nozzles

determined. The flow was visualized to help explain and validate the results found in the experiments.

Approach

Schlieren photographs of Cates' flow in the vectored case showed that the flow did not conform to the geometry exactly. Instead, the flow followed the straight section and smoothly turned to exit the nozzle (3:45), as shown schematically in Fig 4. This indicated that the flow may conform to a smoother surface than that which Cates had used, and this may help the nozzle vector more easily. A new geometry was tried, and several nozzles constructed with variations in length and exit area. Variable secondary injection area was also included in the design. Each nozzle was tested to determine its ability to vector. Then, by varying primary pressures at increments of 20 psi between 154.4 psia and 214.4 psia, and varying secondary pressures by 10 psia increments between 34.4 psia and 104.4 psia, the effects could be examined. Axial and side thrust, pressure distributions along the walls of the nozzle, and primary and secondary mass flows were recorded for analysis.

$$l = 0, \quad AR = 4, \quad L = 19 \ Wt$$
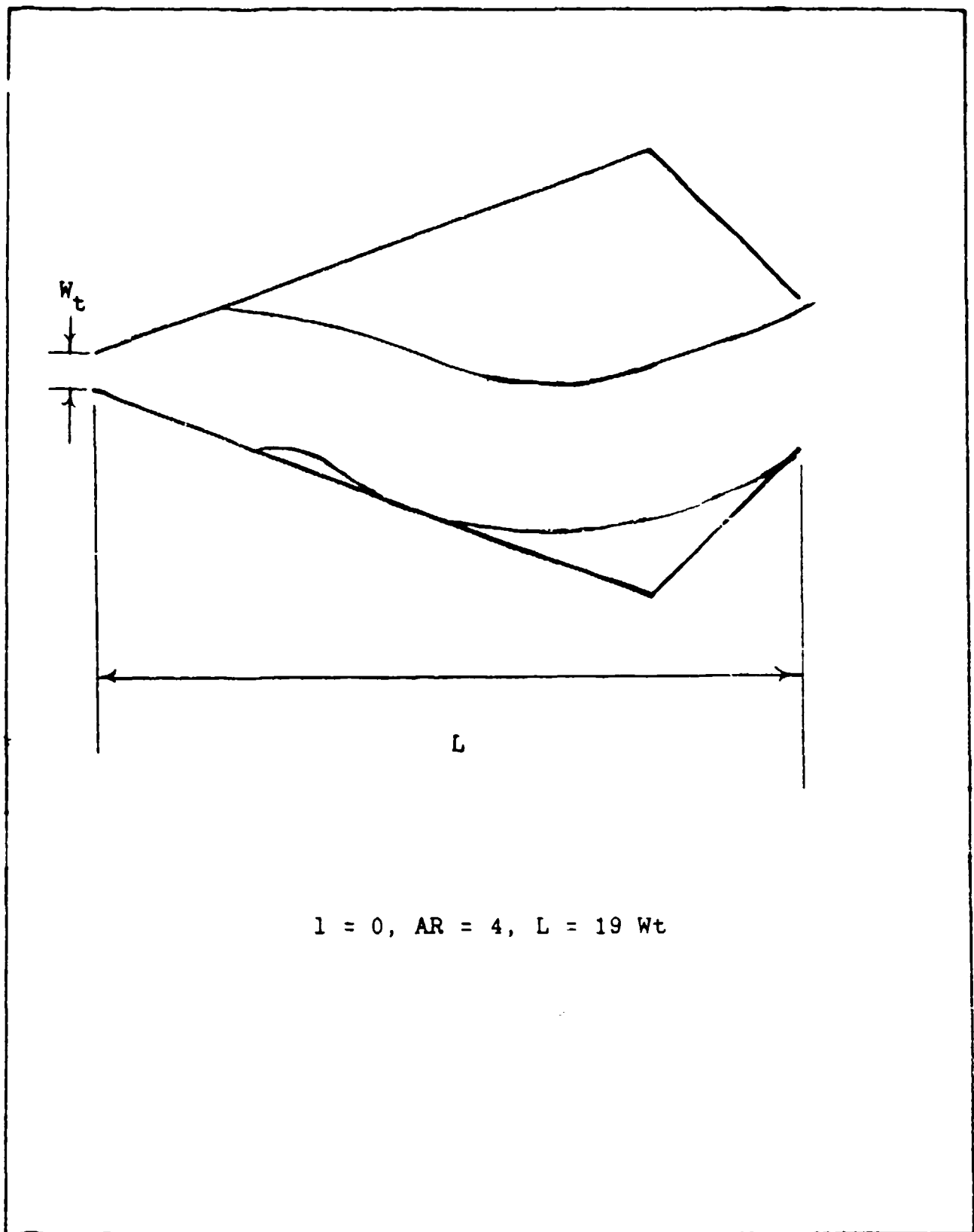
Fig 4. Schematic of Vectored Flow in Operable Nozzle (3:45)

II. Nozzle Design

Design Philosophy

The guidelines established by Fitzgerald and Kampe (5:10-20) for the design of an axisymmetric nozzle could not be used for two dimensional nozzle design. Schlieren photographs of the vectored flow in Cates' study (3:45), drawn in Fig 4, suggested a straight line and a circle joined smoothly would provide a suitable nozzle enclosure. Also, a length of 19 Wt (Wt is the width of the throat = 0.25 in) and an exit area to throat area ratio of 4 was the only nozzle Cates successfully operated as a CJTVC nozzle (3:41). These parameters were used as guidelines to design the nozzles in the present investigation. Appendix A contains the details of the calculation of the measurements of the nozzles. Six nozzles were fabricated and tested, and the geometries and nomenclatures for each are listed in Fig 5. Everything upstream of the throat was the same for each nozzle, as was the location of the secondary injection port, the exit angle, and the divergence angle. The throat was not smooth; it was the intersection of two flat planes at an included angle of 130 deg. Secondary injection was chosen to be at 3 Wt downstream of the throat (halfway between the two injection ports Cates used). Based on Brown's results (2:50), the exit angle was fixed at 45 degrees and the divergent angle was fixed at 20 degrees. The thickness was also constant for all the nozzles, at 3 Wt.
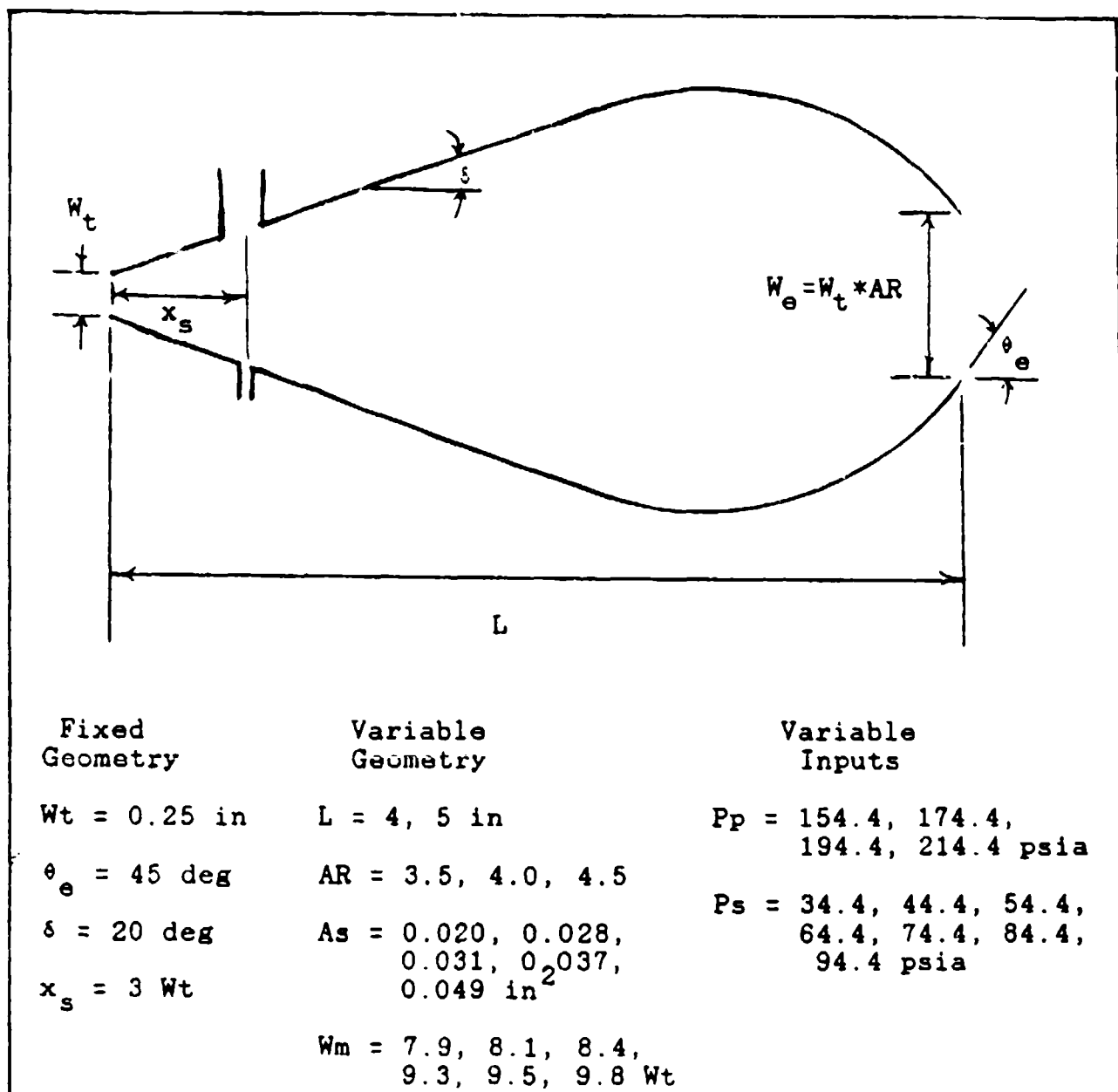
Fig 5. Geometry of Experimental Nozzles

Fixed Geometry	Variable Geometry	Variable Inputs
W_t = 0.25 in	L = 4, 5 in	Pp = 154.4, 174.4, 194.4, 214.4 psia
θ_e = 45 deg	AR = 3.5, 4.0, 4.5	
δ = 20 deg	As = 0.020, 0.028, 0.031, 0.037, 0.049 in^2	Ps = 34.4, 44.4, 54.4, 64.4, 74.4, 84.4, 94.4 psia
x_s = 3 Wt	Wm = 7.9, 8.1, 8.4, 9.3, 9.5, 9.8 Wt	

Table I. Nomenclature of Nozzles Used

Exit to Throat Area Ratio	Length	
	Short (16 Wt)	Long (20 Wt)
Narrow (3.5)	SN	LN
Medium (4.0)	SM	LM
Wide (4.5)	SW	LW

If the nozzle was used in the bracket with the extension, an "E" is added to this nomenclature.

13

Cates used one circular cross-section with a secondary
injection area to nozzle throat area of 0.15 (3:9). In this
study, circular cross-sectional secondary areas of 11%, 15%,
17%, 20%, and 26% of the nozzle throat area were used. Also,
a slot with an area of 17% of the throat area was tested, to
examine the effect of the shape of the secondary injection
port. Table II lists the size and nomenclature of the
different secondary injection areas.

Table II. Nomeclature and Size of Secondary Injection Ports

A_s/A_t =	% of A_t	Cross-Sectional Shape, Dimensions
0.11	10.9	Circular, dia = 0.161 in
0.15	14.6	Circular, dia = 0.187 in
0.17	16.8	Circular, dia = 0.200 in
0.20	19.9	Circular, dia = 0.218 in
0.26	26.2	Circular, dia = 0.250 in
slot	16.8	Rectangular, 0.50 in by 0.0625 in

Explanation of Experimental Nomenclature

The original bracket the nozzles were tested in extended
50 percent past the exit, which provided a two-dimensional
flow region outside the nozzle. Figure 6 is a schematic
drawing of this bracket. This affected the ability of the
nozzle to vector. The tests done with the extension will be
denoted by an "E" attached to the end of the two-letter
designation of the nozzle. For instance, the LME nozzle was
the test using the LM nozzle, but it was mounted in the
bracket with the extension. The tests denoted LM used a
bracket that ended at the nozzle exit.

14
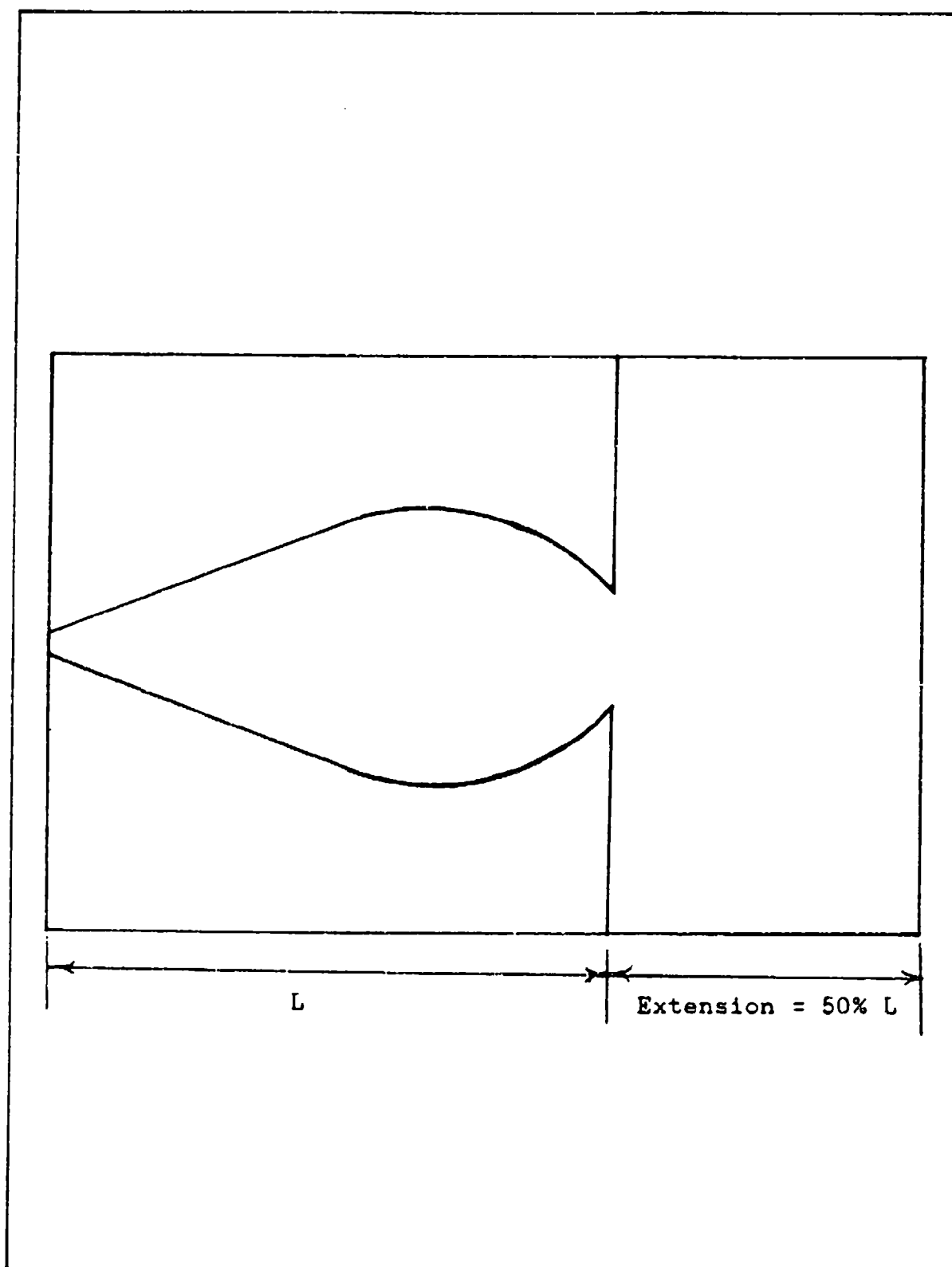
Fig 6.   Schematic of Nozzle Bracket with Extension.

13

III. Experimental Apparatus

Plexiglas Nozzle Halves

The nozzles when assembled formed the shape shown in
Fig 5. There were two halves to each nozzle, identical in
shape. The static pressure ports to determine wall pressures
were located downstream at the same distance from the throat
on each side. These were at 13, 33, 47, 61, 75, and 89
percent of the length in the 16 Wt nozzle, and 10, 30, 45,
60, 75, and 90 percent of the length in the 20 Wt nozzle.
The injection ports were both at 3 Wt distance downstream of
the throat, which was 19 percent of the length in the 16 Wt
nozzle and 15 percent of the length in the 20 Wt nozzle.
The ports on each half had different shapes. One side had a
slot 0.0625 by 0.50 in wide, and the other side had a 0.25
inch diameter hole. Inserts of 0.161, 0.187, 0.200, and
0.218 inches in diameter were made to fit in the original
port, which provided the capability of changing secondary
area.

Nozzle Bracket

The nozzles halves were secured in a bracket, which was
attached to a settling chamber. For most of the data runs,
the bracket was 50 percent longer than the 20 Wt nozzle.
This significantly altered the characteristics of vectoring,
and was removed for final runs to determine the exact
effect. The walls of the bracket were 0.75 in clear

16

plexiglas, each bolted to an aluminum bracket. The bracket
was held together with eight bolts to secure the two
plexiglas nozzle pieces. Masking tape sealed the space
between the nozzle halves and the clear plexiglas. The
nozzle pieces were cut into the geometries shown earlier, and
were secured by three bolts into the bracket to ensure proper
spacing. The nozzle assembly, with several of the nozzles
and secondary injection ports, is shown in Fig 7.

Test Stand

Figure 8 is a schematic of the test stand, Fig 9 is a
picture of the apparatus configured for schlieren
photography, and Fig 10 is a view of the nozzle set up on the
force stand for a data run. The nozzle bracket, bolted to
the settling chamber, was aligned horizontally for data runs
and vertically for visualization. The settling chamber hung
from a two-degree-of-freedom pendulum attached to a steel A-
frame. The load cell, shown in Fig 11 with the adapter for
the nozzle bracket, supported the end of the bracket, and
used foil-backed strain gauges to measure the forces in the
axial and side directions. The strain gauges used a source
of ten volts, and the output was collected by the data
aquisition system.

Secondary Injection System

The secondary flow was supplied independently of the
primary flow. A flexible hose was attached to the secondary
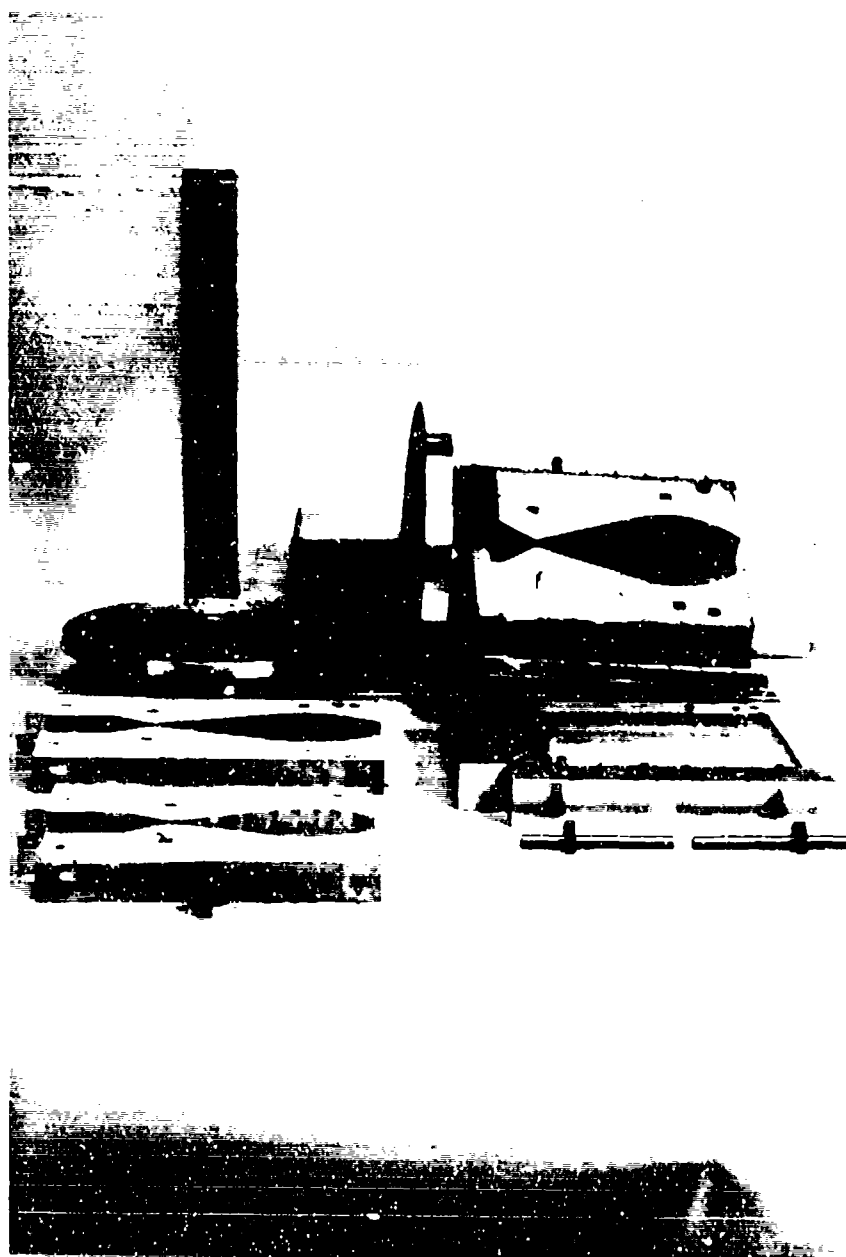
Fig 7. Picture of Nozzle Bracket and Nozzles

18
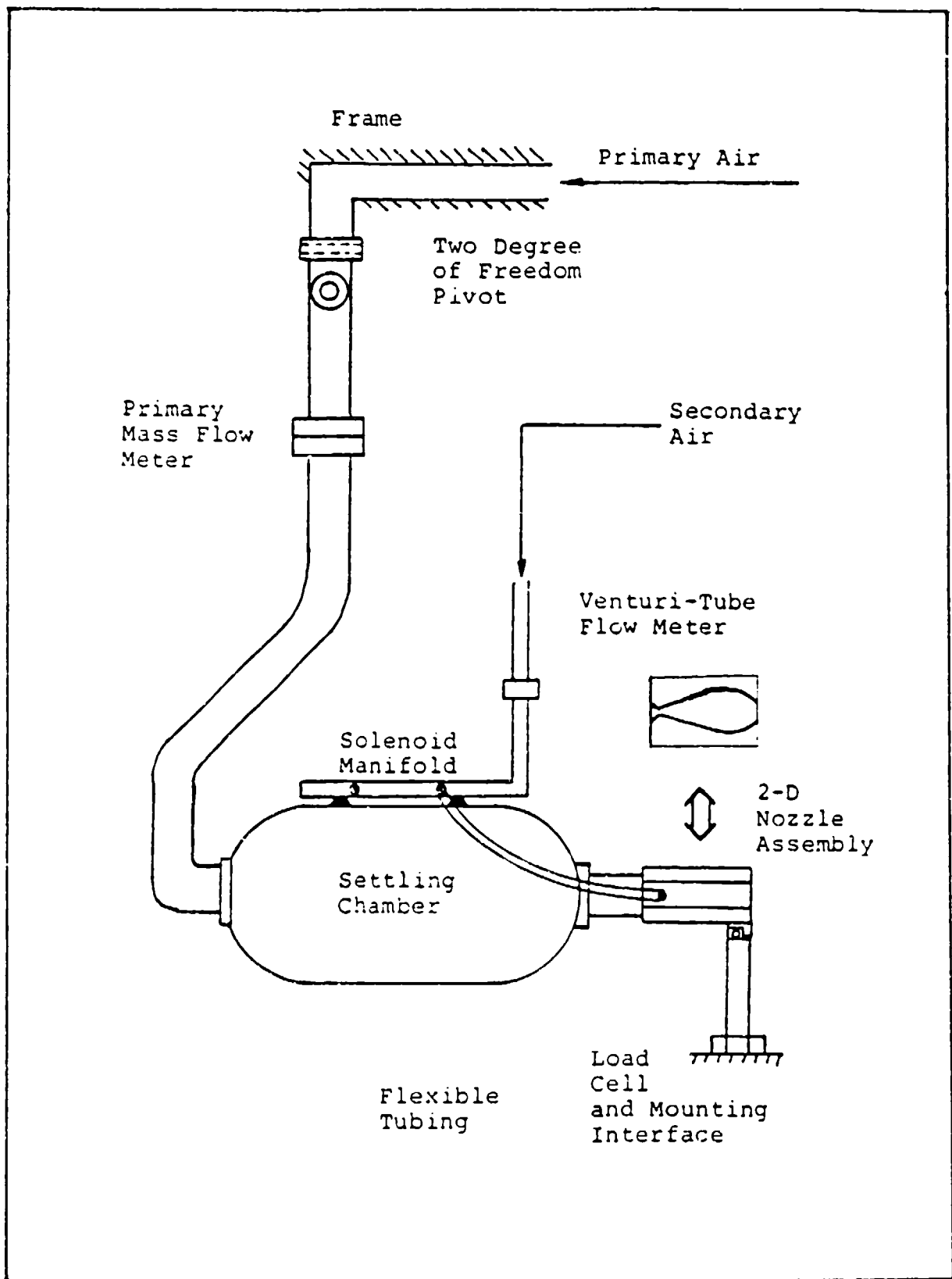
Fig 8.   Schematic Drawing of Apparatus (3:13)
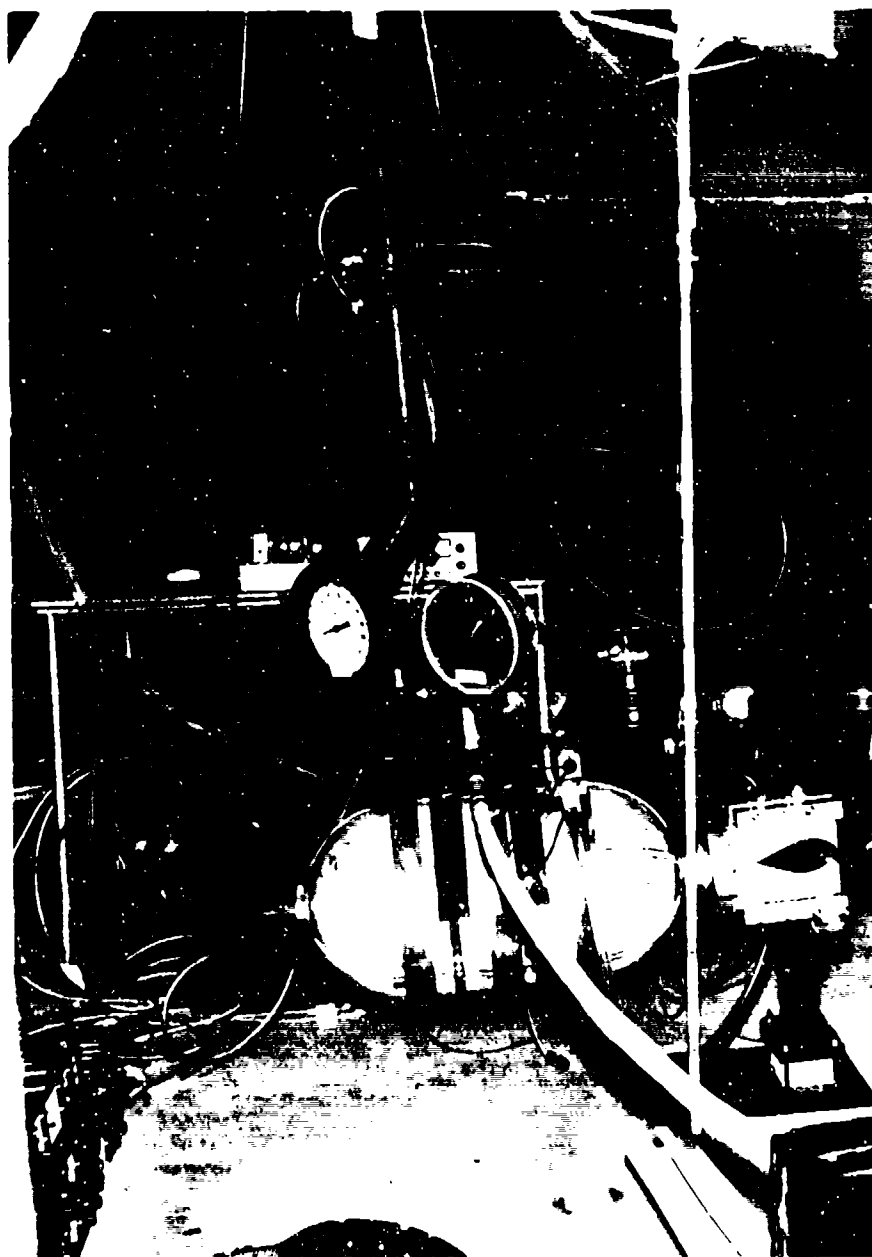
Fig 9. Test Stand Configured for Schlieran Photography
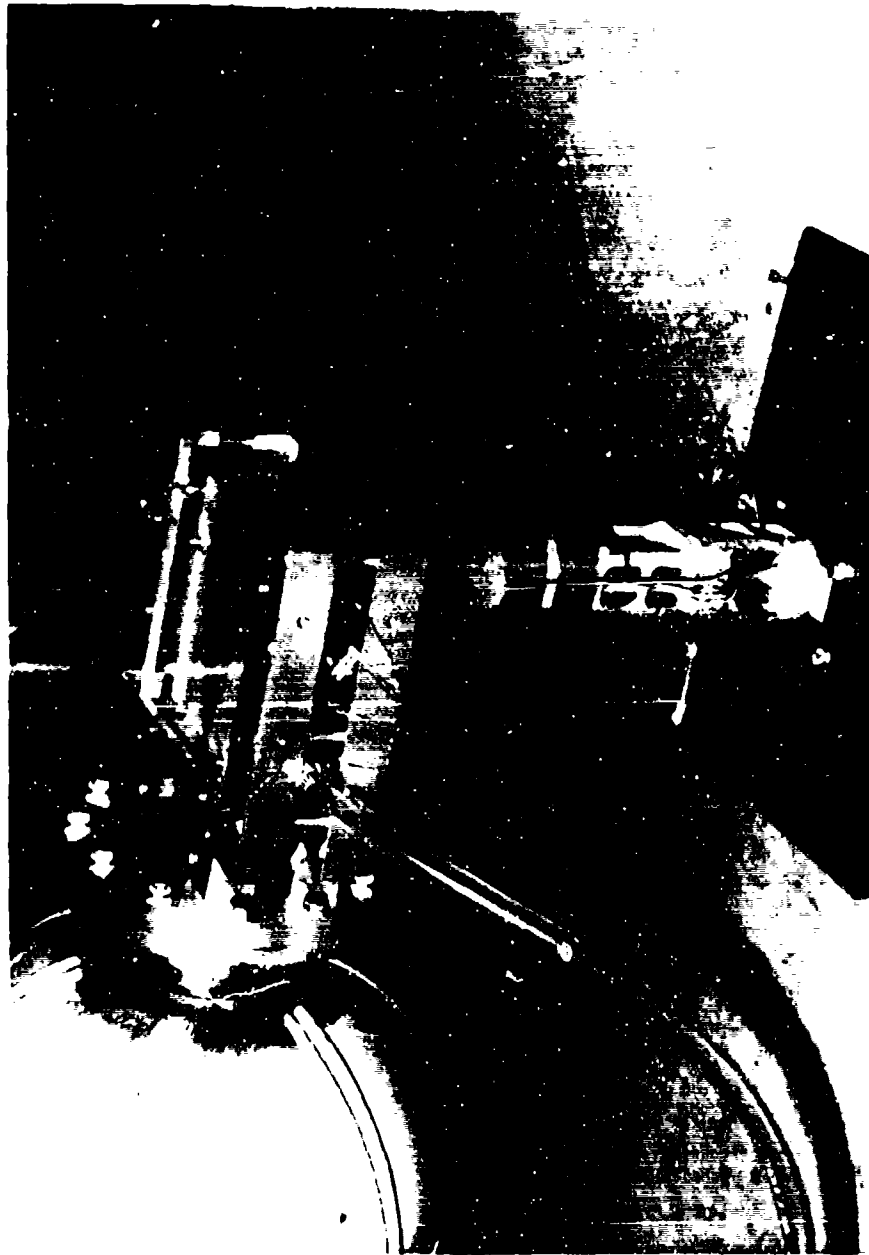
Fig 10. Test Stand Configured for Forces
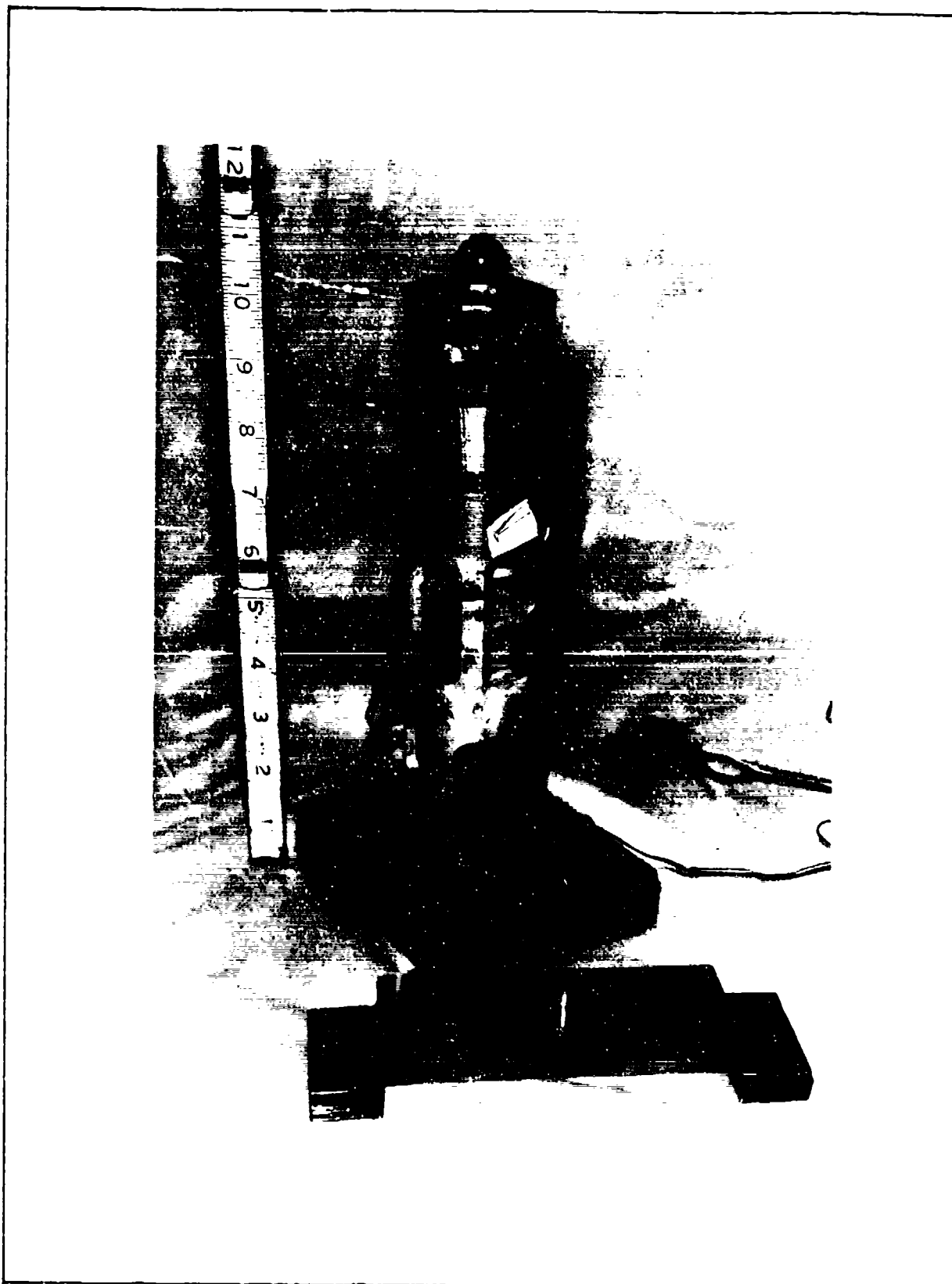
Fig 11. Load Cell with Adapter for Nozzle Bracket

22

injection ports of each nozzle, and was connected to a solenoid valve at the other end. These solenoid valves were connected to a manifold that was bolted to the top of the settling tank. The solenoid valves had a maximum response of 11 Hz, which corresponds to the valves opening and closing in 90 msec. The manifold was supplied air at selected pressure values controlled by a regulator/dome valve. A venturi meter between the valve and the manifold was used to determine the secondary injection air mass flow rate. The regulator valve was supplied by a high pressure line, different from the one used in the primary supply. A pressure gauge was mounted on the manifold, and by using the regulator valve, the desired secondary stagnation pressure was set before each run.

Static Pressure Ports

Pressure transducers were mounted on a cart near the test stand, and were connected to the static pressure ports by 0.0625 in flexible tubes. These transducers were bellows-type, operated by an excitation of ten volts. The output of the transducers was connected to the data aquisition system.

Mass Flow Measurement

A 1.125 in diameter standard ASME orifice was installed in the primary flow line, and a 0.375 in diameter venturi meter was installed in the secondary flow line. Pressure taps for each meter were connected to pressure transducers, whose output was recorded by the data aquisition system.

23

Temperature of the primary flow was assumed to be 67 F, and it was assumed to be 77 F in the secondary flow. Deviations from these temperatures resulted in negligible differences in mass flow measurements, and this is shown in Appendix B.

Data Aquisition System

The data aquisition system was comprised of an HP-85A computer and an HP-3497A data scanner. Voltages from the static pressure wall transducers, the mass flow pressure transducers, and force sensors were read by the HP-3497A and recorded on tape cartridges using the HP-85A. The system recorded twelve static wall pressure measurements, two mass flow pressure measurements, and two force measurements about once every five seconds.

Flow Visualization

A schlieren optical system, Fig 12, was used for flow visualization. Two 7.25 in diameter spherical mirrors with focal lengths of 44 in were used, as well as a spark lamp for still pictures and a zirchonium steady lamp for movies. A Polaroid camera was used with Polaroid type 42 film (ASA 200) for still pictures, and a high-speed (100 frames/sec) 16mm Locam movie camera was used for movies.

System Control

The HP-85A computer was programmed to control the opening and closing of the solenoid valves and record the

24
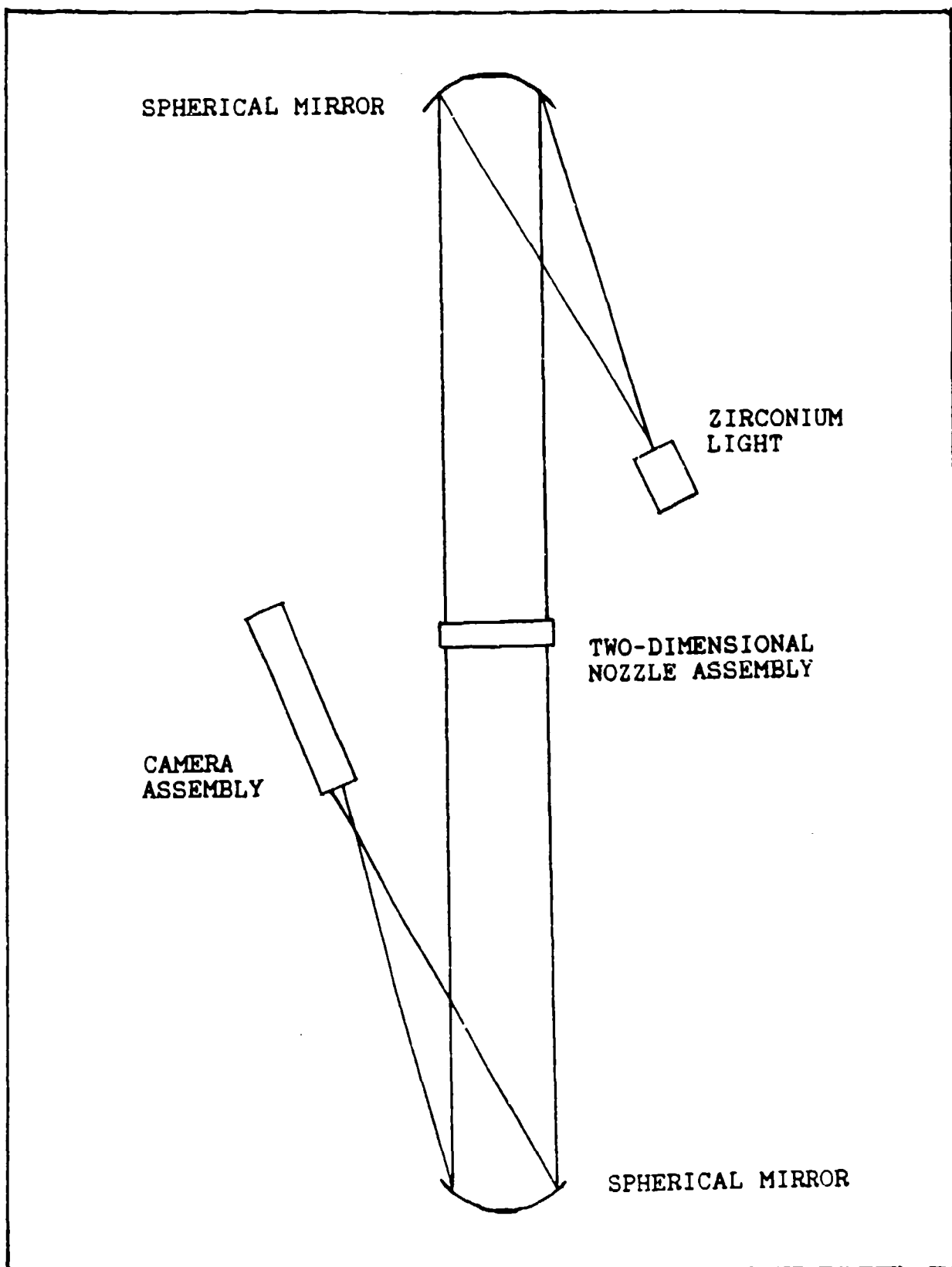
Fig 12. Optical Arrangement for Schlieren Photography

data from the HP-3497A onto tape.

The control of the primary and secondary pressures was not handled by the HP-85A. The secondary stagnation pressure was set via the regulator valve connected to the manifold before each test. The primary static pressure was set by a control panel inside the control room, using a closed circuit TV to monitor the primary pressure gauge.

IV. Experimental Procedure

The procedure for a data gathering run was as follows:

1. The secondary pressure was set by the regulator valve.

2. The solenoid valve commands were stored in a data file to be used by the controlling program.

3. The test control program was loaded into the computer. This program read the valve commands, created a data file for the test, and read the no-load value of the pressure transducers and force sensors.

4. Once the HP-3947A was ready to aquire data from the pressure and force sensors, the primary pressure was set.

5. The test was started.

6. At the end of the test, the primary supply was vented by the operator.

7. The secondary supply was shut off and the data recorded by the computer was stored on tape.

After a data aquisition run, another program would read the values of the sensors and calculate the static port pressures, the mass flows, and the forces.

The flow visualization runs differed in the mounting of the nozzle vertically instead of horizontally. Because of this, no force measurements were made during these runs.

V. Results and Discussion

Non-Dimensional Parameters

Because of some unique characteristics, non-dimensional parameters will be used for many of the results. Thrust, either axial or side, will be made dimensionless by dividing by the product of the throat area and primary pressure (in psia). Secondary pressure and wall pressure will be made dimensionless by dividing by the primary pressure. Distance downstream of the throat, x, will be made dimensionless by dividing by L, the length of the nozzle. Non-dimensional quantities will sometimes be denoted by "N-D".

Effect of Nozzle Geometry on Operable CJTVC Nozzles

An "operable" CJTVC nozzle implies that the jet is axial until the introduction of secondary flow, when the jet vectors as shown in Fig 2. The CJTVC nozzle appears to operate in the axial case by having separated regions of a relatively low pressure around the jet. In the vectored case, a high pressure region downstream of the separation point pushes the jet over to the opposite wall. CJTVC nozzles are very dependent on the geometry to operate correctly, as the exit has to be large enough to allow the jet to leave the cavity, but small enough to allow the pressure buildup in the cavity in the vectored case to keep the jet attached to the wall.

Two of the nozzles constructed for the experiments

28

vectored.   Table III lists the nozzles and geometry of each,
and which of the nozzles were operable as a CJTVC nozzle.

Table III.   Nozzles Investigated as CJTVC Nozzles

Nozzle	Operable as CJTVC?	$\frac{L}{Wt}$	$\frac{We}{Wt}$	$\frac{L}{We}$
LN	No	20	3.5	5.71
LM	Yes	20	4.0	5.00
LW	No	20	4.5	4.44
SN	Yes	16	3.5	4.57
SM	No	16	4.0	4.00

The last parameter, length divided by the width of the
exit, seems to be the most critical.   The nozzles that were
operable, LM and SN, each had an L/We in the middle of the
nozzle geometries tested (5.00 and 4.57, respectively).   The
nozzles that had an L/We less than than 4.57, SM and LW, were
not operable for very different reasons than LN, which had an
L/We greater than 5.00.

LW and SM never vectored from the axial case using any
Ps/Pt or As combination.   Figure 13 is a non-dimensional
pressure distribution and schlieren photograph of the LW
nozzle with and without secondary injection at Pp = 194.4
psia.   Ps/Pp for the injection is 0.54, and As/At = 0.26.   As
can be seen from the picture, the jet is not attached to the
wall.   But because the jet is not completely axial, there is
a small contribution to side force of about 0% of the axial
force.   By comparing Fig 13 to Fig 14, which is the vectoring
case at the same Ps/Pp with the LM nozzle, the pressure in

29

Side B　　　　　　　　　　　　　　Side B

Side A　　　　　　　　　　　　　　Side A

Ps/Pp = 0.0　　　　　　　　　　Ps/Pp = 0.54
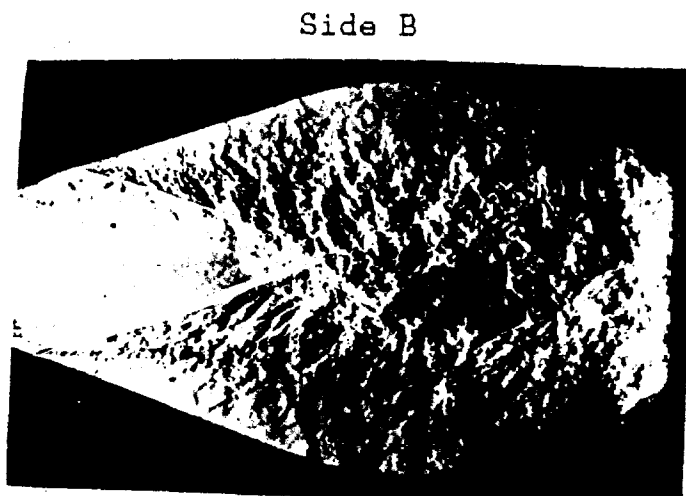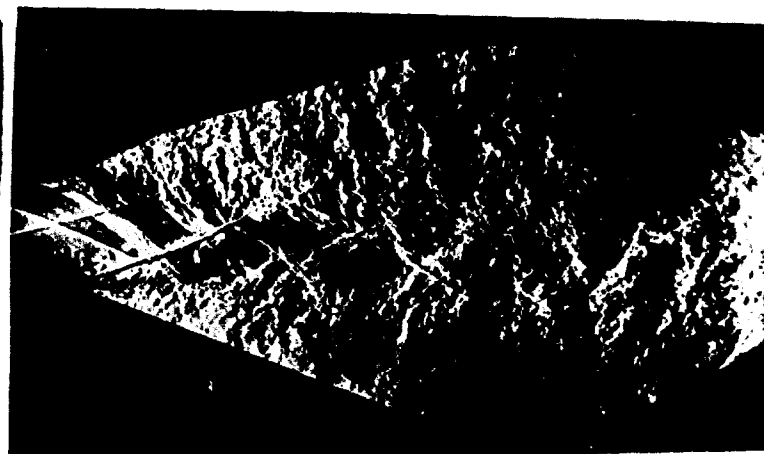
Sec. Injection from Side B at X/L=0.15
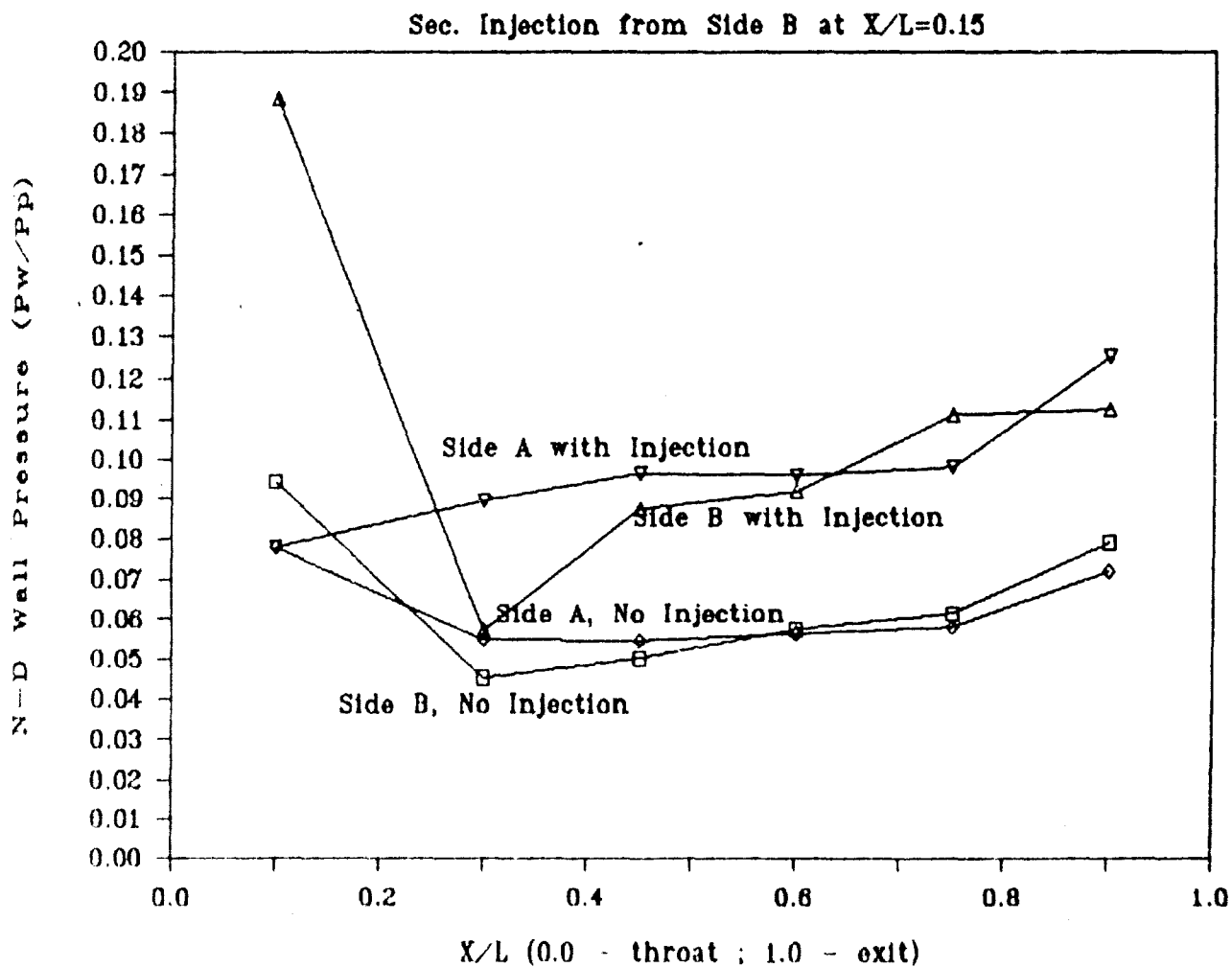
Fig. 13　　Effect of Exit Too Large for Vectoring
　　　　　　LW, Pp = 194.4 psia

Side B

Side B

Side A

Side A

Ps/Pp = 0.0

Ps/Pp = 0.54
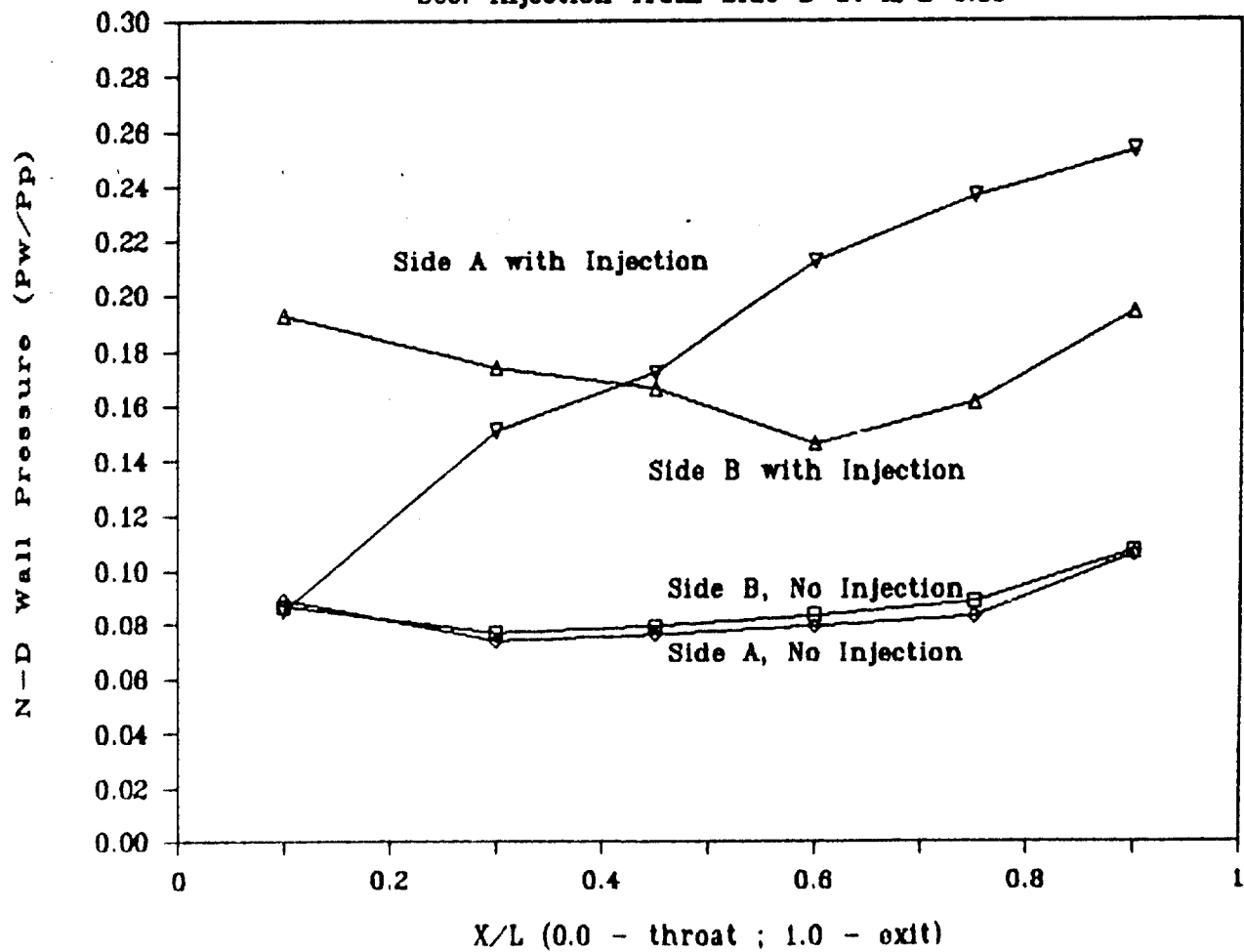
Fig 14. Exit Correctly Sized for Vectoring
LM, Pp = 194.4 psia

31

the cavity in the LW nozzle is very low. In the SM and LW nozzles, the exit seems to be too wide for successful CJTVC operation. If the exit is too wide, the secondary pressure cannot build high enough to push the jet to the wall. Instead, the primary flow will be moved over to allow the secondary flow to exit, as was noted by Cates (3:34).

The MN nozzle was a case of the exit area being too small. With or without secondary injection from both sides, the nozzle would not be stable in the axial position. This could be because of the following reasoning. If the exit is too narrow, the whole jet does not exit, and some of it recirculates in the nozzle cavity, building the pressure inside the cavity. In a perfectly symmetrically nozzle, this would not be a problem with axial operation. However, small imperfections cause the pressure on one of the sides of the jet to be slightly greater than the other side. This difference vectors the jet to the wall, and the axial case becomes very hard to maintain.

Both the LM and SN nozzles vectored, but the LM nozzle vectored under more variations in secondary injection area and secondary pressure. This may imply that the LM nozzle is closer to the optimum design of a two-dimensional CJTVC nozzle than the SN nozzle.

Vectoring Domain

Figure 15 is a graph of N-D secondary mass flow versus N-D secondary pressure at a constant primary pressure of

32
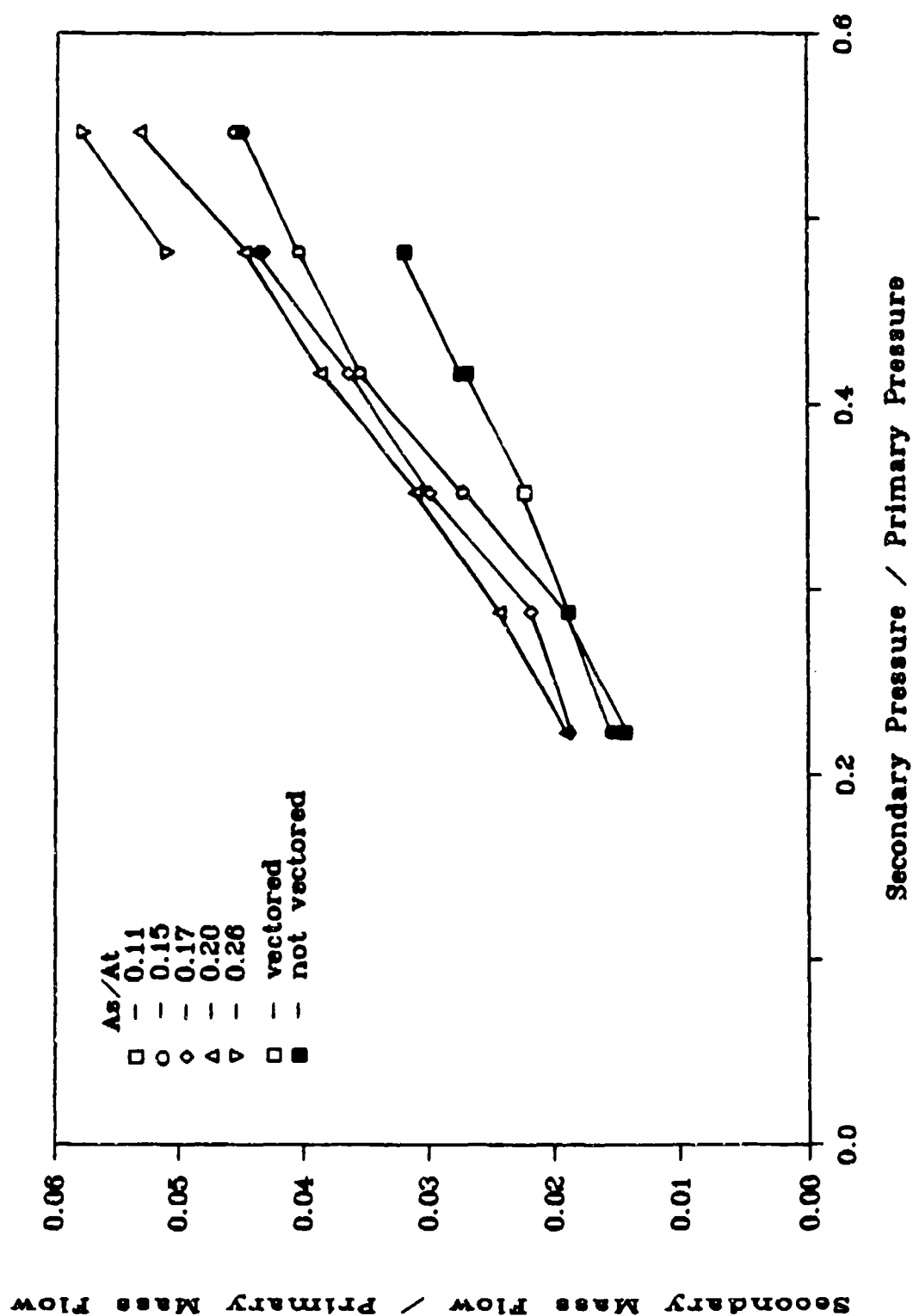
Fig 15. Effect of Ps and As on Vectoring
LME, Pp = 154.4 psia, $\dot{m}_p$ = 0.74 lbm/sec

33

154.4 psia, and it provides a domain where the LME nozzle vectors. Vectoring cases are indicated by an open symbol, and non-vectoring cases are denoted by a darkened symbol. The minimums of the domain occur when there is insufficient secondary pressure or mass flow for vectoring. For instance, the minimum Ps/Pp is around 0.28, as experiments to the left of this line with too small a Ps/Pp did not vector, and most of the cases to the right did. But coupled closely with the minimum pressure required is a minimum mass flow necessary for vectoring. At an $As/At = 0.11$, only one vectoring combination was observed, even though the Ps/Pp ratio was much larger than the minimum. So there seems to be both a requirement on secondary mass flow and secondary pressure for vectoring to occur.

Vectoring also depends on the area of the secondary injection. In Fig 15, at a Ps/Pp of 0.42, the nozzle does not vector at a mass flow ratio of 0.024 and $As/At = 0.11$. But it vectored at a lower Ps/Pp of 0.29 with a smaller mass flow ratio of 0.021 and a larger $As/At = 0.17$. Therefore, vectoring depends on the secondary area, mass flow, and pressure.

The combination of these minimum requirements may imply that vectoring is a function of the secondary stream momentum - the product of secondary injector stream velocity and secondary mass flow. With a small area, the mass flow is low, which gives a small secondary momentum. Also, low pressure implies that the velocity through the secondary

34

injector is low, which also results in a reduced secondary momentum. So a minimum secondary momentum requirement may account for the minimum requirements of secondary area, mass flow, and pressure.

An upper limit on vectoring is displayed by the points at a $P_s/P_p = 0.48$, $A_s/A_t = 0.17$, and at $P_s/P_p = 0.56$, $A_s/A_t = 0.15$. In these cases, even though the secondary pressure and mass flow were above the apparent minimums, the nozzle did not vector. It may be that the cases were an extension of the minimum mass flow requirement, but because of the area of the secondary injection and the mass flow at these points, this does not seem to be a plausible explanation. What might be occurring is at these conditions, the secondary injection may be at a large enough pressure and mass flow to penetrate and completely disrupt the jet, instead of just pushing it to the opposite wall. Disrupting the jet would prevent flow from attaching distinctly to one wall, so the resulting flow would not have any side force.

The domain of vectoring changes with increasing primary pressure. Figures 16, 17, and 18 are the same type of graphs as Fig 15, only the primary pressures are 174.4, 194.4, and 214.4 psia, respectively. The minimum secondary pressure and secondary mass flow requirements for vectoring are noticeable in these graphs, particularly in Fig 16. In Fig 17, the minimum P_s/P_p for vectoring is at a value of about 0.30, which is higher than the value in Fig 15. Therefore, the secondary pressure requirement seems to increase with primary
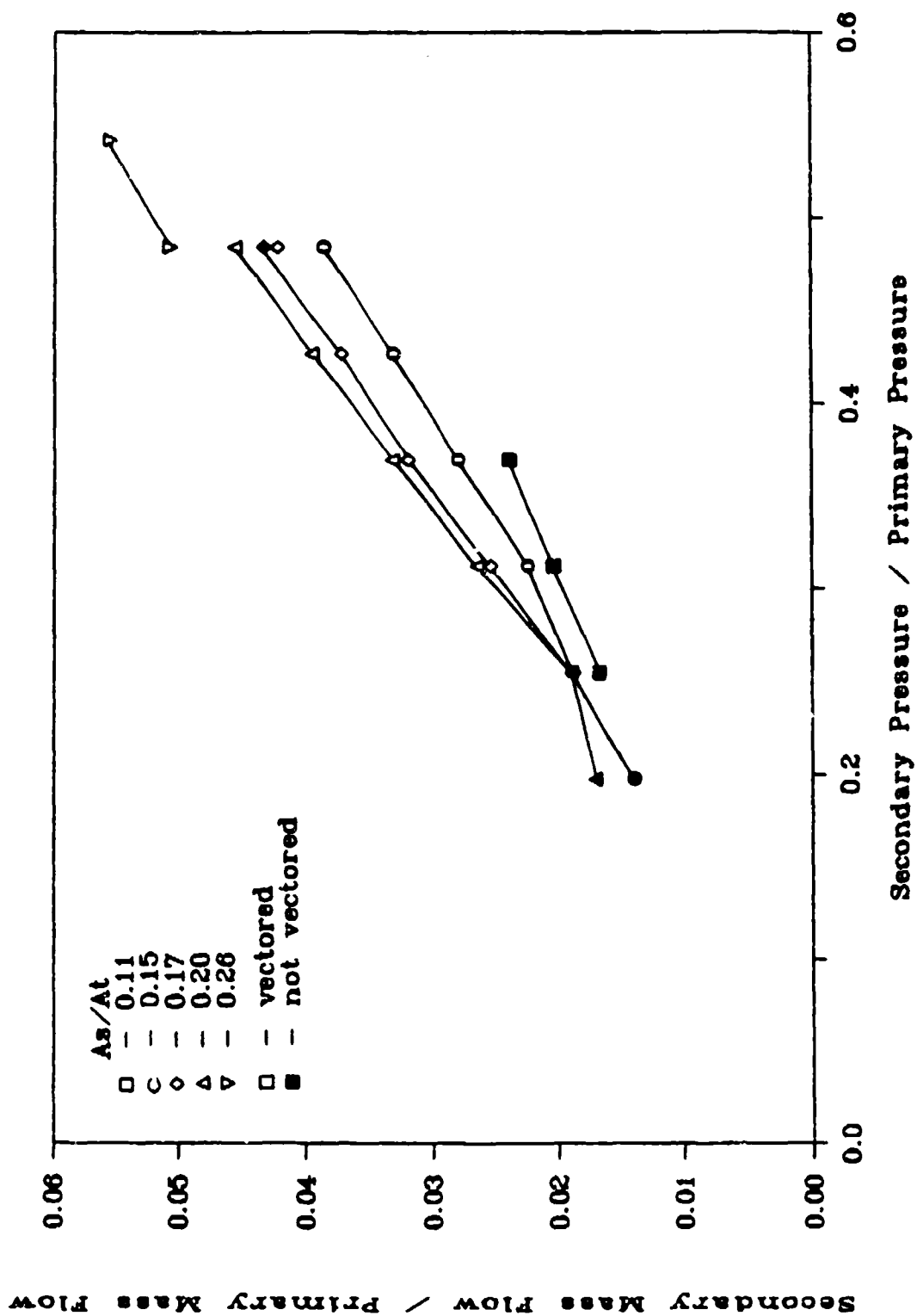
Fig 16. Effect of Ps and As on Vectoring
LME, Pp = 174.4 psia, $\dot{m}_p$ = 0.85 lbm/sec
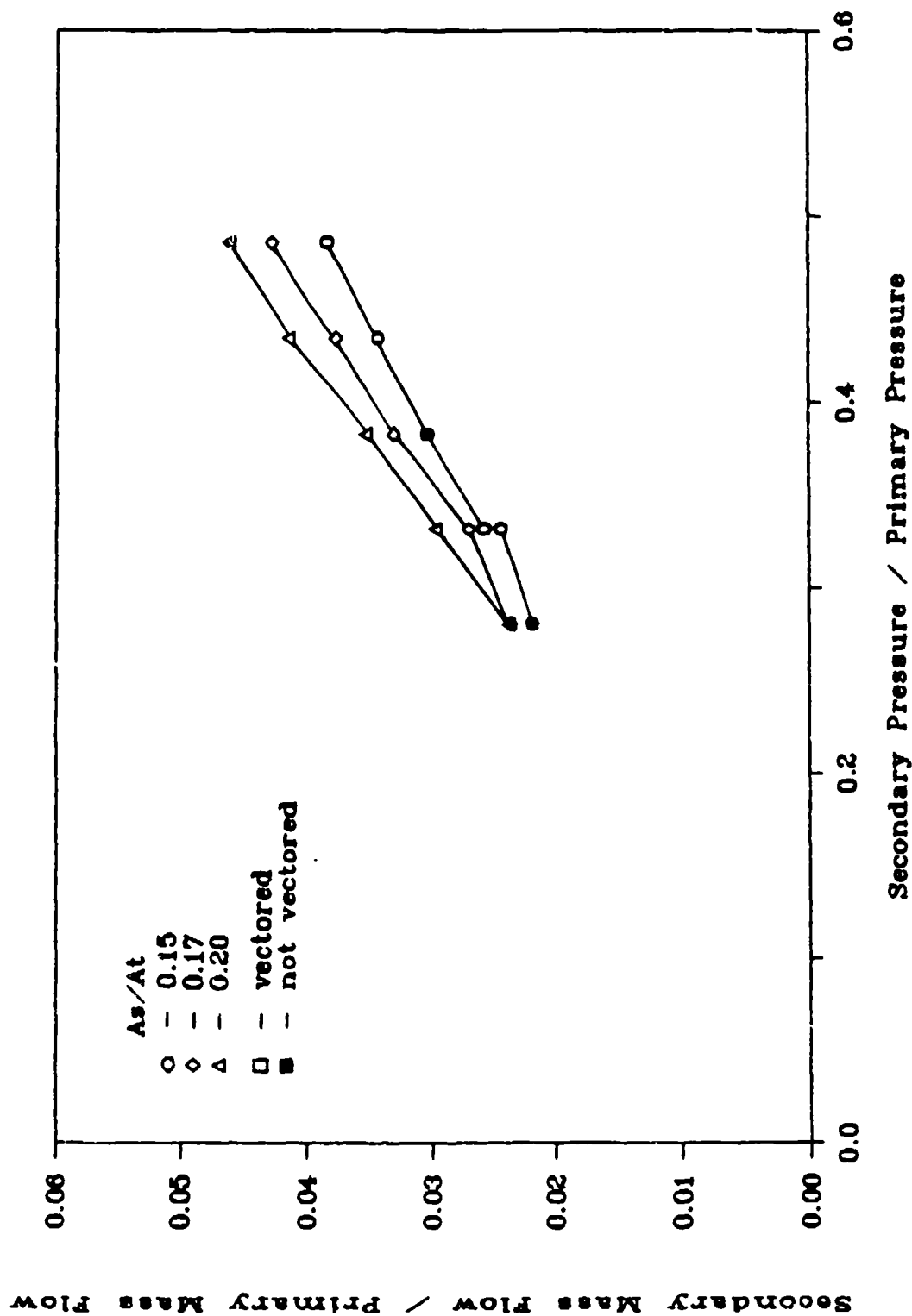
Fig 17. Effect of Ps and As on Vectoring
LME, P_p = 194.4 psia, $\dot{m}_p$ = 0.96 lbm/sec
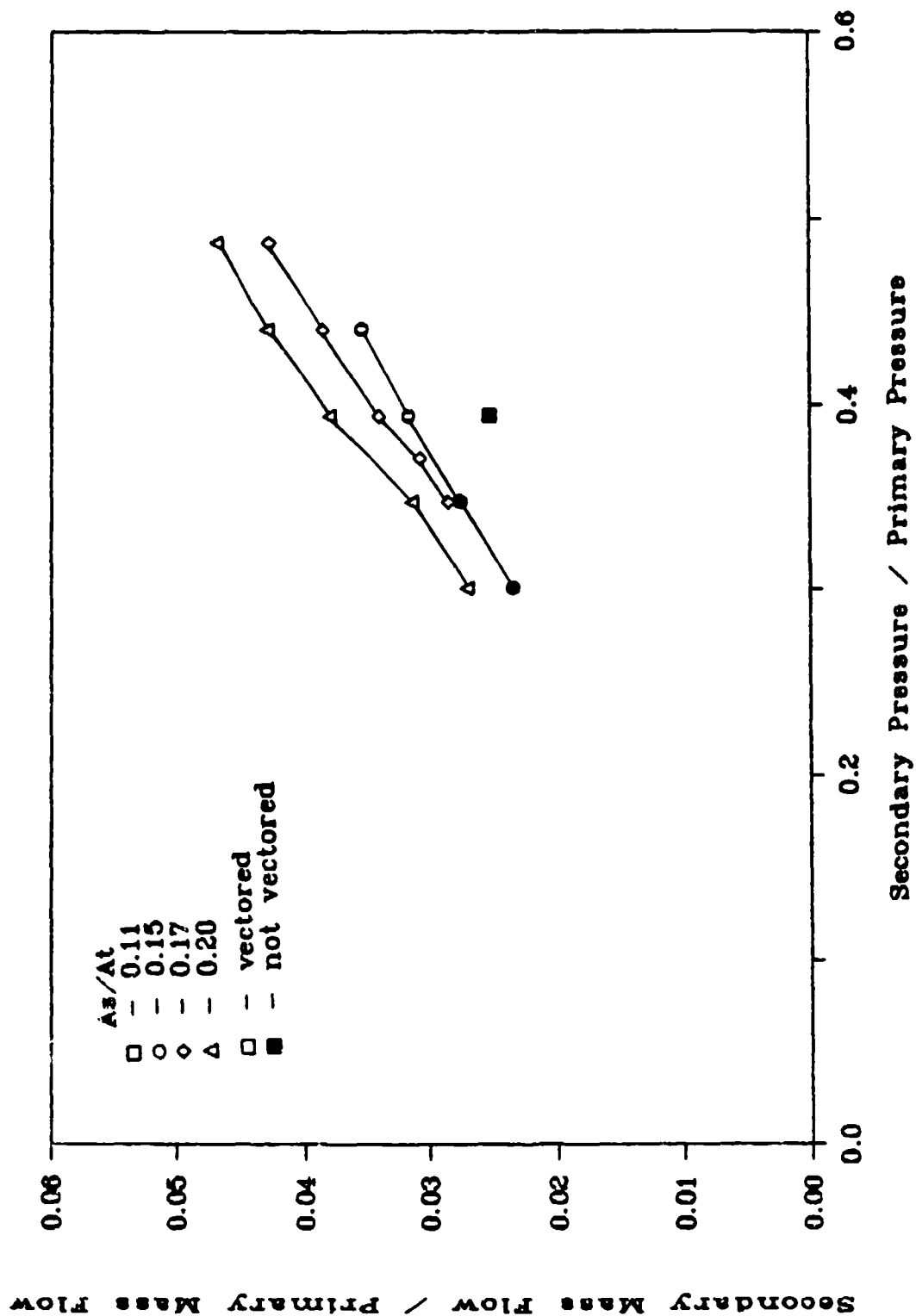
Fig 18. Effect of Ps and As on Vectoring
LME, $P_p = 214.4$ psia, $\dot{m}_p = 1.07$ lbm/sec

pressure increase. Also, using the same graphs for comparison, the minimum mass flow required for vectoring appears to slightly increase.

Too much secondary flow is indicated at the point of $Ps/Pp = 0.49$ and N-D secondary mass flow $= 0.047$ in Fig 17, where the flow did not vector. Because there are flows at the same Ps/Pp and smaller mass flow that did vector, this too implies that there is a maximum to the amount of secondary flow necessary for vectoring.

Figures 19 through 23 display the same information as Figs 15 through 18, but As is held constant on each graph, and Pp is varied. These graphs together define the operational domain of the system, by indicating under what primary pressures, secondary pressures, and secondary injection areas the LME nozzle will vector. Approximate minimum values are $Ps/Pp = 0.25 - 0.30$, secondary mass flow of 2-3% of the primary mass flow, and a minimum $As/At = 0.17$. Fig 19 seems to be in the non-vectoring range, since most of the cases do not vector. Fig 20 is on the border, with about half the cases vectoring. Figs 21 - 23 seem to be in the domain of vectoring, since most of the cases vector. The maximum values for secondary mass flow and pressure can be seen as the darkened points in the upper right of Figs 21 and 22. They occurred at about $Ps/Pp = 0.50$ and N-D secondary mass flow of 0.045.

A domain of vectoring, with both minimum and maximum secondary pressure and mass flow, has not been mentioned in

Fig 19. Effect of Ps and Pp on Vectoring
LME, As/At = 0.11

40
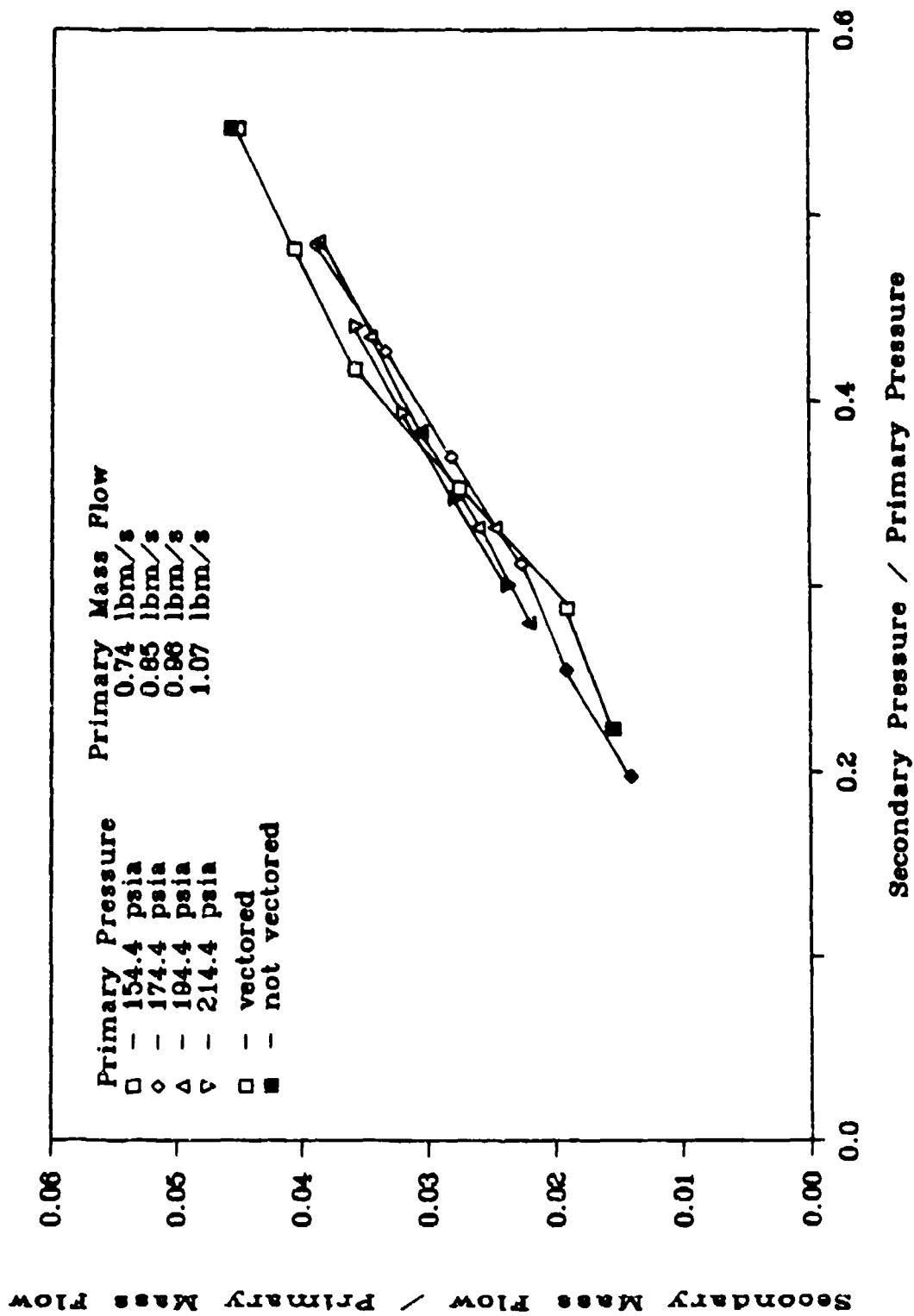
Fig 20. Effect of Ps and Pp on Vectoring
LME, As/At = 0.15

41
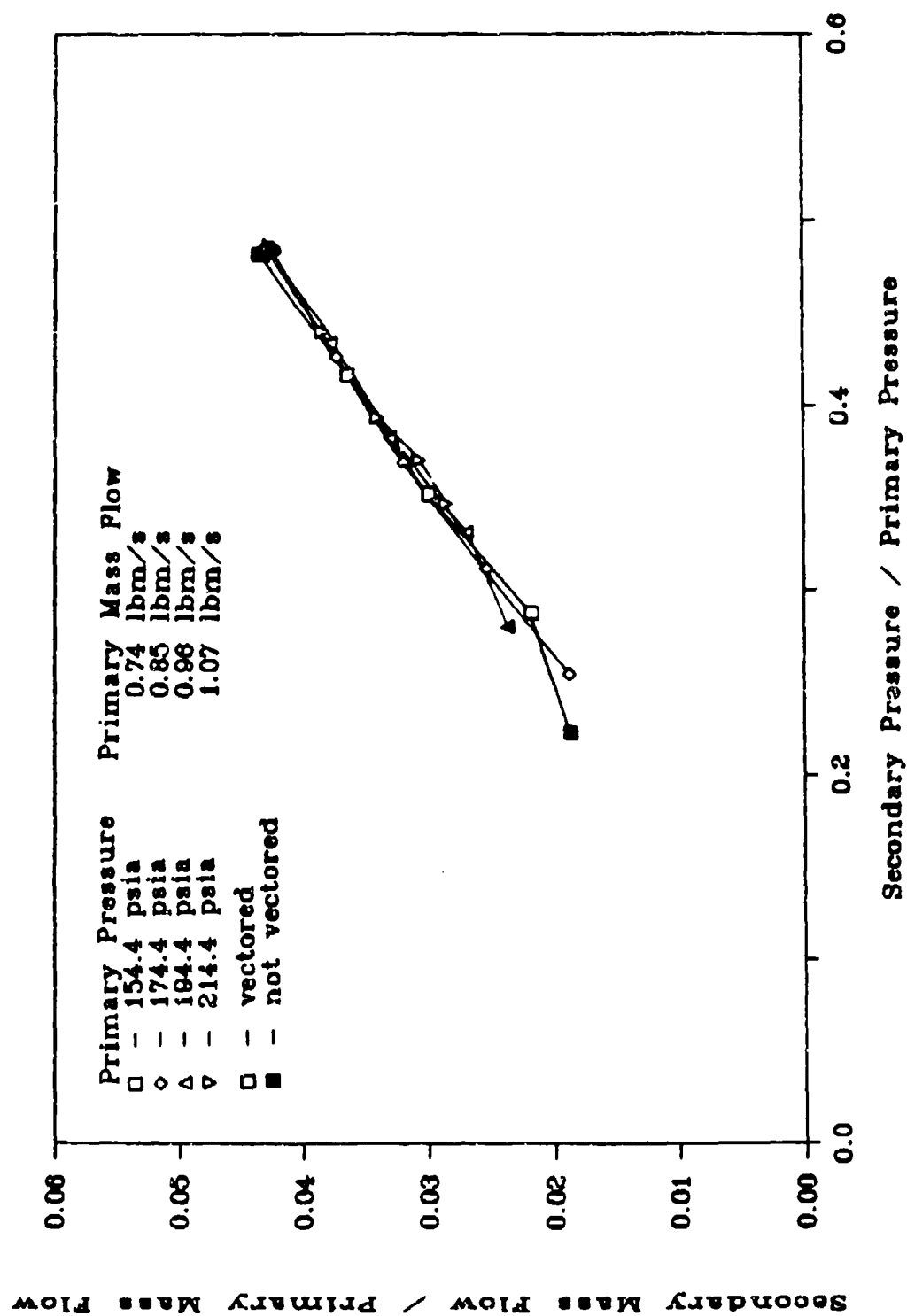
Fig 21. Effect of Ps and Pp on Vectoring
LME, As/At = 0.17
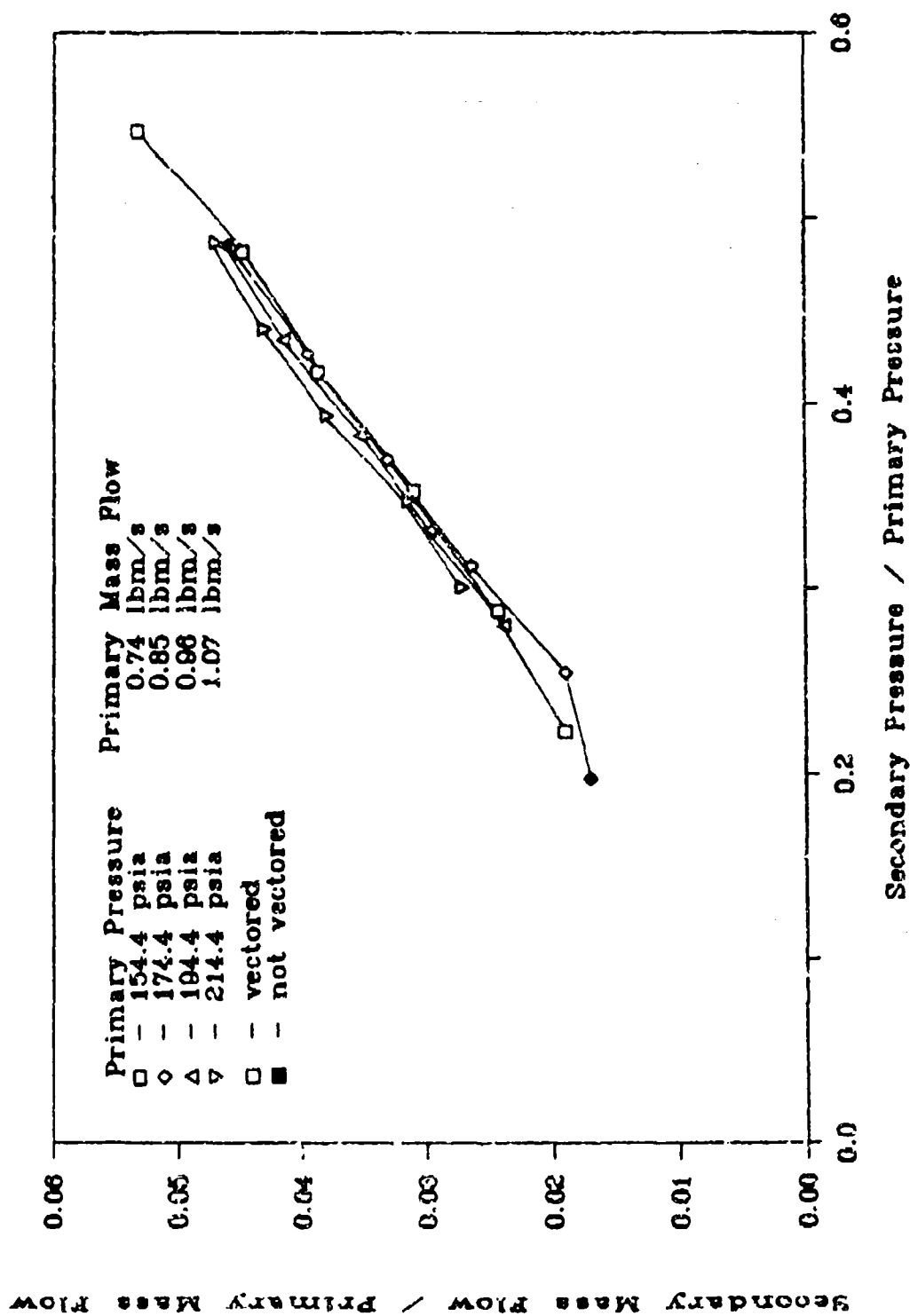
Fig 22. Effect of Ps and Pp on Vectoring
LME, As/At = 0.20

Fig 23. Effect of Ps and Pp on Vectoring
LME, As/At = 0.26

Secondary Pressure / Primary Pressure

Secondary Mass Flow / Primary Mass Flow

Primary Pressure
□ — 154.4 psia
◇ — 174.4 psia
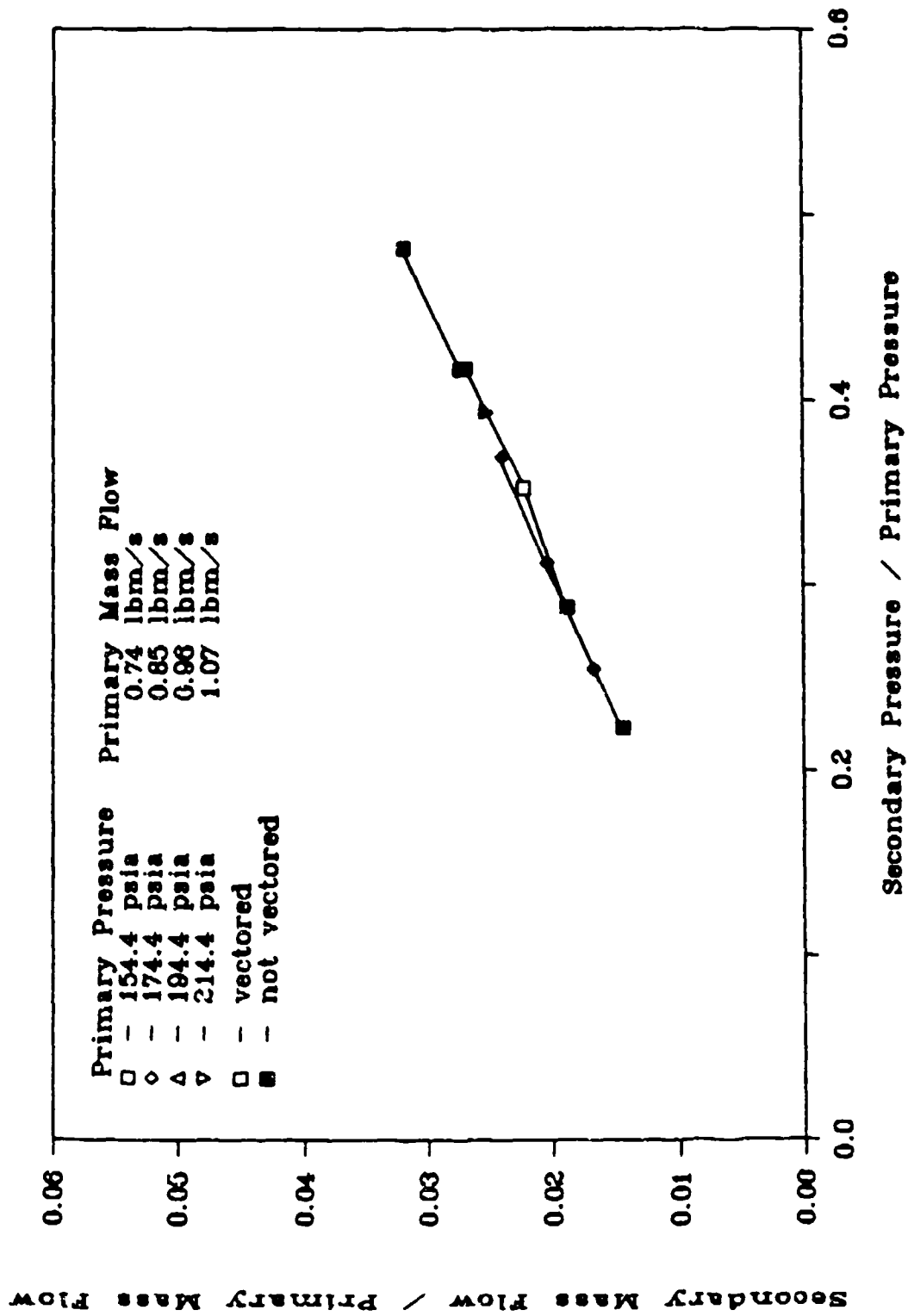
□ — vectored
■ — not vectored

Primary Mass Flow
0.74 lbm/s
0.85 lbm/s
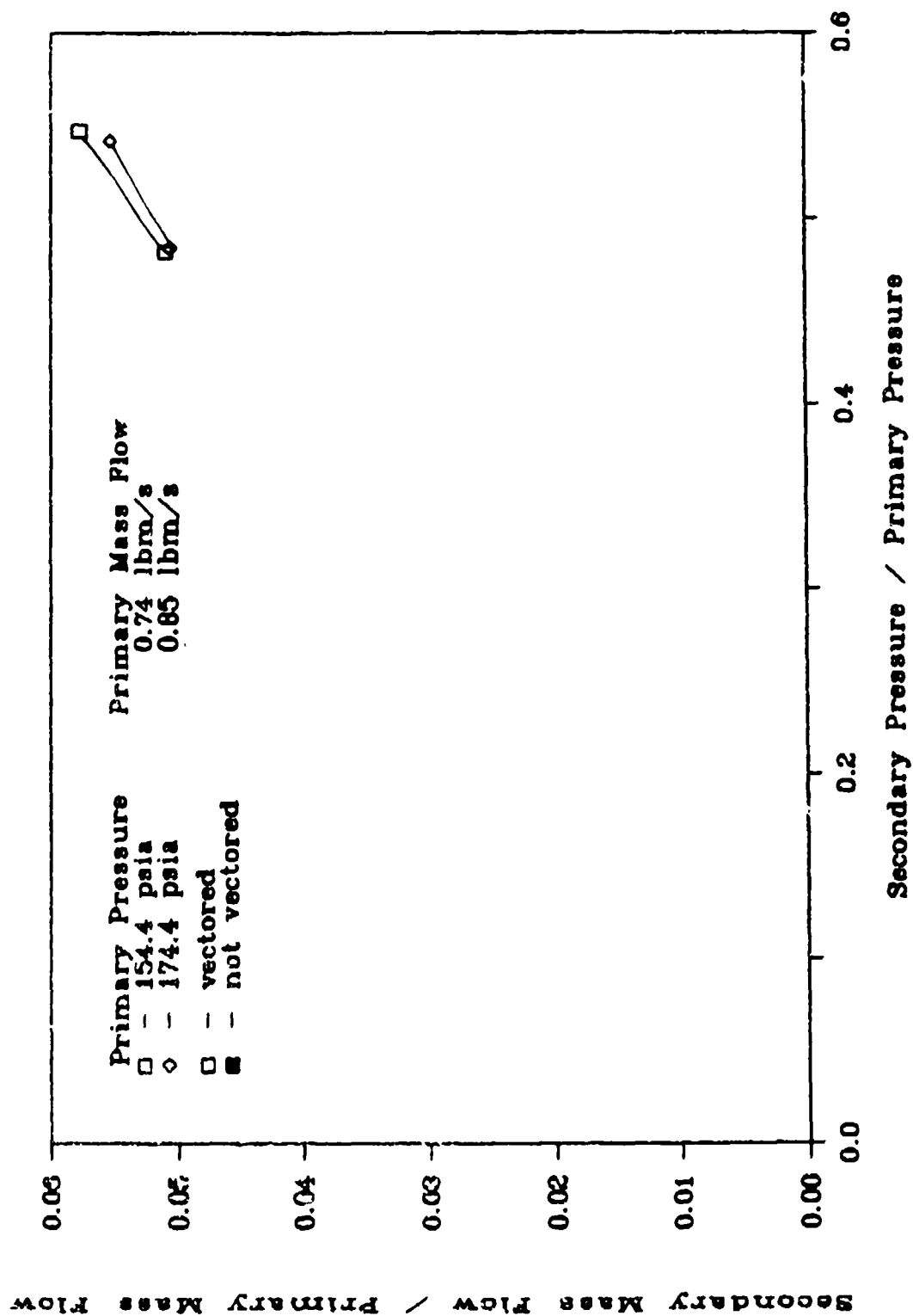
any previous CJTVC work, either axisymmetric or two-dimensional. Any system using this geometrical configuration would have to be designed to operate within this domain.

Thrust Efficiency

Performance of a TVC system is measured by several parameters, including angle of thrust, efficiency of axial and vectored conditions, and amount of input (force or amount of secondary flow) required to vector the flow.

Figure 24 graphs the magnitude of force of several different nozzles at the different primary pressures. The "ideal thrust" is the thrust of an ideally expanded nozzle at the various primary pressures, and the calculation is found in Appendix C. The "overexpanded nozzle" represents the thrust obtained from the test stand using a nozzle with the same 20 degree divergence angle as found in the CJTVC. The "axial CJTVC" is the thrust obtained from the LME nozzle at the various primary pressures with no secondary injection. The "vectored CJTVC" is the total thrust in the vectored case of the LME nozzle (total thrust equals the square root of the sum of the squares of side and axial forces), using the case for which Ps is a minimum for vectoring. The graph shows that the vectored case produces more total thrust than the axial case, and the thrust is about equal to the thrust produced by the overexpanded nozzle. Figure 25 is a graph of the efficiency of the nozzles, measuring total thrust produced relative to the theoretical thrust produced at the

45
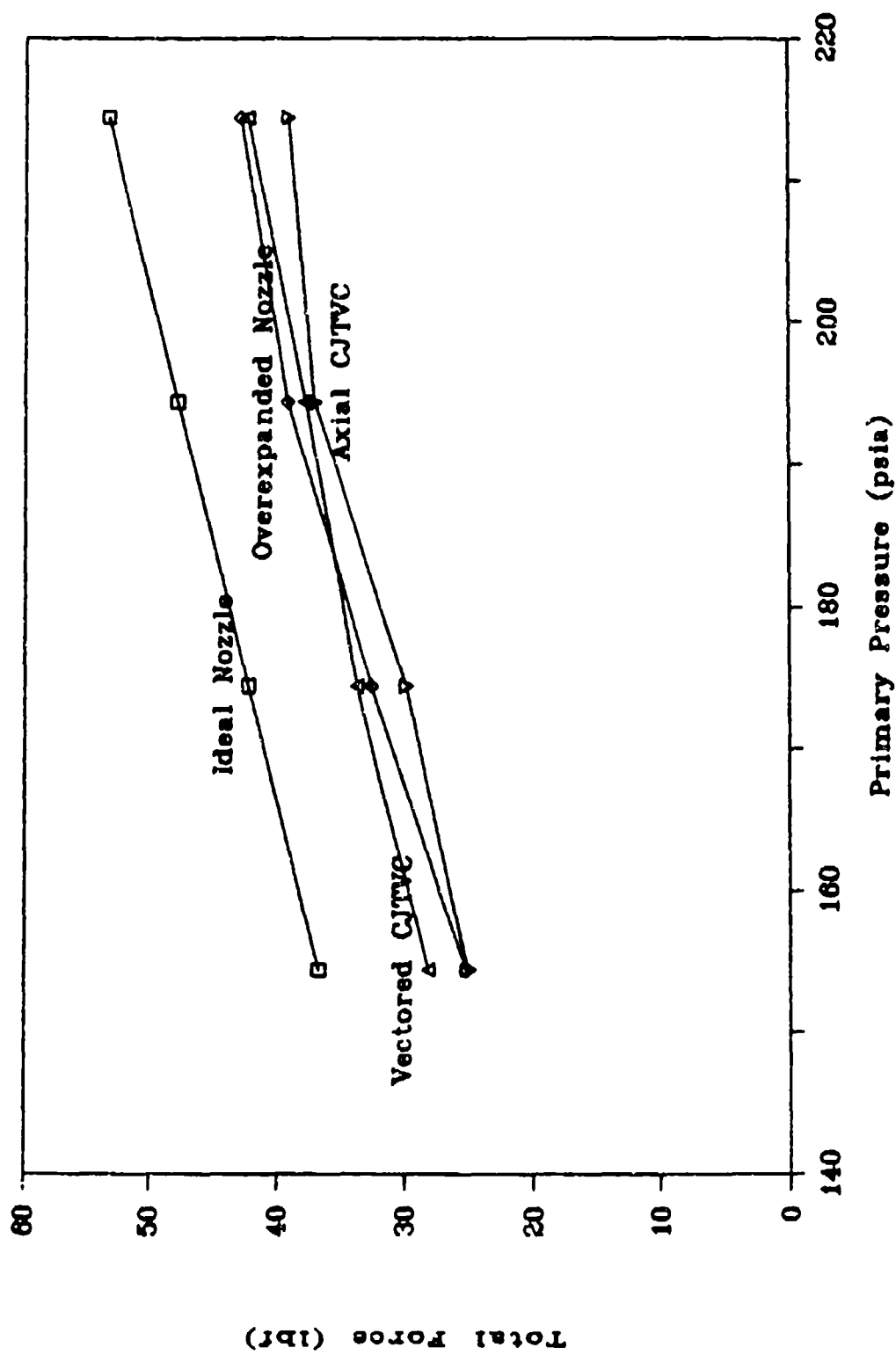
Fig 24. Effect of Pp on Thrust of Various Nozzles
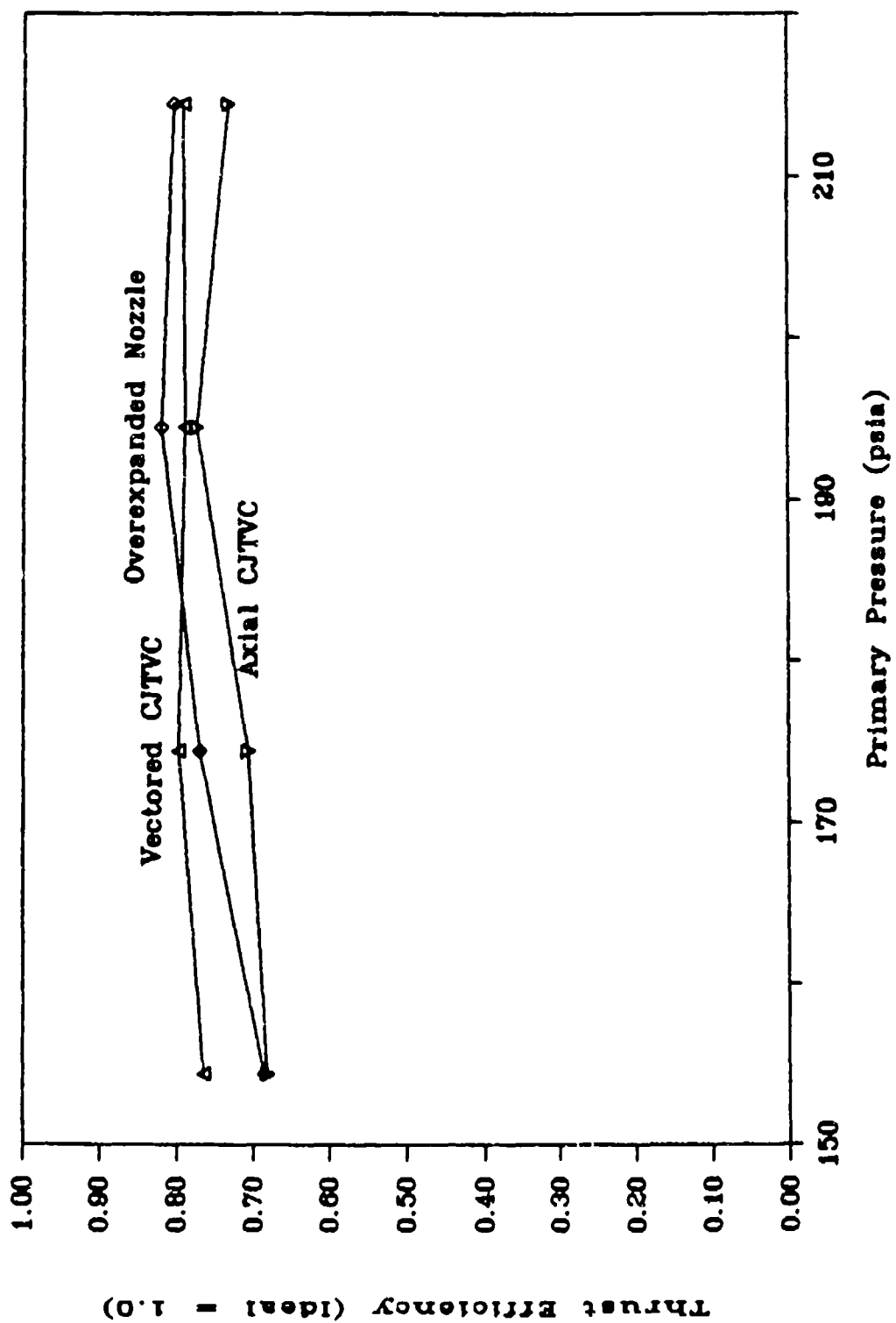
Fig 25. Effect of Pp on Efficiency of Various Nozzles

primary pressure by an ideally expanded nozzle. As can be seen from the graph, in the vectored case, the efficiency of CJTVC is approximately the same as the efficiency of the overexpanded nozzle. The axial efficiency is 5 - 10% below the vectored efficiency. The increase in efficiency of the vectored case over the axial case is partially due to the 2-3% extra mass flow from the secondary injection, which is not accounted for in the efficiency calculation. It may also be partially due to less recirculation of the primary jet in the separation region, since there is only one separation region in the vectored case and two regions in the axial case.

The data presented in Figs 24 and 25 are for the nozzle with the extension. Without the extension, the efficency is much improved. At the 174.4 psia primary pressure, the axial force is 33.2 lbf for an efficiency of 78%. And in the vectored case, the total force is 35.4 lbf for an efficiency of 84%. These are ten percent greater than either the vectored flow with the extension or the overexpanded case. The efficiency may be lower with the extension due to the larger losses to friction.

The values for efficiency with the extension are approximately the same values Cates found (3:46). Cates' values increased slightly with primary pressure, and the same trend is evident in this data. The increase in efficiency of the values without the extension over those found by Cates may be due to the smoother geometry of the these nozzles. The values are about five percent higher than Brown's data

48

for the axisymmetric nozzle, but his efficiency also slightly
increased with primary pressure (2:25).

Effect of Vectoring on Axial Force

Axial thrust is not affected severely by vectoring, as
shown in Figs 26, 27, and 28. Dimensionless axial force
versus non-dimensional secondary pressure is presented for
the LME nozzle, with As/At = 0.15, 0.17, and 0.20. The
dashed line represents an unknown value of force in the Ps/Pp
range between non-vectoring and vectoring. The graphs show
that before vectoring, any increase in secondary pressure can
slightly increase axial force. After vectoring, the axial
force drops a maximum of ten percent, then starts to increase
as the secondary pressure is increased. The data from Cates'
nozzles exhibited the same drop in axial force when vectoring
(3:42).

Response Time of Vectoring

High speed movies were made to find the response time
of vectoring and the return to axial. At a Pp = 154.4 psia
and Ps/Pt = 0.48, the jet moved from the axial condition to
the vectored condition in less than 30 msec. However, after
the valve was shut, the jet stayed attached for 250 msec, and
then returned to the axial condition in less than 20 msec.
The response of the jet moving from the axial to vectored
case was the same 30 msec using the same Pp but Ps/Pt =
0.74. But when the valve was closed, the jet stayed attached

49

Fig 26. Effect of Vectoring on Axial Force
LME, As/At = 0.15
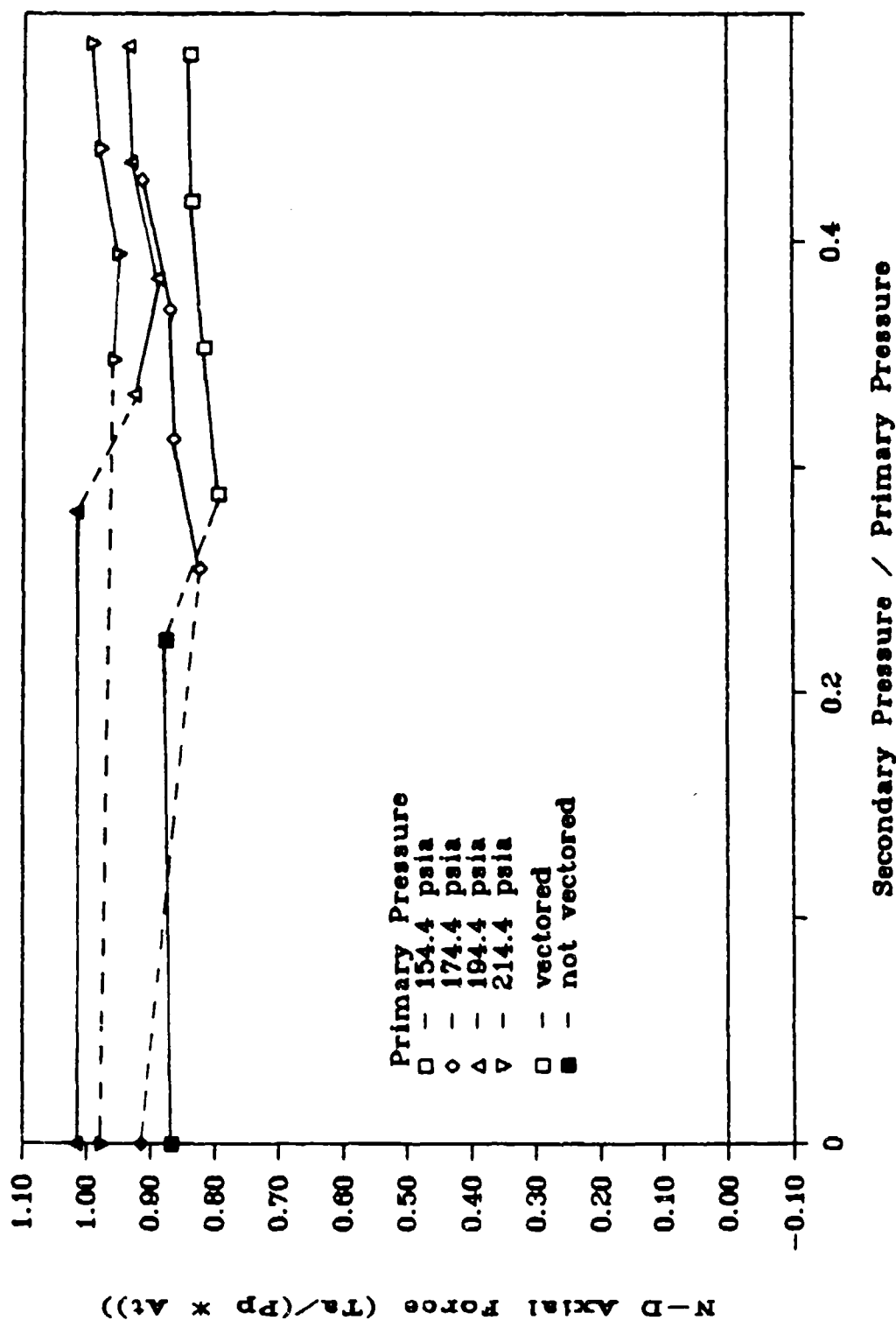
Fig 27. Effect of Vectoring on Axial Force
LME, As/At = 0.17

Secondary Pressure / Primary Pressure

N-D Axial Force (Ta/(Pp * At))

Primary Pressure
□ — 154.4 psia
◇ — 174.4 psia
△ — 184.4 psia
▽ — 214.4 psia

□ — vectored
■ — not vectored

Fig 28. Effect of Vectoring on Axial Force
LME, As/At = 0.20

52

for 80 msec, then moved to the axial case in 20 msec. Using a Pp = 214.4 psia and Ps/Pt = 0.49, the jet took slightly longer, 50 msec, to move from the axial to the vectored case. But the time for the return was smaller - the jet remained attached to the wall for about 60 msec after the secondary injection was turned off, then moved back to axial in 20 msec.

These times are all for the solenoid valves, which have a maximum frequency of 11 Hz. This response corresponds to the valves opening and closing in 90 msec, which may affect the jet response. With these valves, for larger Pp, the jet takes slightly longer to move to the wall after the valve is opened, but the response time is within 50 msec for these tests. The jet has the tendency to remain attached to the wall after the valve is closed for a varying amount of time, between 50 and 250 msec. The delay involved in leaving the wall might be alleviated through the use of secondary injection from the wall that the jet is attached.

Side Force From Vectoring

The magnitude of side force produced by vectoring for As/At = 0.15, 0.17, and 0.20 for the LME nozzle at different Ps/Pp is displayed in Figs 29, 30, and 31. Unlike the N-D axial force, all the N-D side force in the vectoring cases fall roughly on a line in each figure, even with variance in primary pressure. Using linear regression on the vectoring cases, these lines have the following equations for the
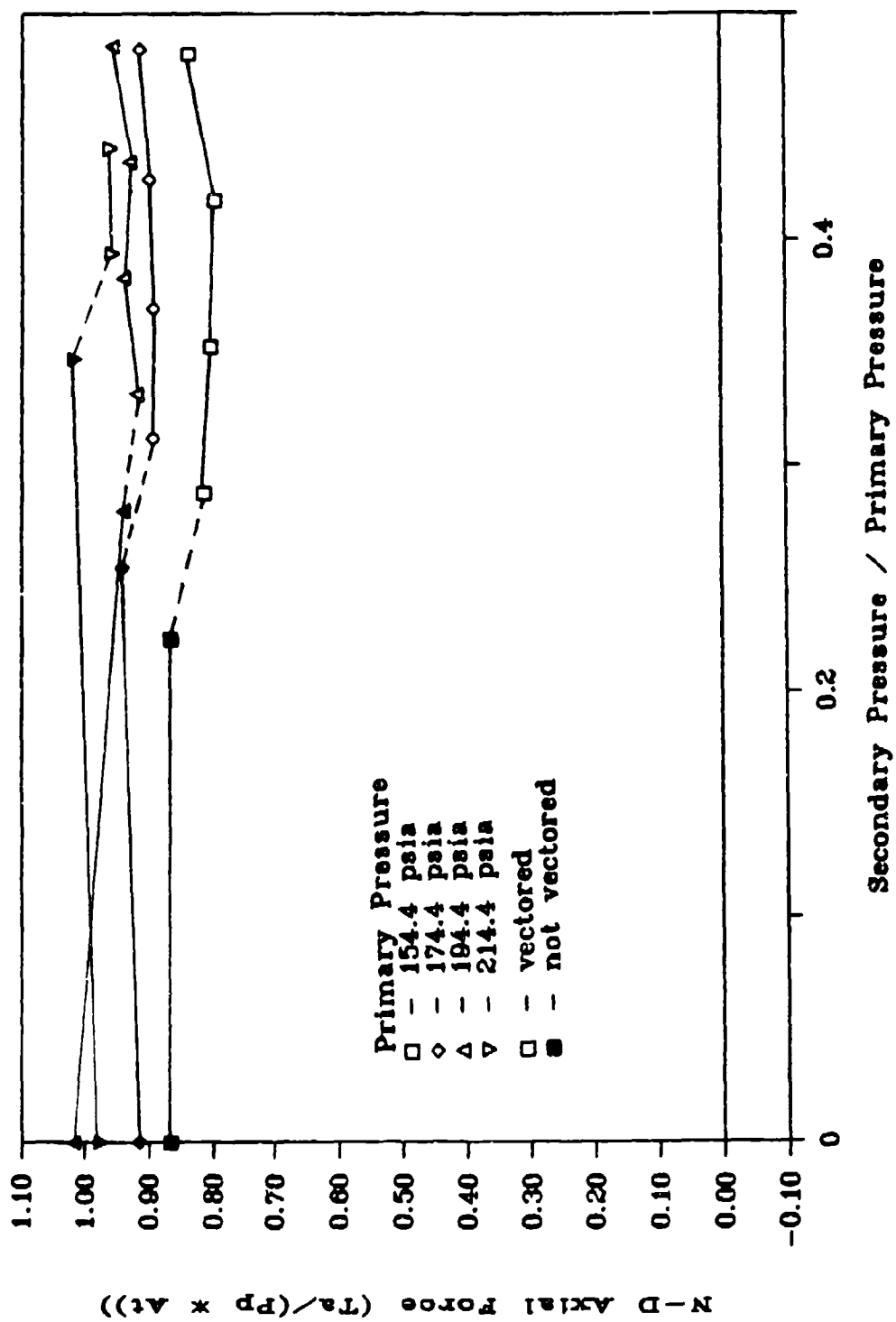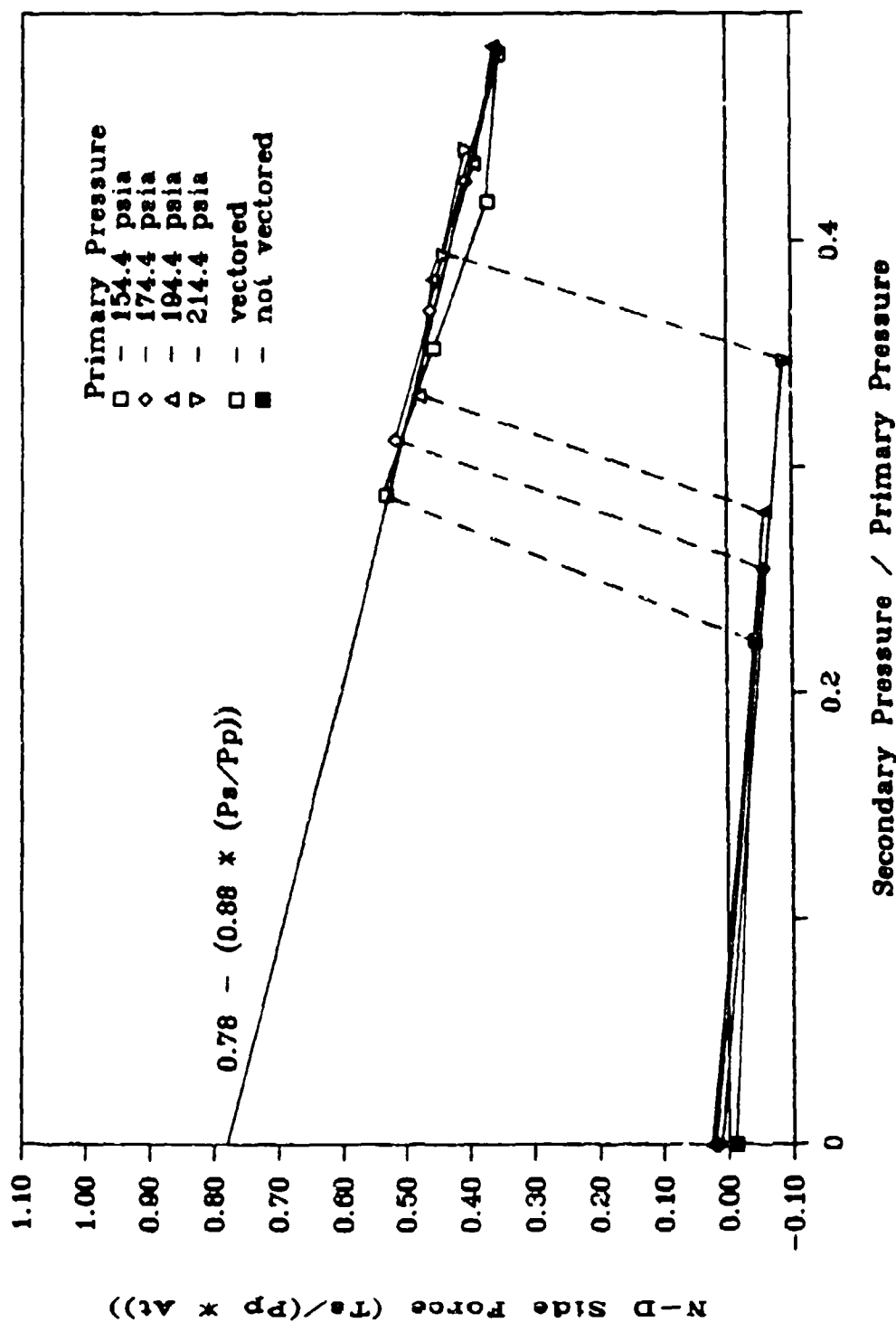
Fig 29. Effect of Vectoring on Side Force
LME, As/At = 0.15
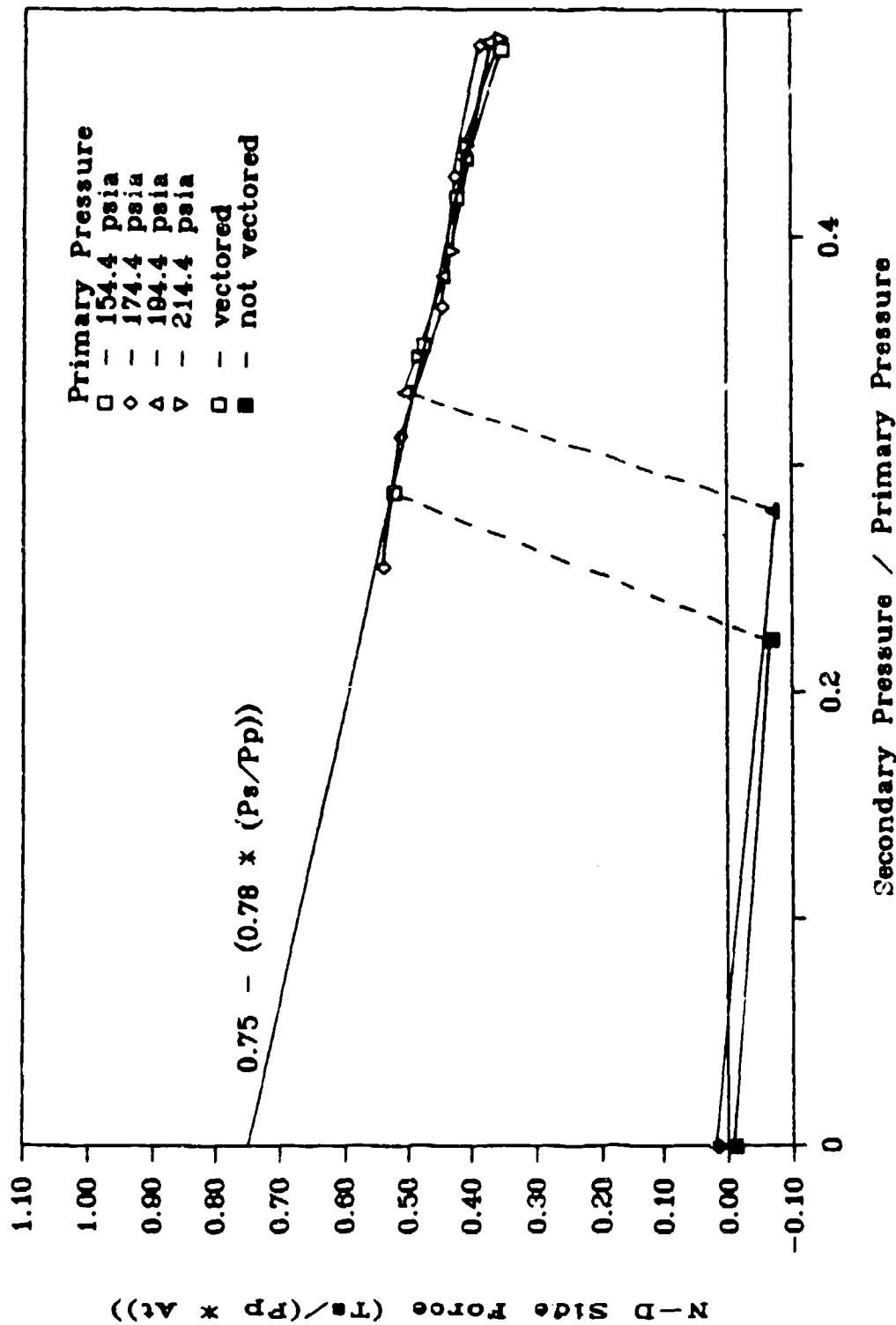
Fig 30. Effect of Vectoring on Side Force
LME, $A_s/A_t = 0.17$

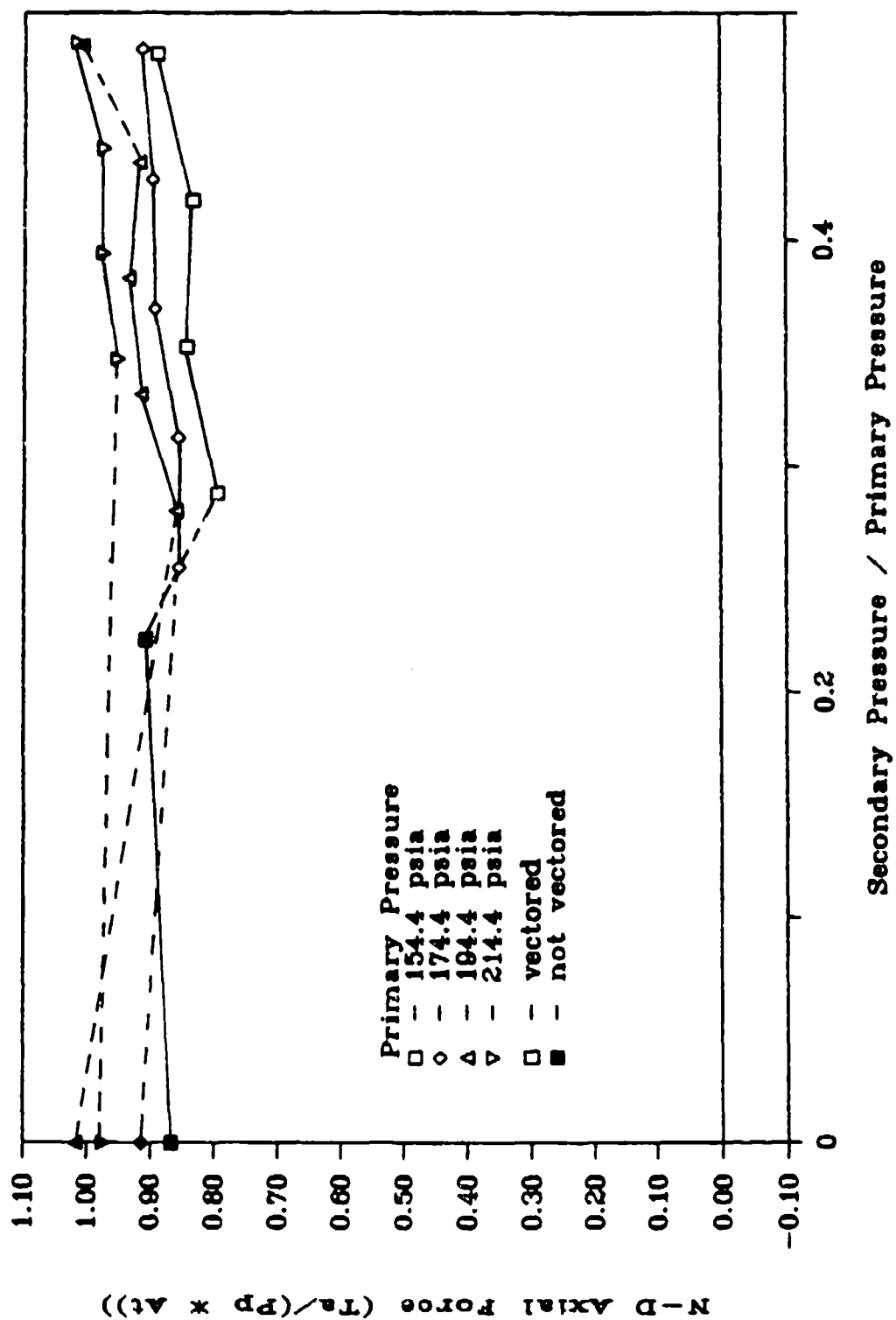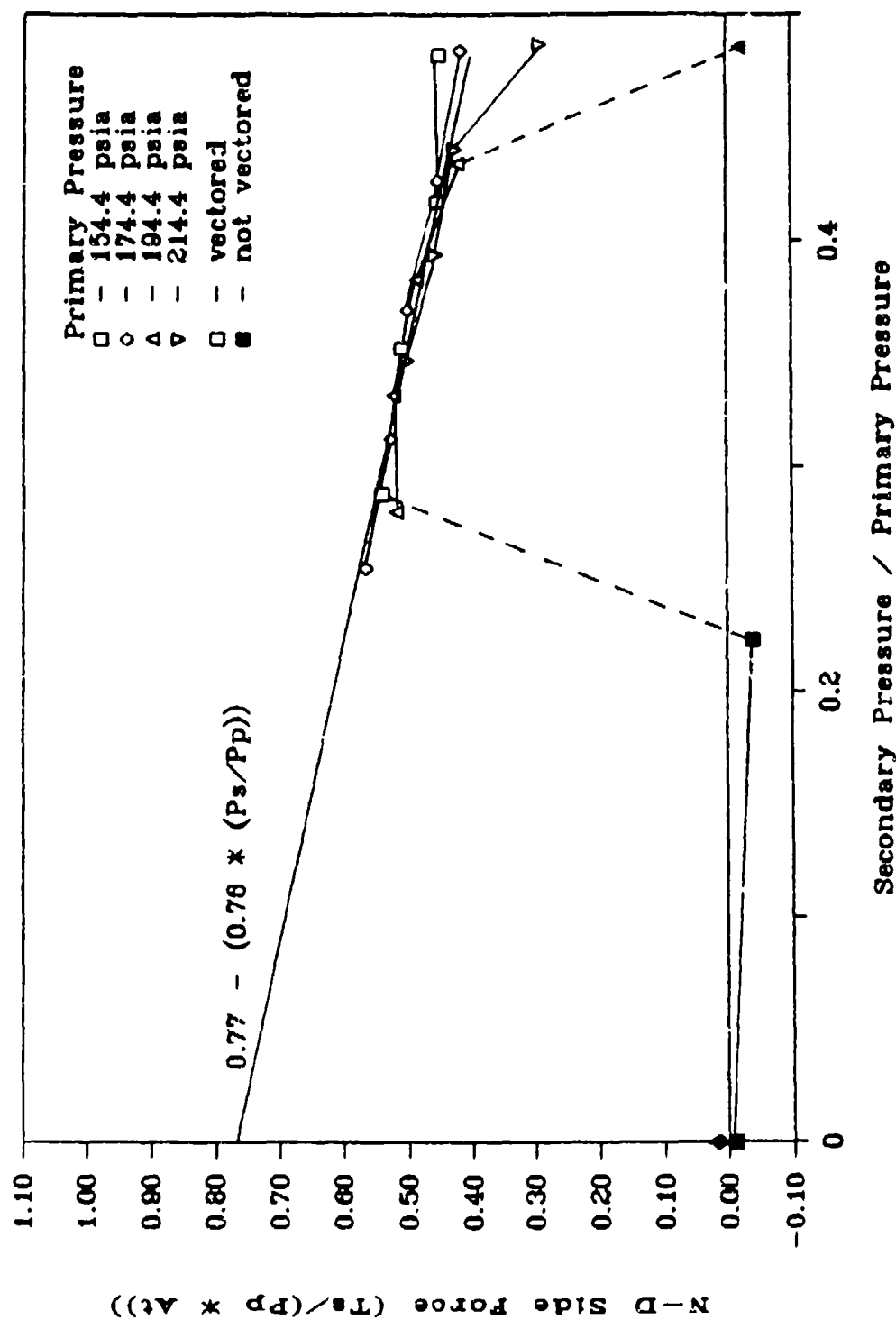Fig 31.   Effect of Vectoring on Side Force
LME, As/At = 0.20

various values of As/At:

As/At = 0.15:   N-D Side Force = 0.78 - (Ps/Pp) * 0.88
As/At = 0.17:   N-D Side Force = 0.75 - (Ps/Pp) * 0.78
As/At = 0.20:   N-D Side Force = 0.77 - (Ps/Pp) * 0.76

These equations can be used to predict the magnitude of side force available from vectoring, by multiplying the N-D side force by Pp * At, which gives the magnitude of side force for the vectoring cases only.

Notable from Fig 29 is the increase in Ps/Pp required for vectoring at the higher primary pressure. At a N-D Ps of 0.28, the nozzle has vectored for the Pp of 154.4 psia, but not for the Pp = 174.4 psia. The same situation occurs at a Ps/Pp= 0.35, and primary pressures of 154.4 psia and 214.4 psia. This confirms that for a fixed area, the minimum secondary pressure requirement for vectoring increases with Pp. Also notable is the maximum point to the flow in Fig 31 at Pp = 194.4 psia, Ps/Pp = 0.48, where the side force drops to nearly zero.

Angle of Thrust

The angle of thrust was calculated to be the arctangent of the side force divided by the axial force. Because the N-D side force did not change with Pp, but N-D axial force increased with increasing Pp, it would be expected that the angle of thrust would then decrease as Pp was increased. Figures 32, 33, and 34 show plots of the thrust angles for the LME nozzle, for As/At = 0.15, 0.17, and 0.20,

57
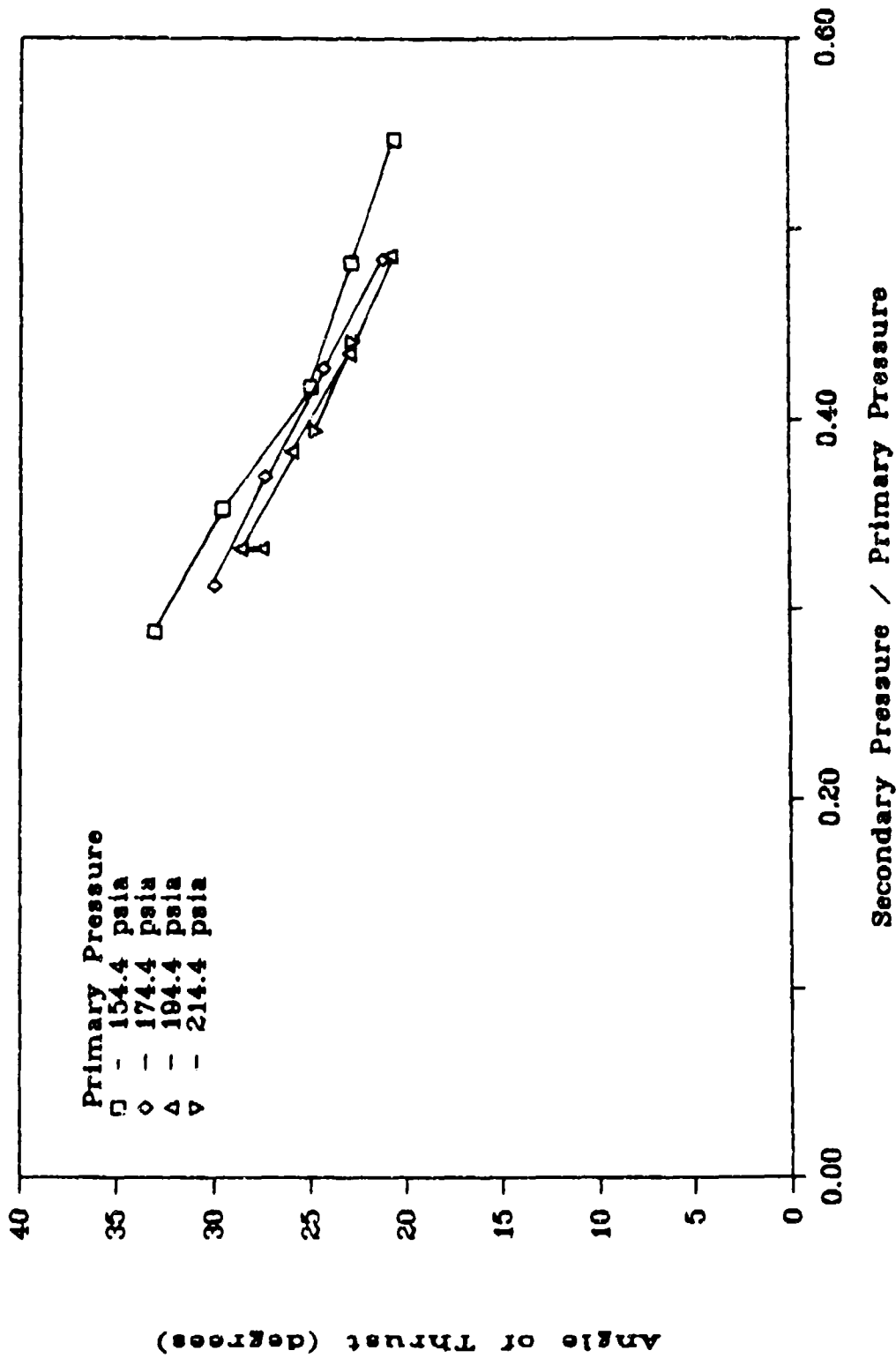
Fig 32. Effect of Ps and Pp on Angle of Thrust
LME, As/At = 0.15
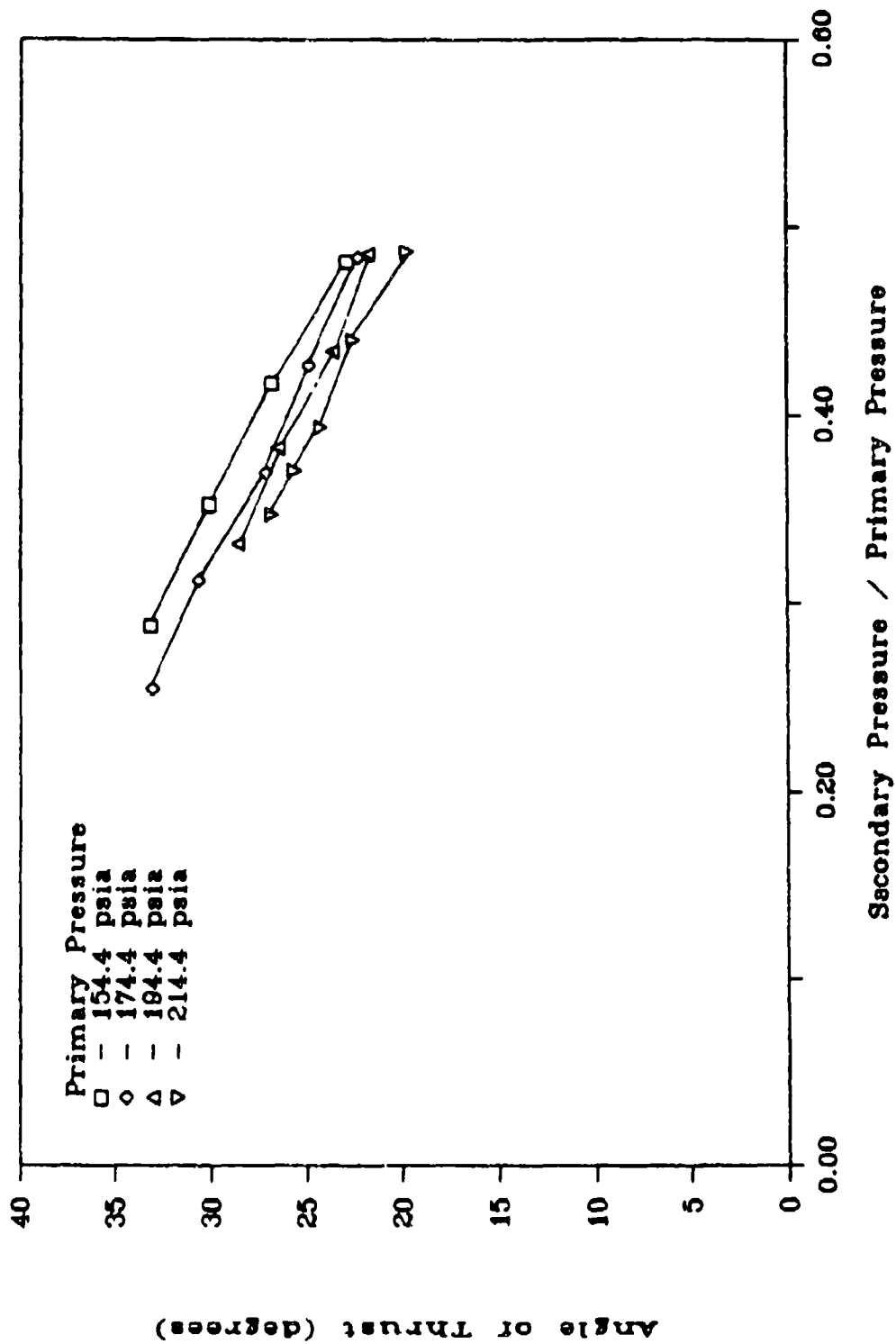
Fig 33. Effect of Ps and Pp on Angle of Thrust
         LME, As/At = 0.175
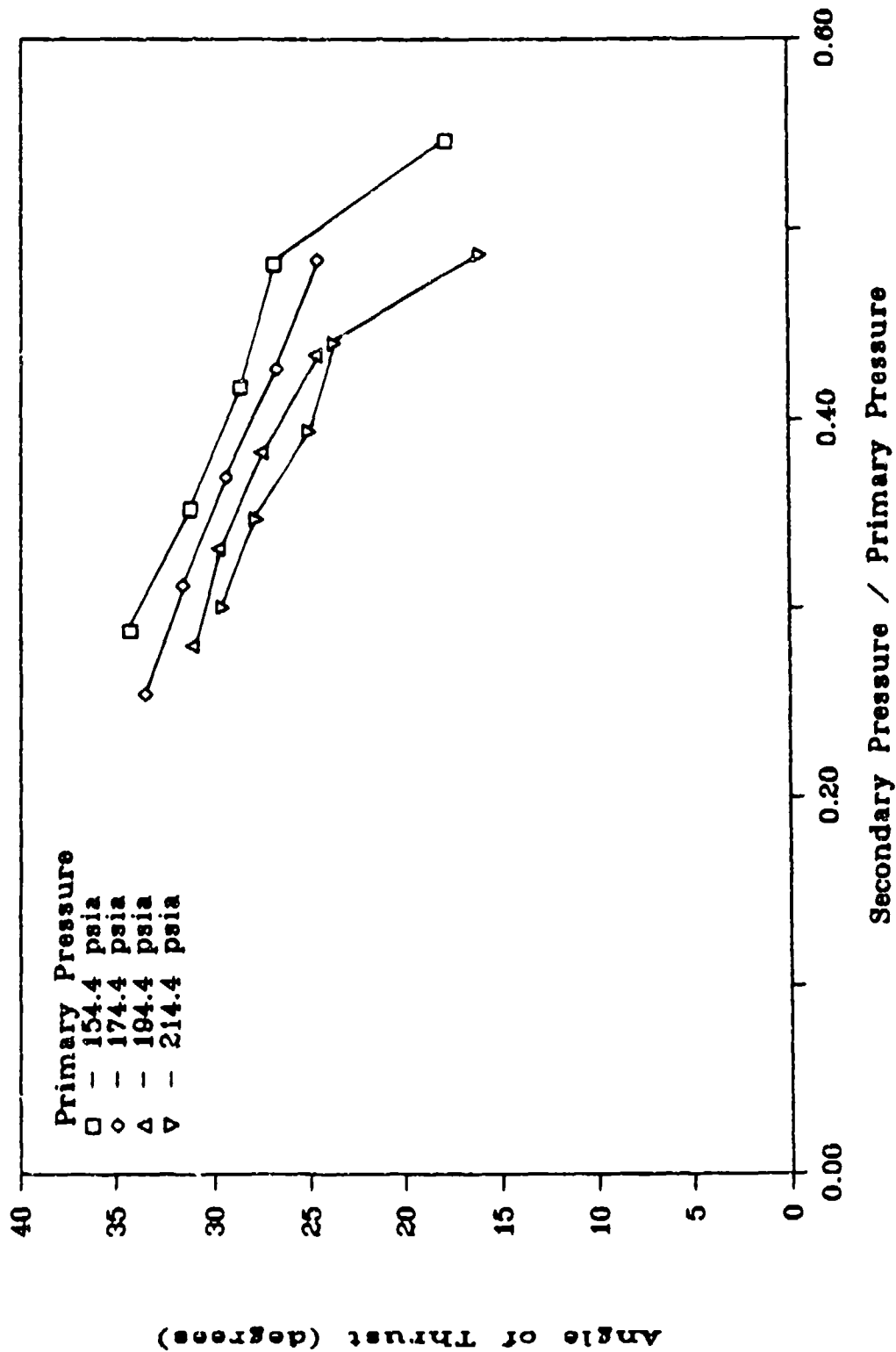
Fig 34. Effect of Ps and Pp on Angle of Thrust
LME, As/At = 0.20

60

respectively. As can be seen from these graphs, the lower primary pressures have larger thrust angles, confirming the expectations. The reason for the lower primary pressures having larger thrust angles is not clear. It might be because the jet's ability to attach to the wall after separation might be better at the lower Pp. Figures 35, 36, and 37 show flows in the LM nozzle at Pp = 154.4, 194.4, and 214.4 psia, with Ps/Pp values of 0.352, 0.331, and 0.347, respectively. These figures compare schlieren photographs and wall pressure distributions of the different primary pressures at similar dimensionless secondary pressure. The primary jet in the flow at Pp = 154.4 psia in Fig 35 is attached to the wall a short distance after separating. In the higher Pp flows, the jet does not appear to attach to the wall as well. The pressure distributions indicate that at a Pp of 154.4 psia, the pressure at X/L = 0.30 is about the same as the axial pressure, and there is a large jump to the attached pressure. This seems to indicate that as the flow moves downstream, the flow is separated then attached. However, in the flows at higher Pp, the pressure at X/L = 0.30 is higher than the axial case, but lower than the attached case. Because the pressure at that point is in between the axial and attached pressures, it appears that the flow is not attached there. What may be happening is that there is a small separation region in the flow, preventing the jet from attaching completely, as shown schematically in Fig 38. So it appears that attachment to the wall is delayed

61

Side B

Side A

Ps/Pp = 0.35

Sec. Injection from Side B at X/L=0.15

X/L (0.0 — throat ; 1.0 — exit)
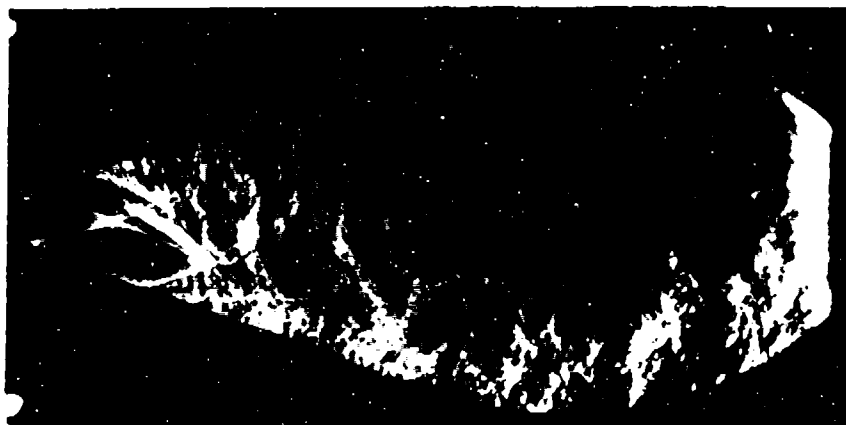
Fig 35.   Wall Pressure Distribution of Vectored Condition
LM, As/At = 0.20, Pp = 154.4 psia, Ps/Pp = 0.35

Side B

Side A

Ps/Pp = 0.33
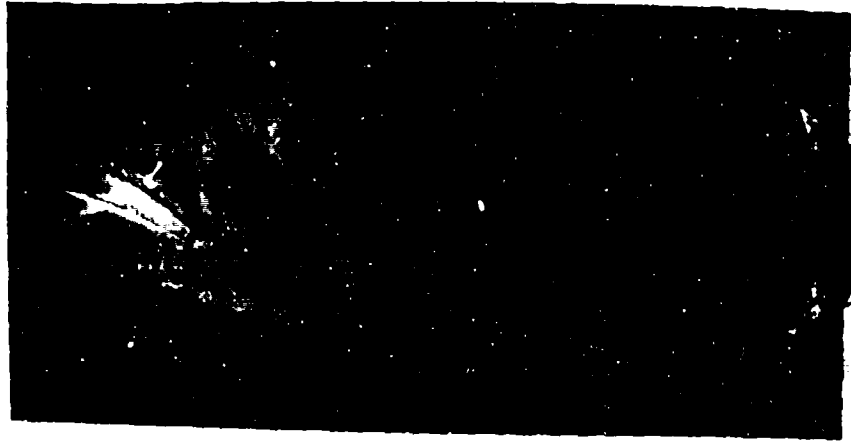
Sec. Injection from Side B at X/L=0.15

Fig 36. Wall Pressure Distribution of Vectored Condition
LM, As/At = 0.20, Pp = 194.4 psia, Ps/Pp = 0.33

Side B

Side A

$Ps/Pp = 0.35$

Sec. Injection from Side B at X/L=0.15
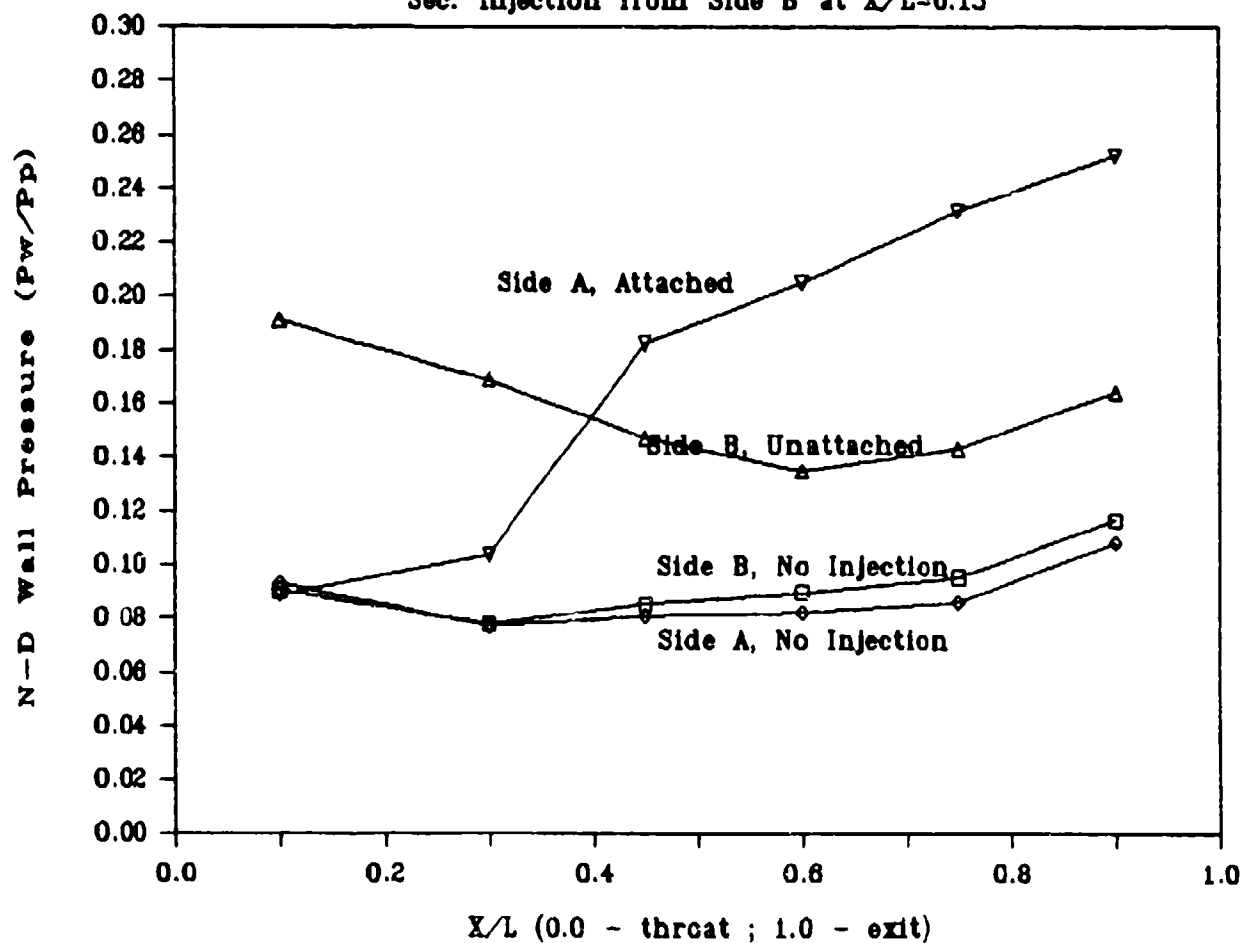
Fig 37. Wall Pressure Distribution of Vectored Condition
LM, As/At = 0.20, Pp = 214.4 psia, Ps/Pp = 0.35
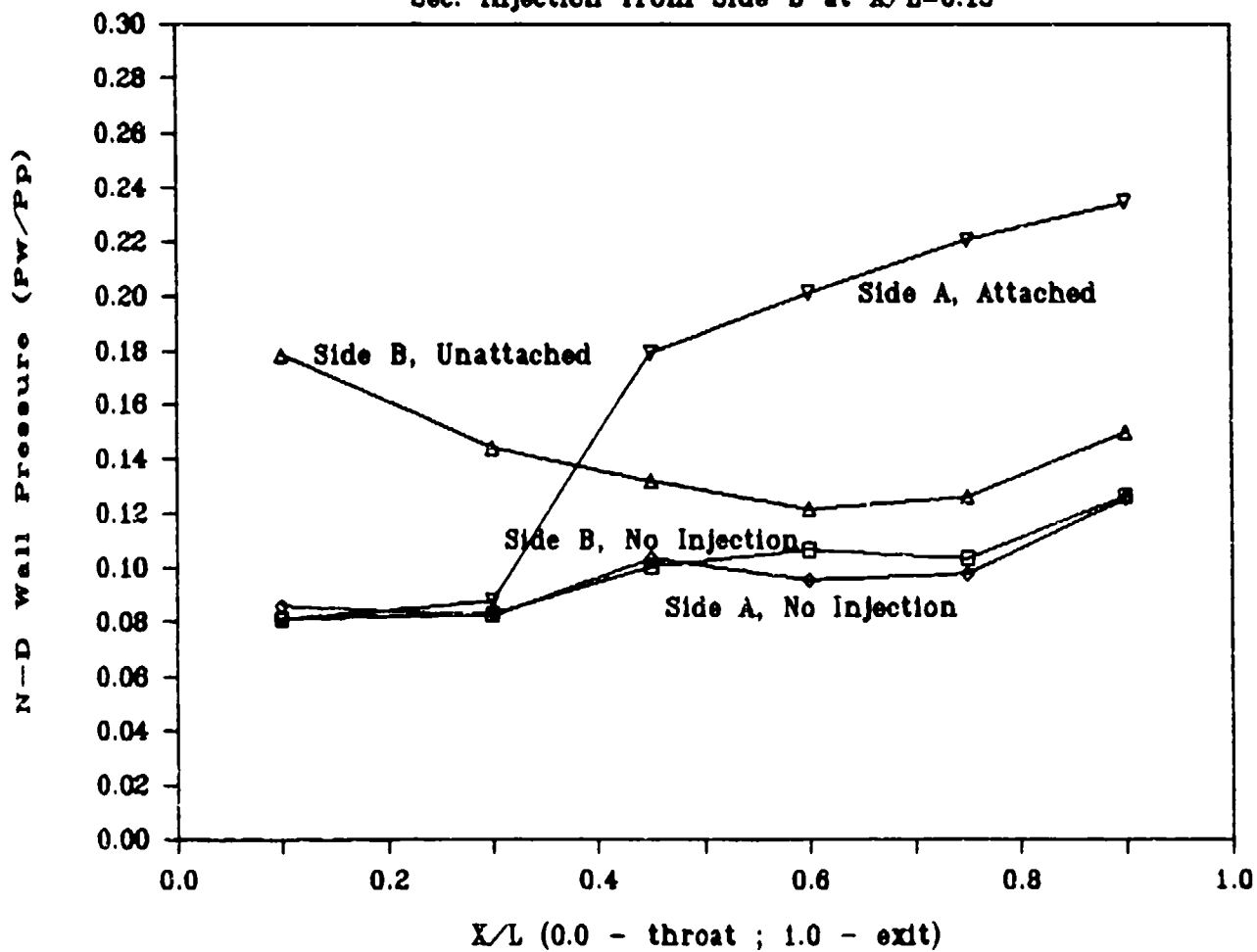
64
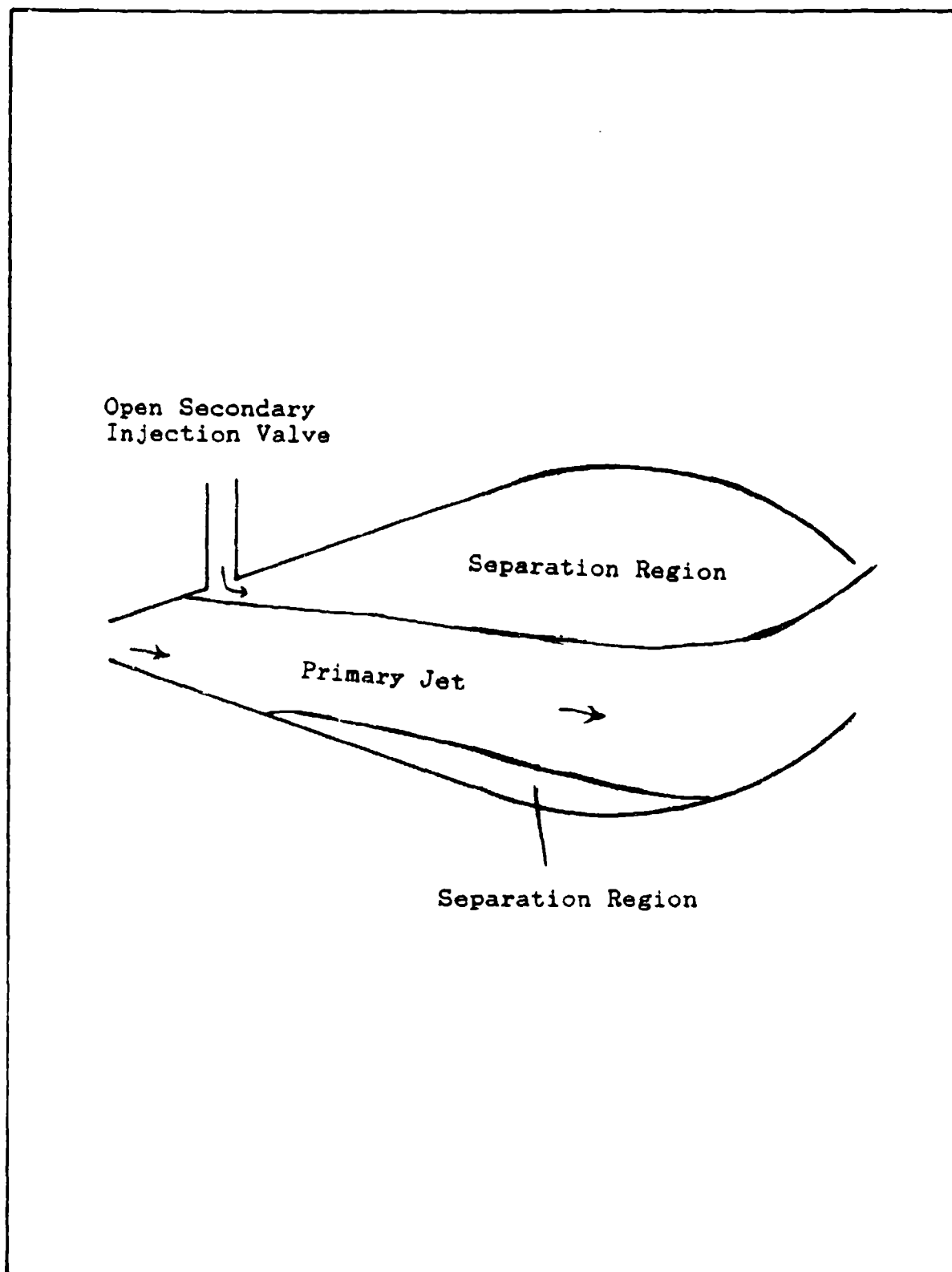
Fig 38.   Schematic of Effect of Large Pp on Jet Attachment

65

in the higher pressure cases. It is also notable that in the range from X/L = 0.45 - 0.60, the pressure in the nozzle at 154.4 psia relative to the axial condition is larger than the same ratio in same X/L range in the nozzles with higher Pp. After that, however, the ratios become equal. So the pressure distribution does seem to indicate that for the nozzles run at a higher primary pressure, the jet might encounter a separation region between it and the wall it is designed to attach to, and therefore it does not attach as well to the wall as the jet at the lower primary pressures. To get the jet to attach better to the wall with higher Pp, a longer straight wall section to which the jet can attach might help.

The location of secondary injection may have also affected the ability of the jet to attach to the wall. The location of secondary injection was at 0.15 for each primary pressure. However, the separation point of the jet will move downstream with increasing primary pressure, and the jet might attach better at the higher Pp with a different x_s.

The thrust angles measured for the LME nozzle range from 17 to 35 deg, decreasing with increasing Pp. The angles reported in Cates' work ranged from 23 - 47 deg for vectoring cases (3:36). The angles also decreased with increasing primary pressure. From Brown's data, the results for the axisymmetric nozzle indicate angles from 20 - 35 degrees, which decrease with increasing primary pressure (2:46). No explanation for the decrease was suggested in either report.

Repeatability and Stability

The data collected would not be useful if the experiments were not repeatable, or if the jet was in a transient mode during the collection of data. Fig 39 shows the pressure distributions of the LM nozzle at a Pp = 174.4 psia, Ps/Pp = 0.43, and As/At = 0.20, in the force test and the photographic test. As can be seen from this figure, the pressures on each wall are very similar, differing in magnitude by a maximum of about 7% at any X/L location. The mass flows in the two cases were similar as well. The primary mass flows were both 0.89 lbm/s, and the secondary mass flows were 0.036 lbm/s and 0.033 lbm/s, respectively.

The high speed movies showed no significant deviations in the jet either in the axial or vectored case, which also validates the data collection.

Effect of Secondary Pressure

Figures 29, 30, and 31 are useful in observing the effects of increasing secondary pressure. Note that in each figure before the jet vectors, with increasing secondary pressure, the side force tends to increase slightly in the direction opposite to the side force obtained after vectoring. An explanation for this trend is shown in the schlieran photographs of Fig 40, 41, 42, and 43. These photographs are of the LM nozzle with As/At = 0.20. The graphs below the pictures are non-dimensional wall pressure versus non-dimensional x location. Figure 40 is the axial

67
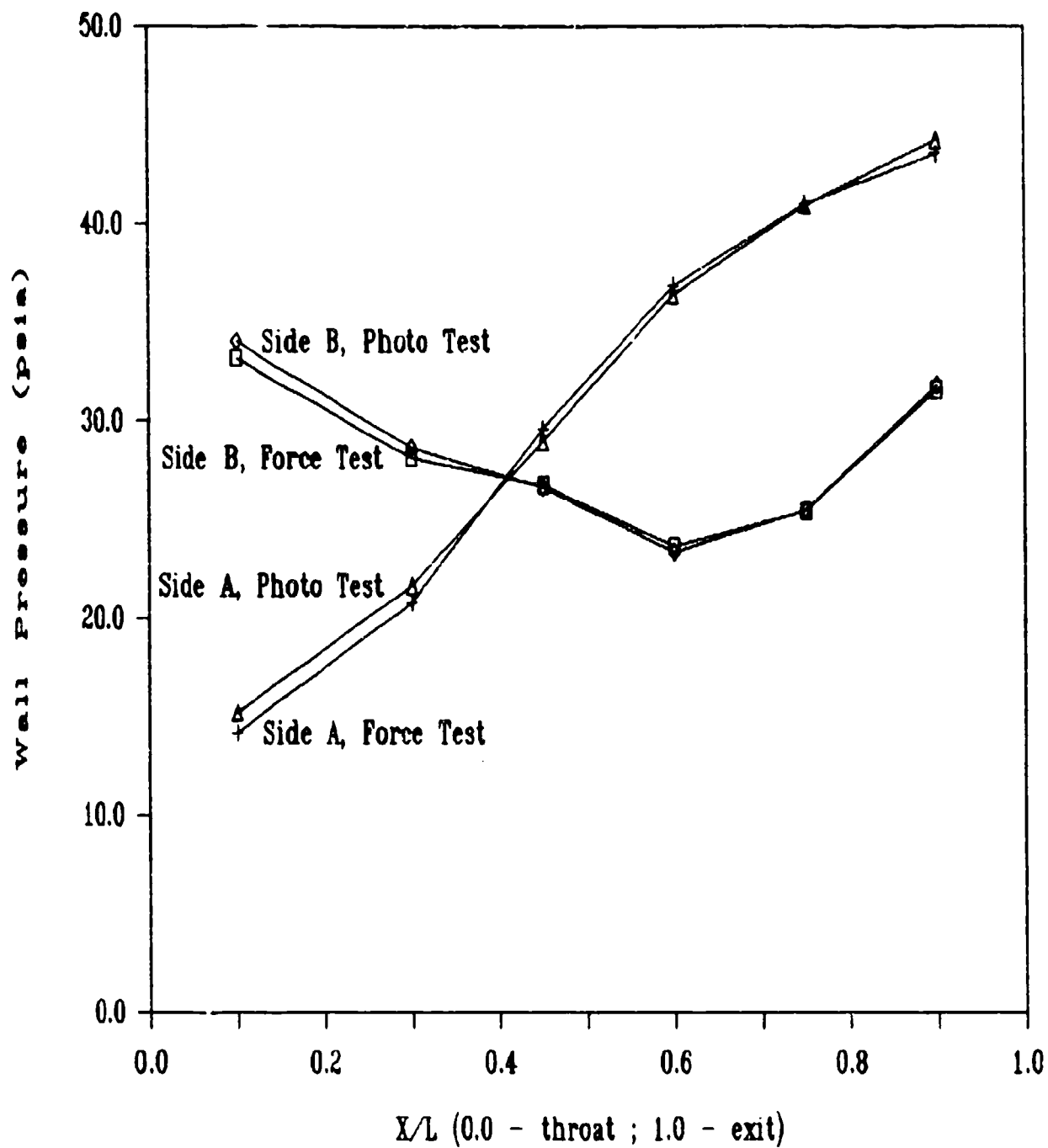
Fig 39. Pressure Distributions for Force and Photographic
Tests of LM, Pp=174.4 psia, Ps/Pp=0.43, As/At=0.20

Side B

Side A

Ps/Pp = 0.00
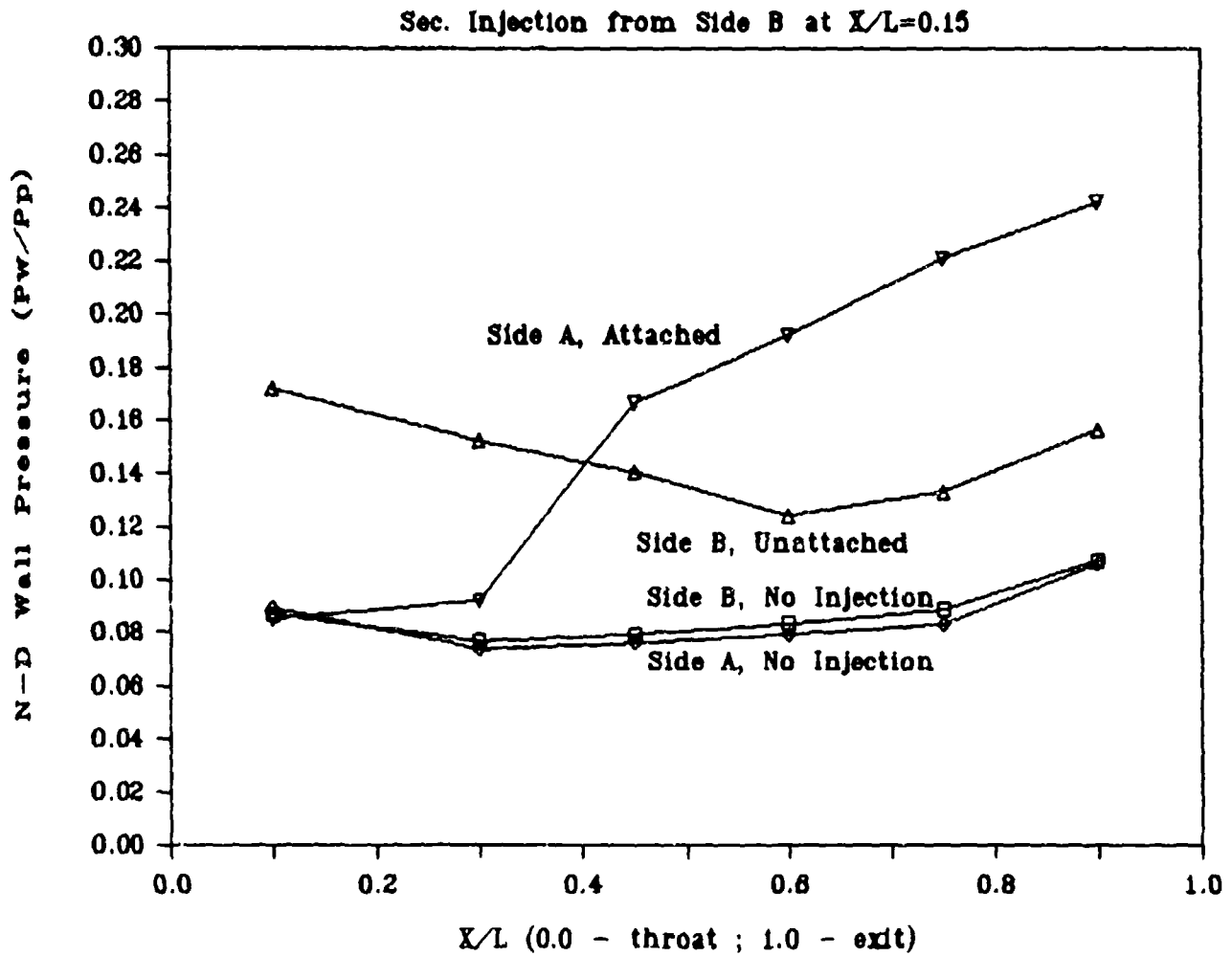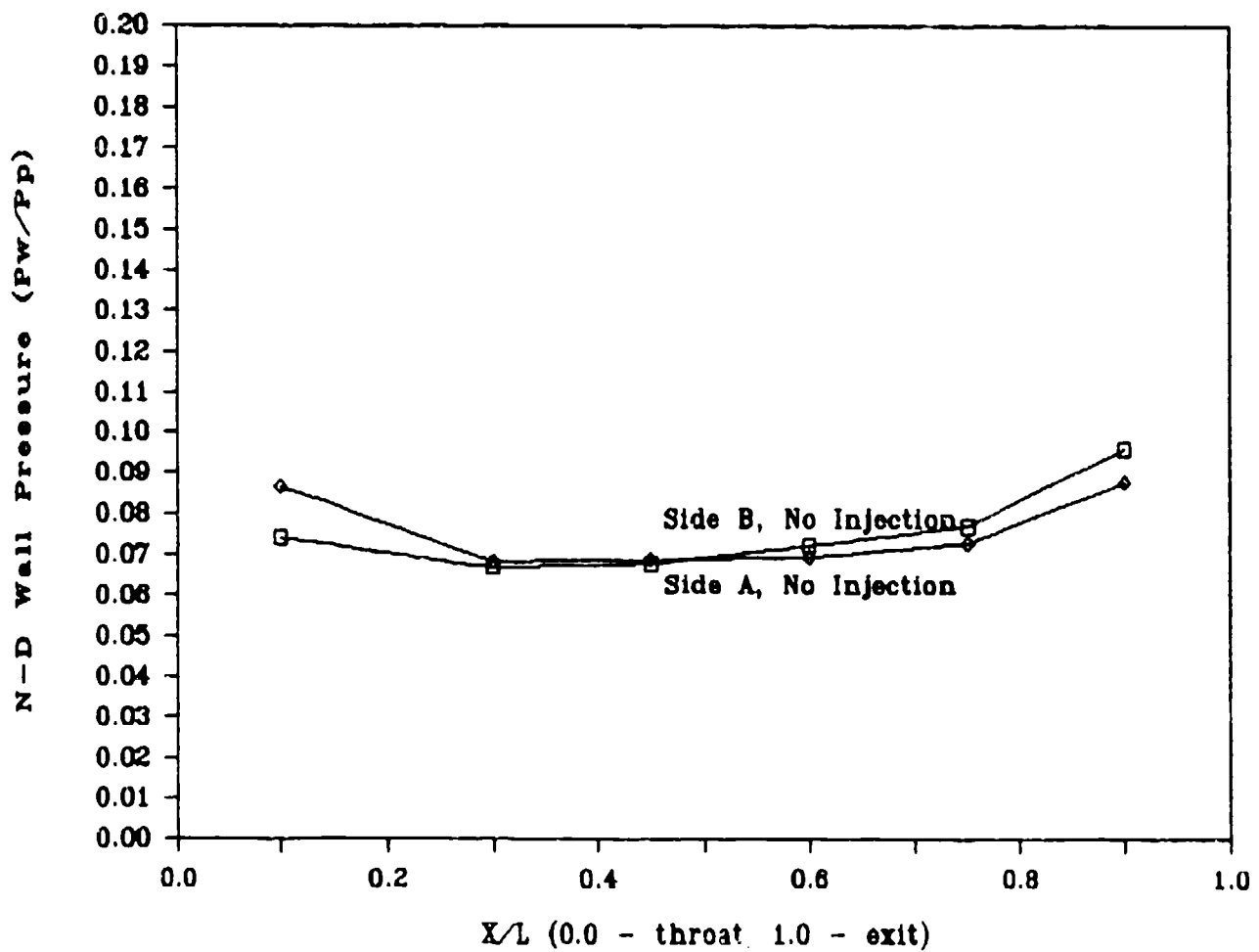

Fig 40. Wall Pressure Distribution of Axial Condition
LM, As/At = 0.20, Pp = 174.4 psia, Ps/Pp = 0.00

Side B

Side A

Ps/Pp = 0.25

Sec. Injection from Side B at X/L=0.15
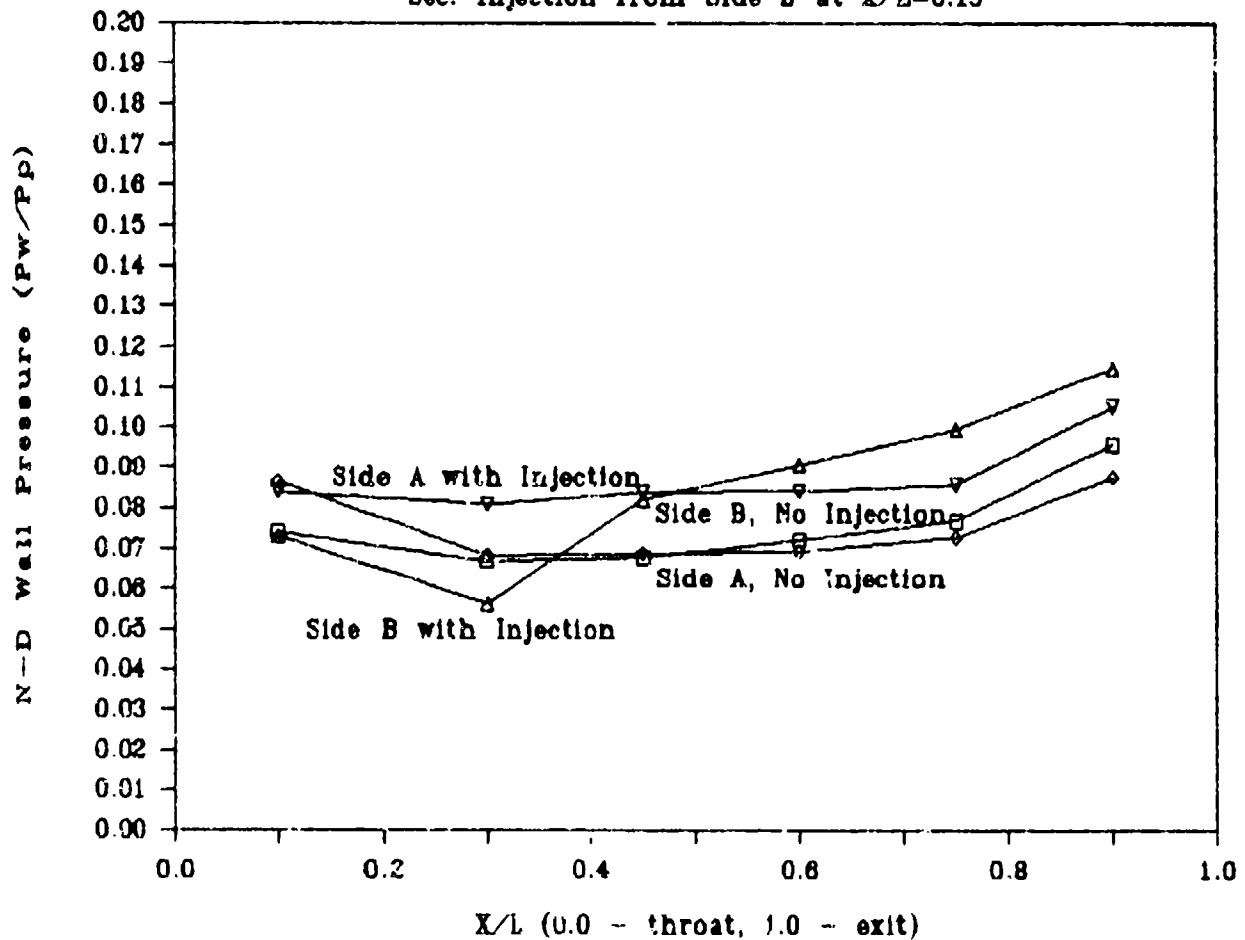
Fig 41. Wall Pressure Distribution of Incomplete Vectoring
LM, As/At = 0.20, Pp = 174.4 psia, Ps/Pp = 0.25

Side B
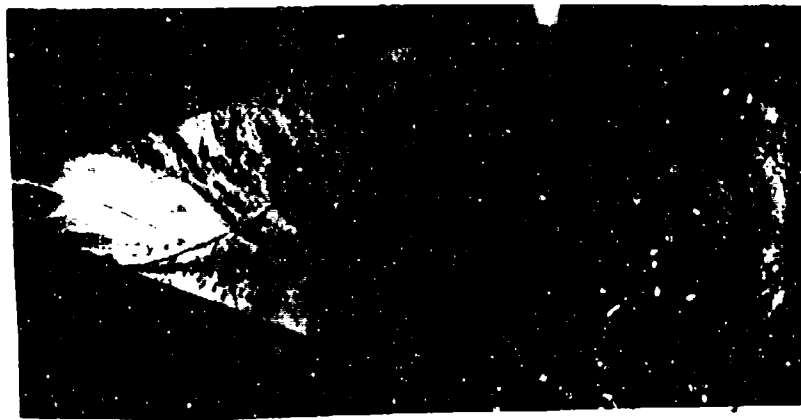
Side A

$Ps/Pp = 0.31$
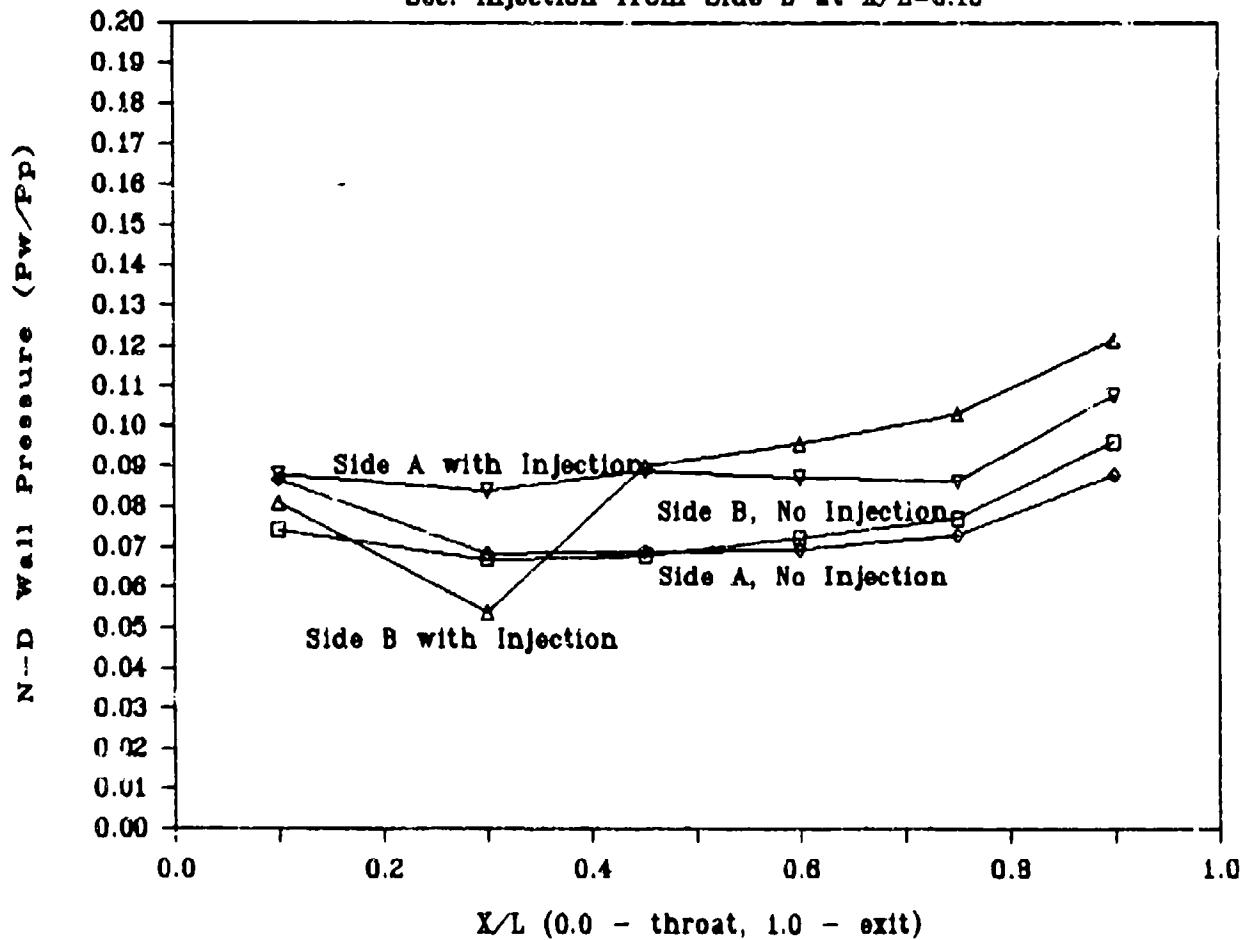
Fig 42. Wall Pressure Distribution of Incomplete Vectoring
LM, As/At = 0.20, Pp ∴ 174.4 psia, Ps/Pp = 0.31

Side B
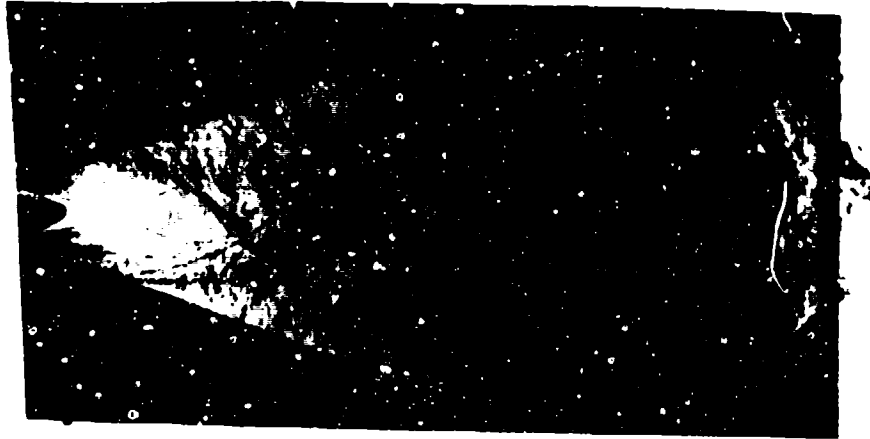
Side A

Ps/Pp = 0.37

Sec. Injection from Side B at X/L=0.15

Side B with Injection

Side A with Injection

Side B, No Injection

Side A, No Injection

X/L (0.0 – throat, 1.0 – exit)
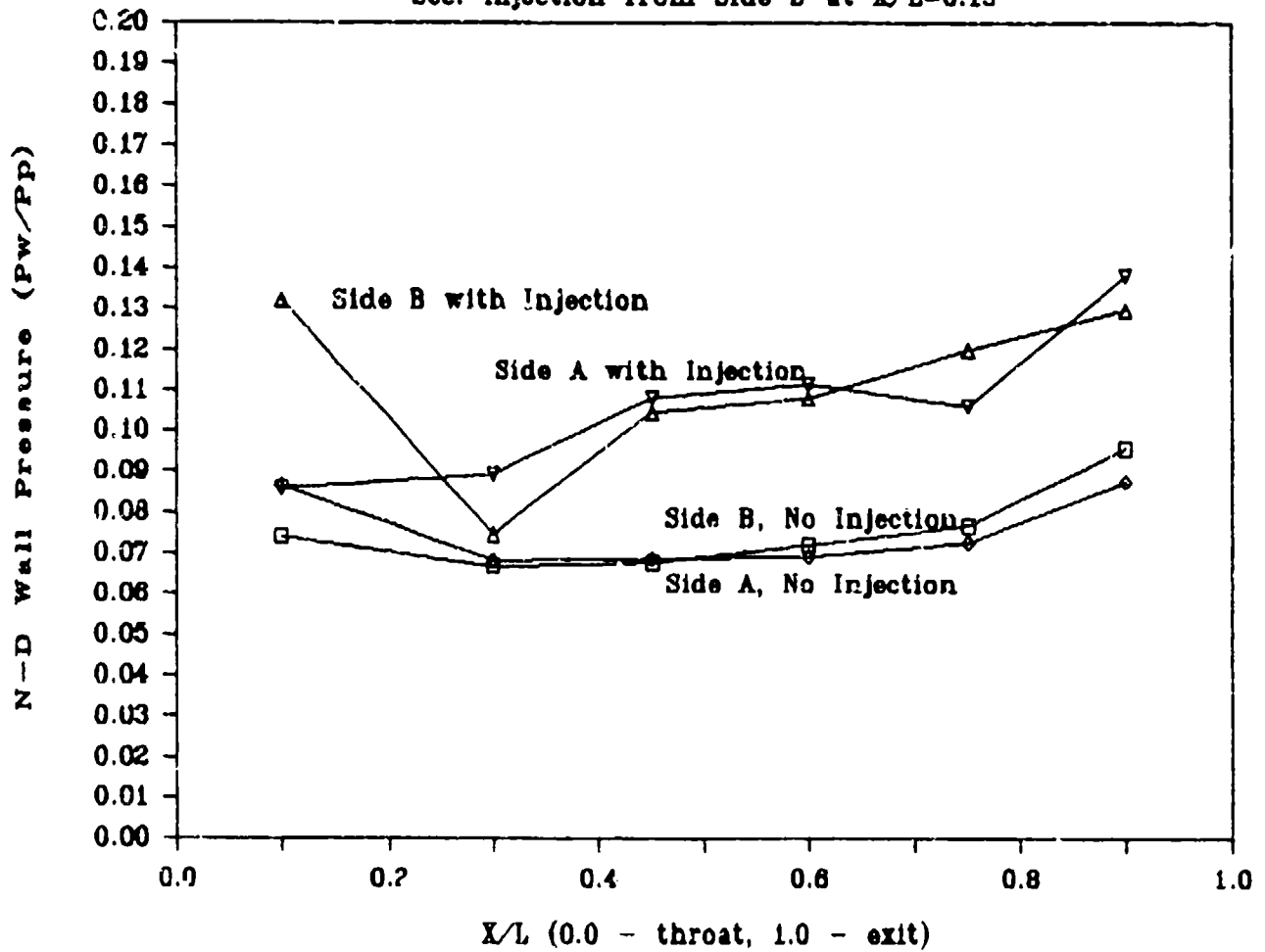
Fig 43.   Wall Pressure Distribution of Incomplete Vectoring
LM, As/At = 0.20, Pp = 174.4 psia, Ps/Pp = 0.37

72

case at a primary pressure of 174.4 psia. Figures 41, 42, and 43 show increases in Ps/Pp of 0.25, 0.31, and 0.37 respectively, but no vectoring occurs. The secondary flow at these pressures disrupts the jet slightly from the injection side, so that the jet is forced away from the wall with the secondary injection. Also, the injection increases the static pressure on the injection side, so that the jet stays nearer the opposite wall. But since the pressure and mass flow are not large enough to vector the jet, it does not attach to the opposite wall. It is just off center, and the more the secondary pressure increases without vectoring, the higher the side force becomes without vectoring. This becomes a maximum of about 10% of the axial force, as shown in Figs 29, 30, and 31.

This effect of slightly increasing side force with secondary injection and without vectoring as defined by Fig 2 will be referred to as "incomplete vectoring". Fig 44 is a drawing of the effect. If the nozzle is incompletely vectored, the axial force can slightly increase as shown in Figs 26, 27, and 28, at the points where no vectoring occurs but there is secondary injection (Ps/Pp > 0).

The jet vectors at a certain secondary to primary pressure ratio, because the pressure in the area just downstream of the throat is large enough to force the jet to attach to the wall opposite the secondary injection. As evidenced by the non-dimensional pressures in Figs 45, 46 and 47 compared to the same points in Figs 40, 41, 42, and 43,

OPEN SECONDARY
INJECTION VALVE

SECONDARY FLOW

PRIMARY JET
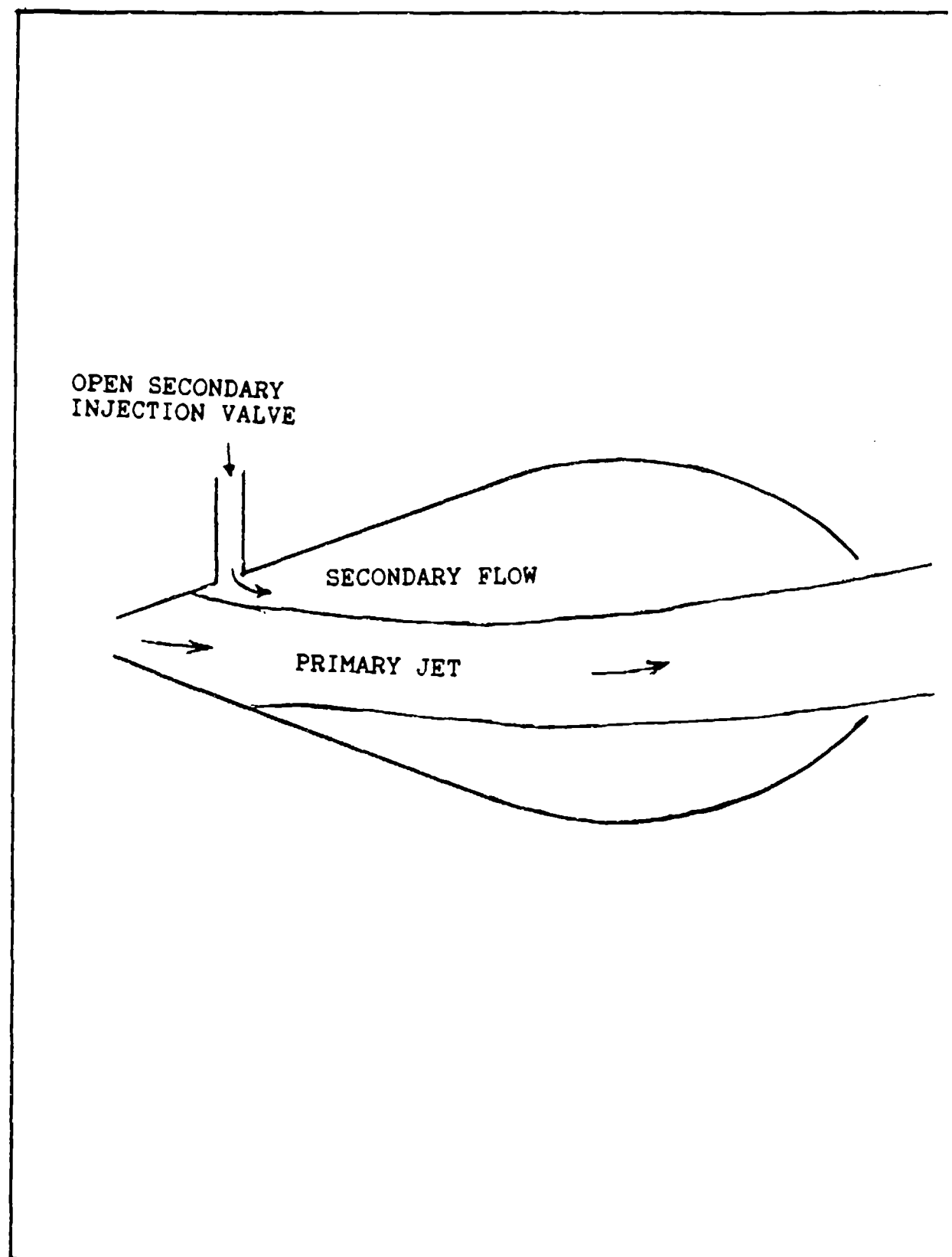
Fig 44.   Illustration of Incomplete Vectoring

Side B
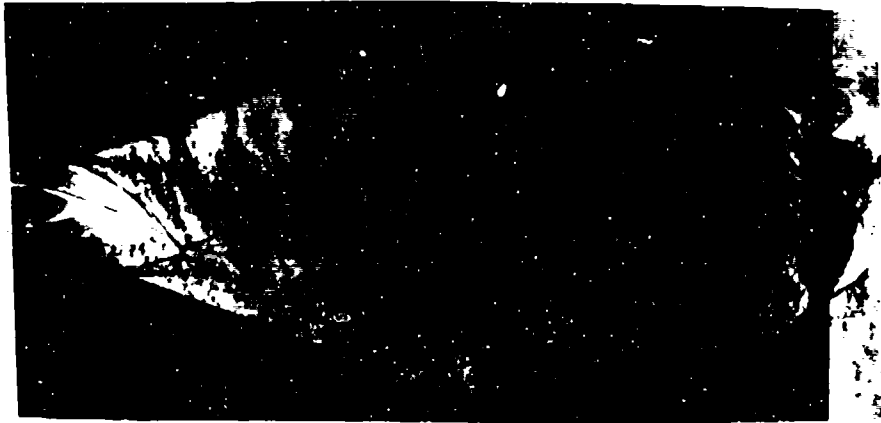
Side A

Ps/Pp = 0.43

Sec. Injection from Side B at X/L=0.15

Fig 45. Wall Pressure Distribution of Vectored Condition
LM, As/At = 0.20, Pp = 174.4 psia, Ps/Pp = 0.43
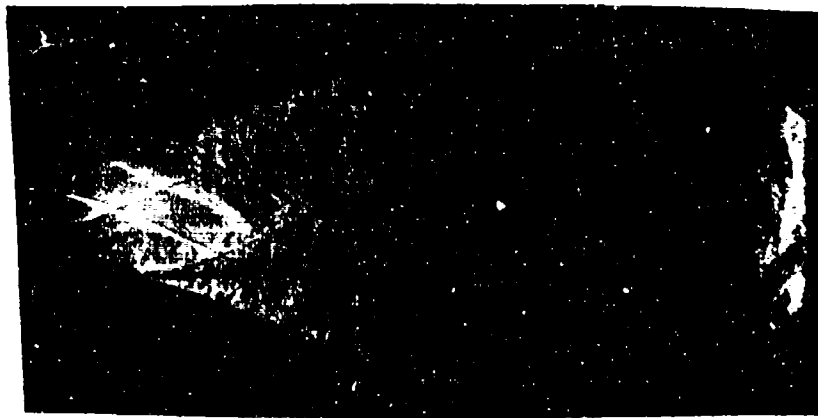
75

Side B

Side A

$Ps/Pp = 0.48$

Fig 46. Wall Pressure Distribution of Vectored Condition
LM, As/At = 0.20, Pp = 174.4 psia, Ps/Pp = 0.48

Side B

Side A

Ps/Pp = 0.54

Sec. Injection from Side B at X/L=0.15

X/L (0.0 – throat, 1.0 – exit)

Fig 47. Wall Pressure Distribution of Vectored Condition
LM, As/At = 0.20, Pp = 174.4 psia. Ps/Pp = 0.54

the pressure in the cavity increases significantly after vectoring. Figures 45, 46, and 47 are vectored cases of the same nozzle and primary pressure used for the incomplete vectored discussion, only now the Ps/Pp = 0.43, 0.48 and 0.54, respectively.

Increasing secondary pressure past the minimum point required for vectoring has a detrimental effect on side force, as shown in Figs 29, 30, and 31 at the points were the nozzle vectored. Increasing secondary pressure too much will result in no side force. This was discussed as a maximum to the secondary flow, and it is shown in Fig 31, at Pp = 194.4 psia and a Ps/Pp = 0.48. The decrease in side force and possible lack of vectoring is due to the disruption of the flow by too much secondary flow. Figs 48, 49, 50, and 51 show the LM nozzle at a primary pressure of 154.4 psia, with Ps/Pp equal to 0.42, 0.48, 0.55, and 0.61, respectively. Particularly when compared to the photograph in Fig 35, which had the same primary pressure and a Ps/Pp = 0.35, the increase in turbulence in the flow with increasing secondary pressure is evident. Cates found the same trends in side force after vectoring (3:43,44), but did not indicate a maximum in the amount of secondary flow. Brown (2:40) showed that for an axisymmetric CJTVC, the side force increases with increasing secondary pressure, and no maximum secondary pressure was encountered. Lambert (9:31) confirmed this trend for the axisymmetric case. The reverse trend of the axisymmetric nozzle compared to the two-dimensional nozzle

Side B

Side A

Ps/Pp = 0.42

Sec. Injection from Side B at X/L=0.15

X/L (0.0 — throat; 1.0 — exit)
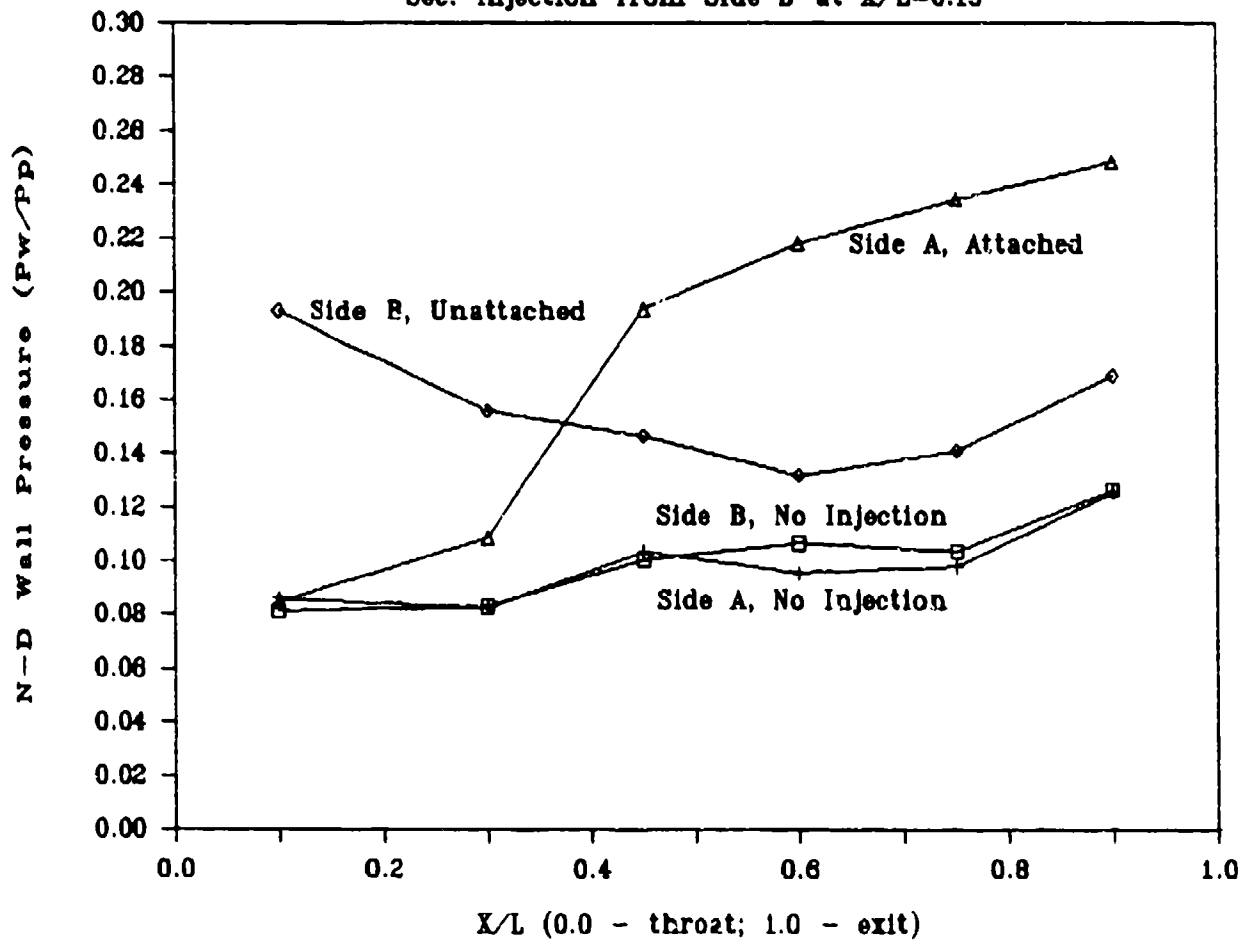
Fig 48. Wall Pressure Distribution of Vectored Condition
LM, As/At = 0.20, Pp = 154.4 psia, Ps/Pp = 0.42

Side B
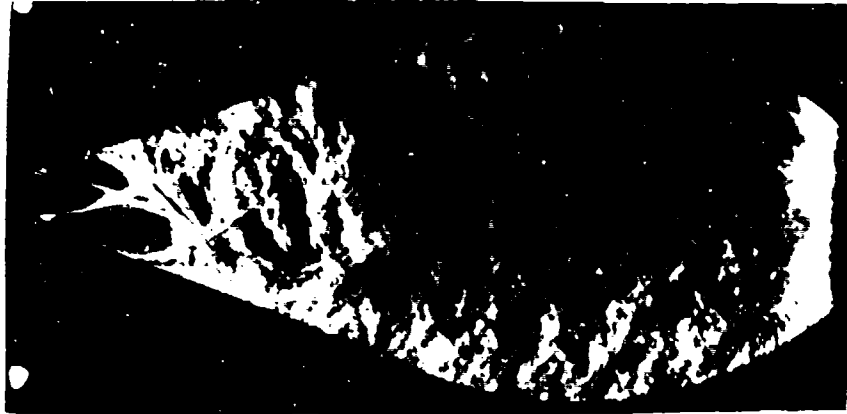
Side A

Ps/Pp = 0.48

Sec. Injection from Side B at X/L=0.15
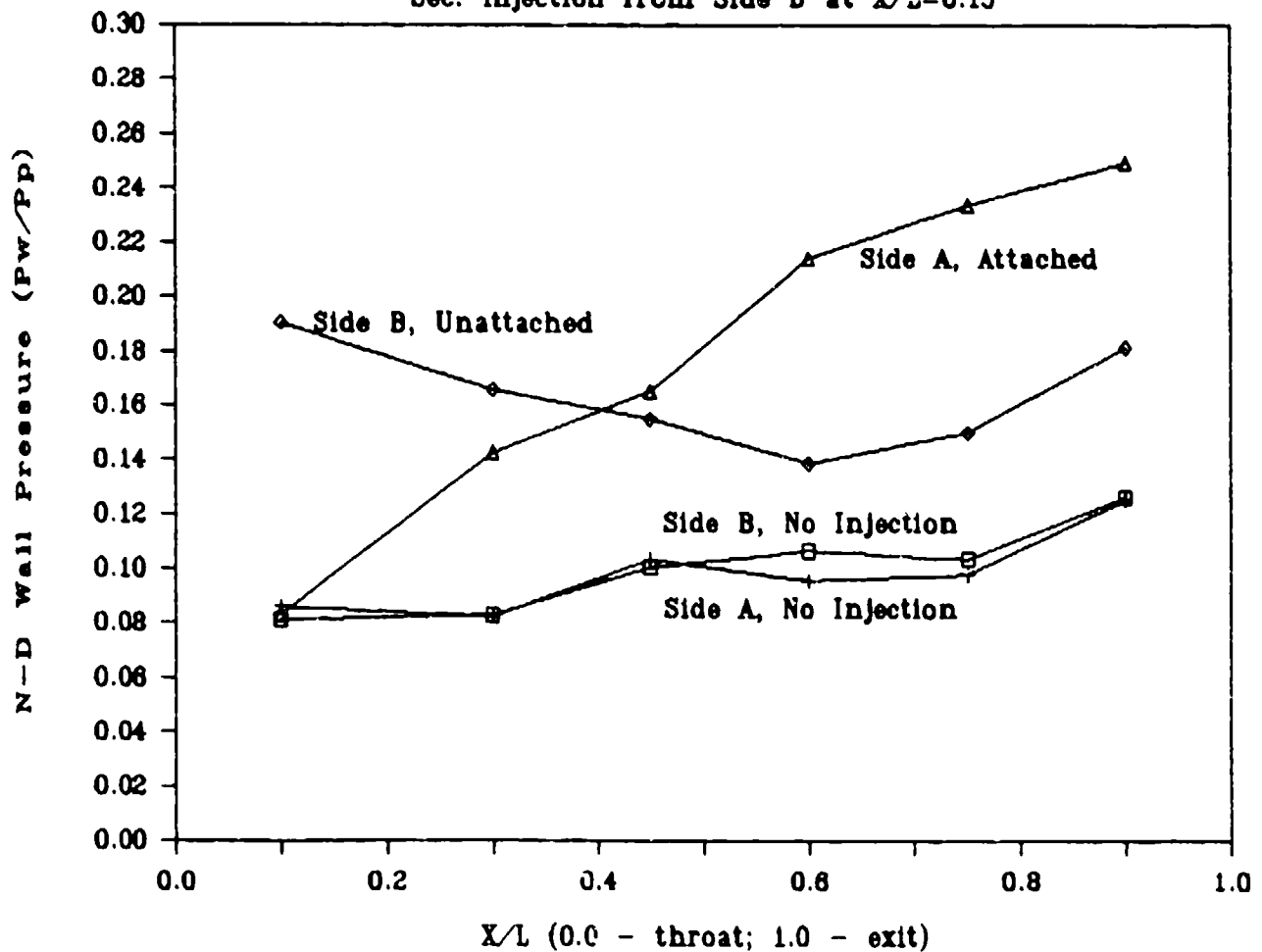
Fig 49. Wall Pressure Distribution of Vectored Condition
LM, As/At = 0.20, Pp = 154.4 psia, Ps/Pp = 0.48

Side B

Side A
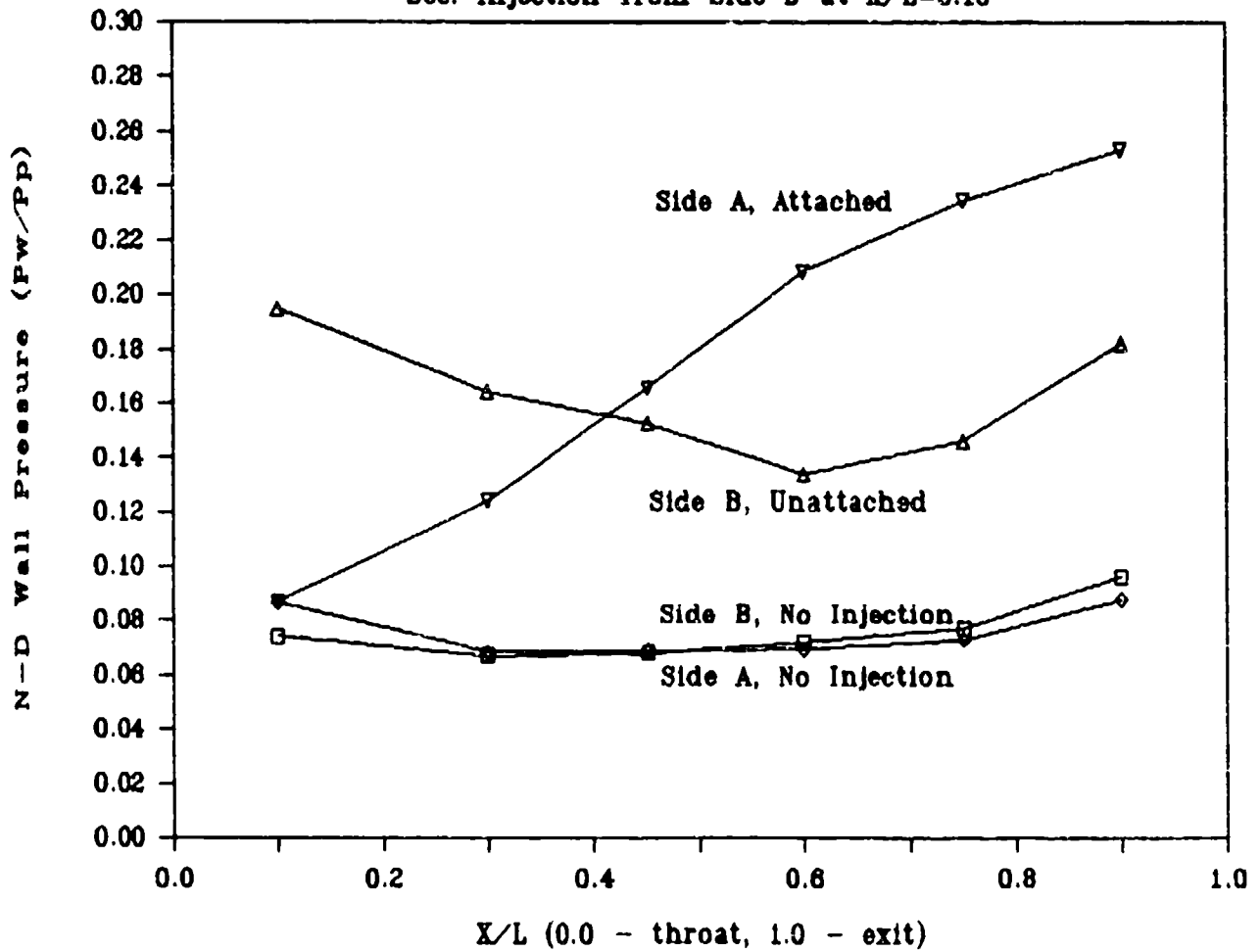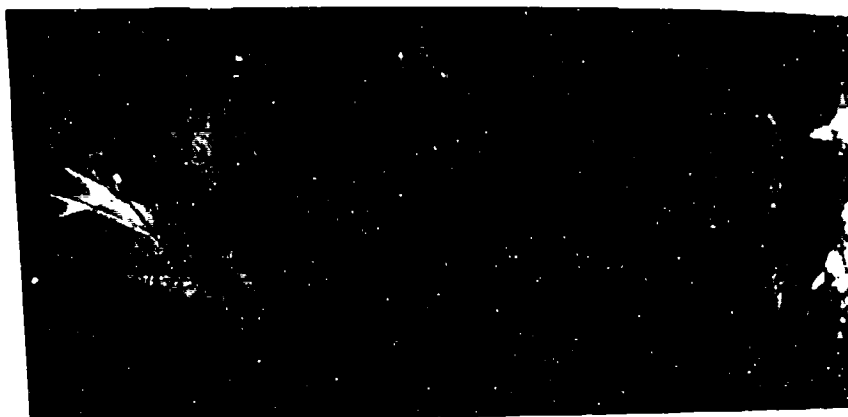
Ps/Pp = 0.55

Sec. Injection from Side B at X/L=0.15

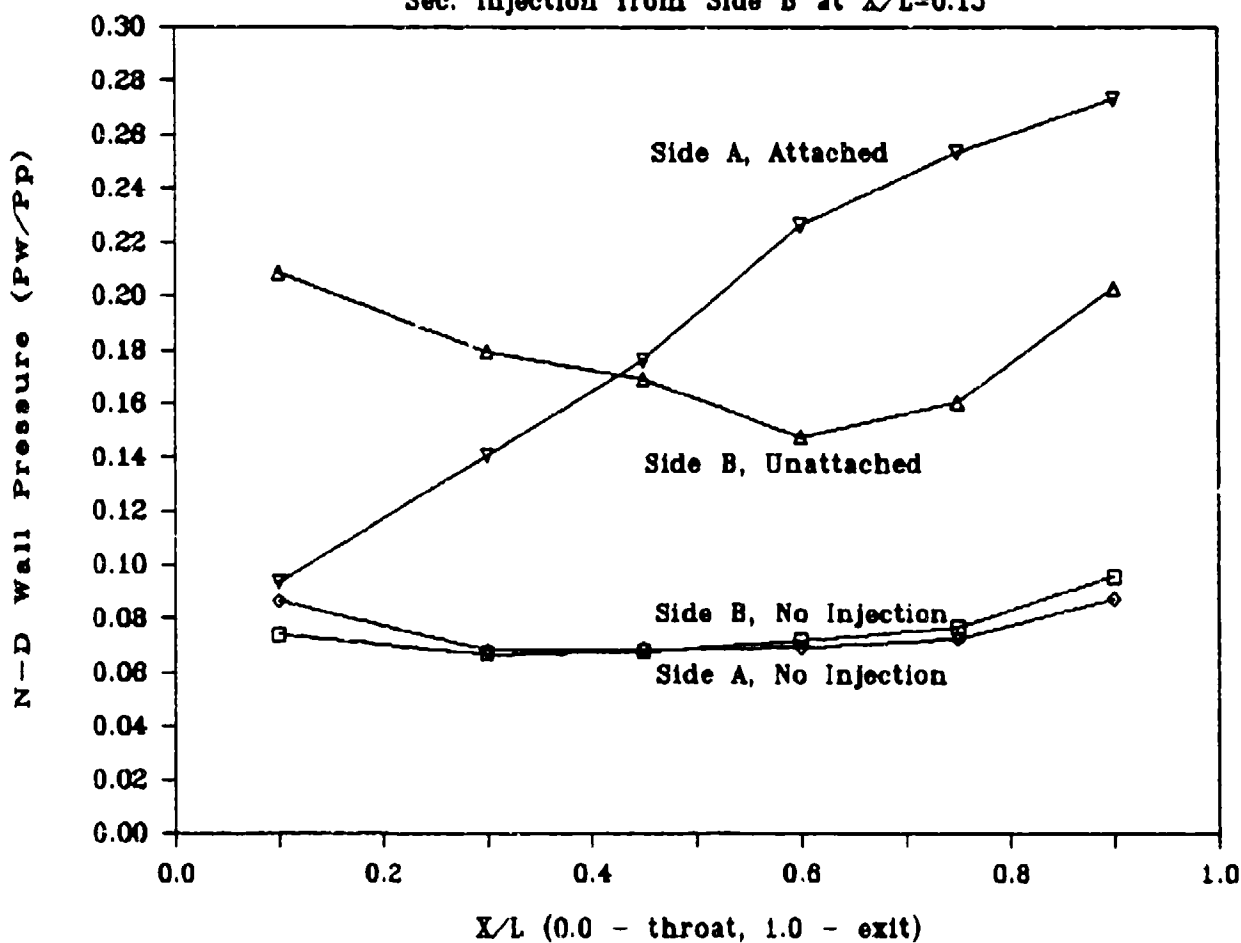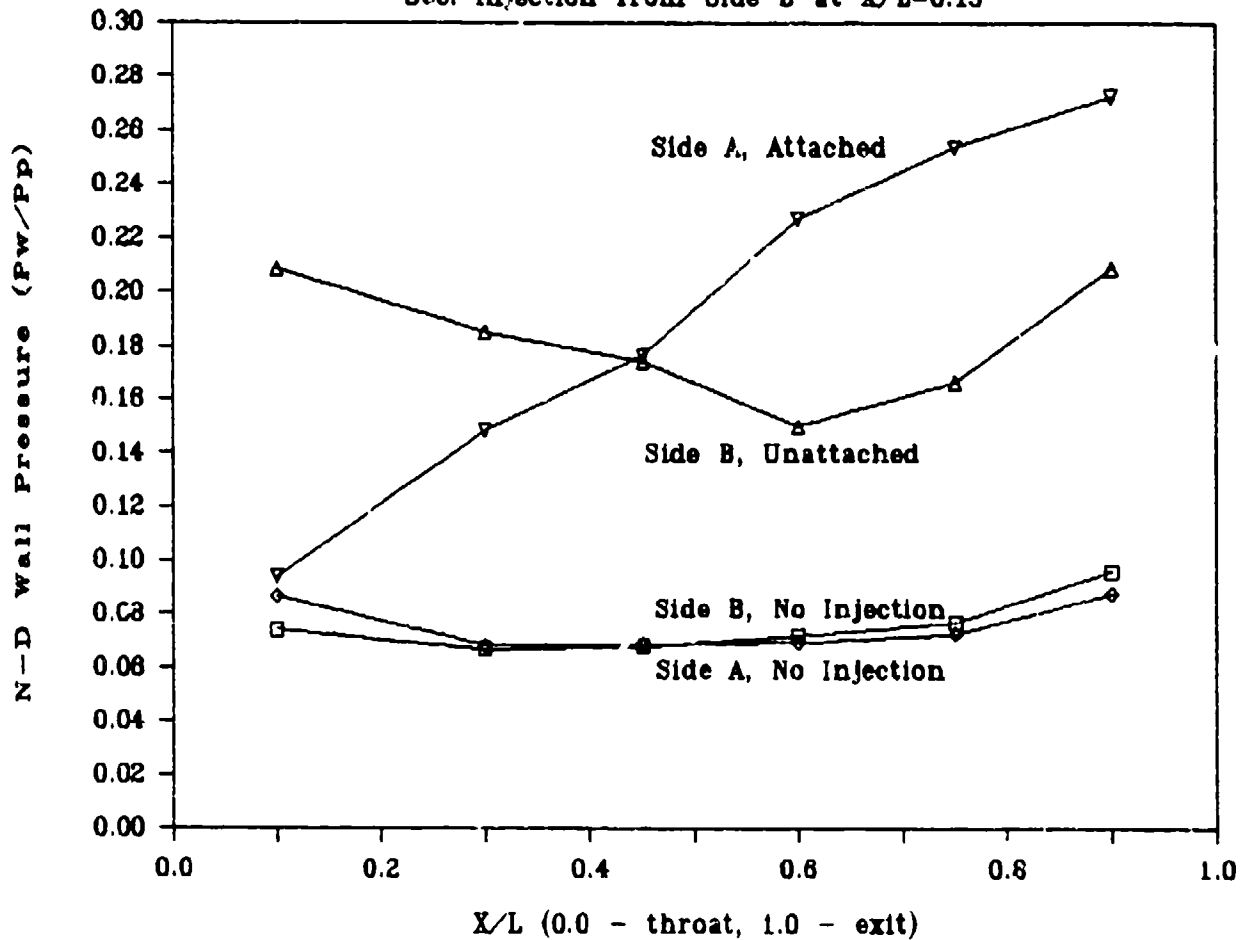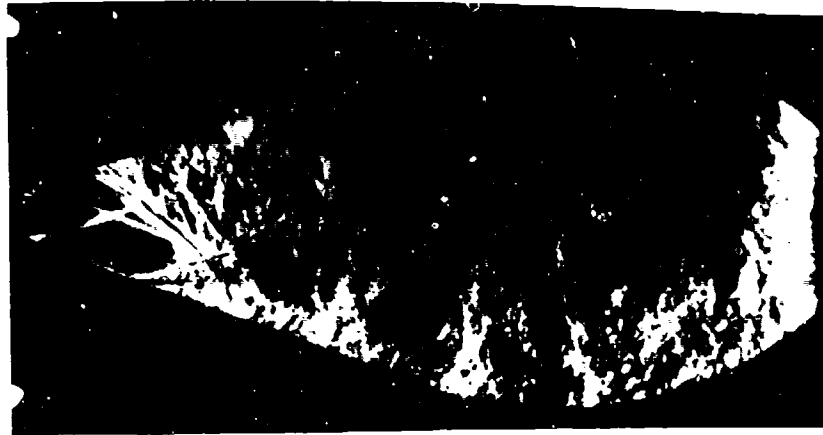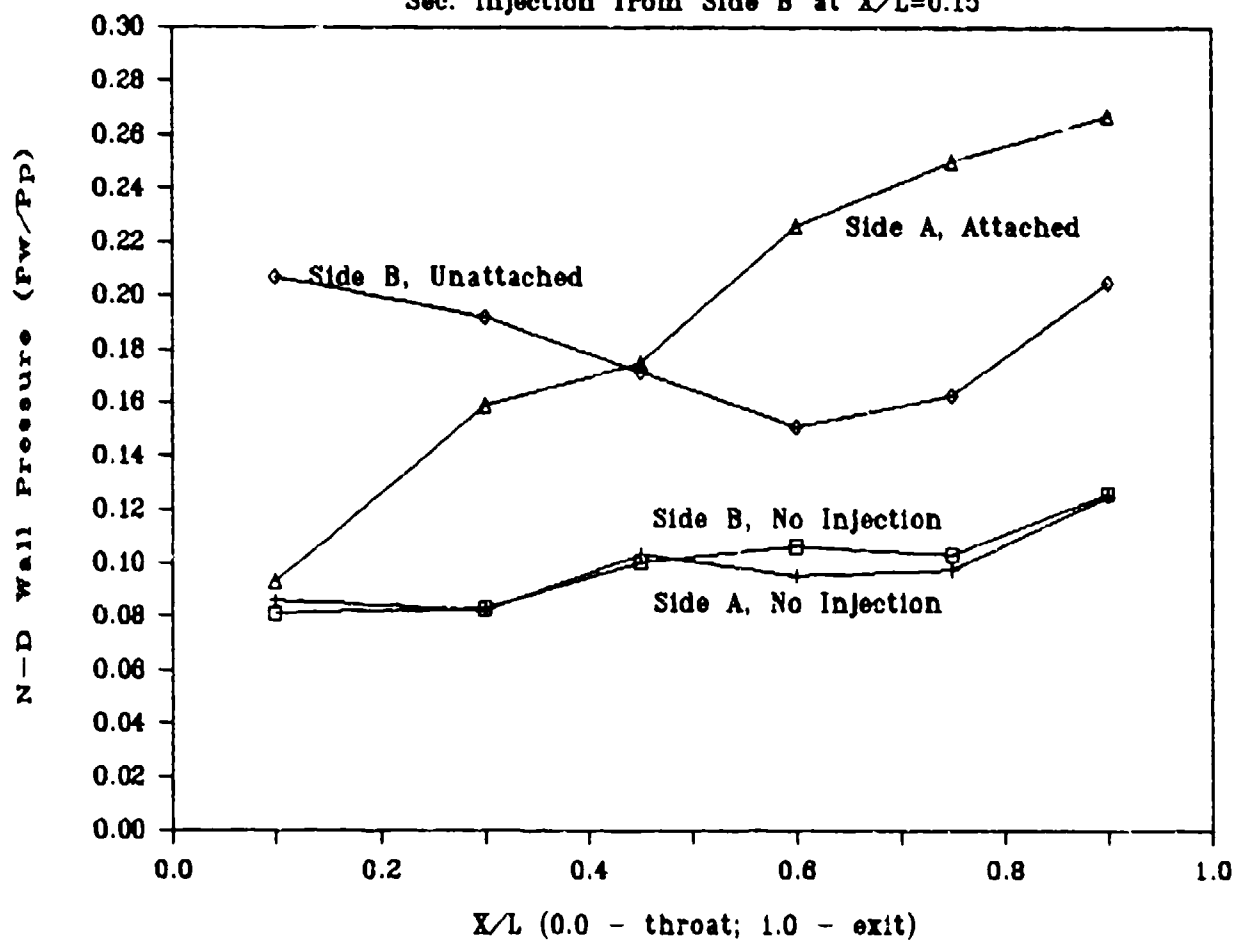Fig 50.   Wall Pressure Distribution of Vectored Condition
          LM, As/At = 0.20, Pp = 154.4 psia, Ps/Pp = 0.55

Side B

Side A

Ps/Pp = 0.61
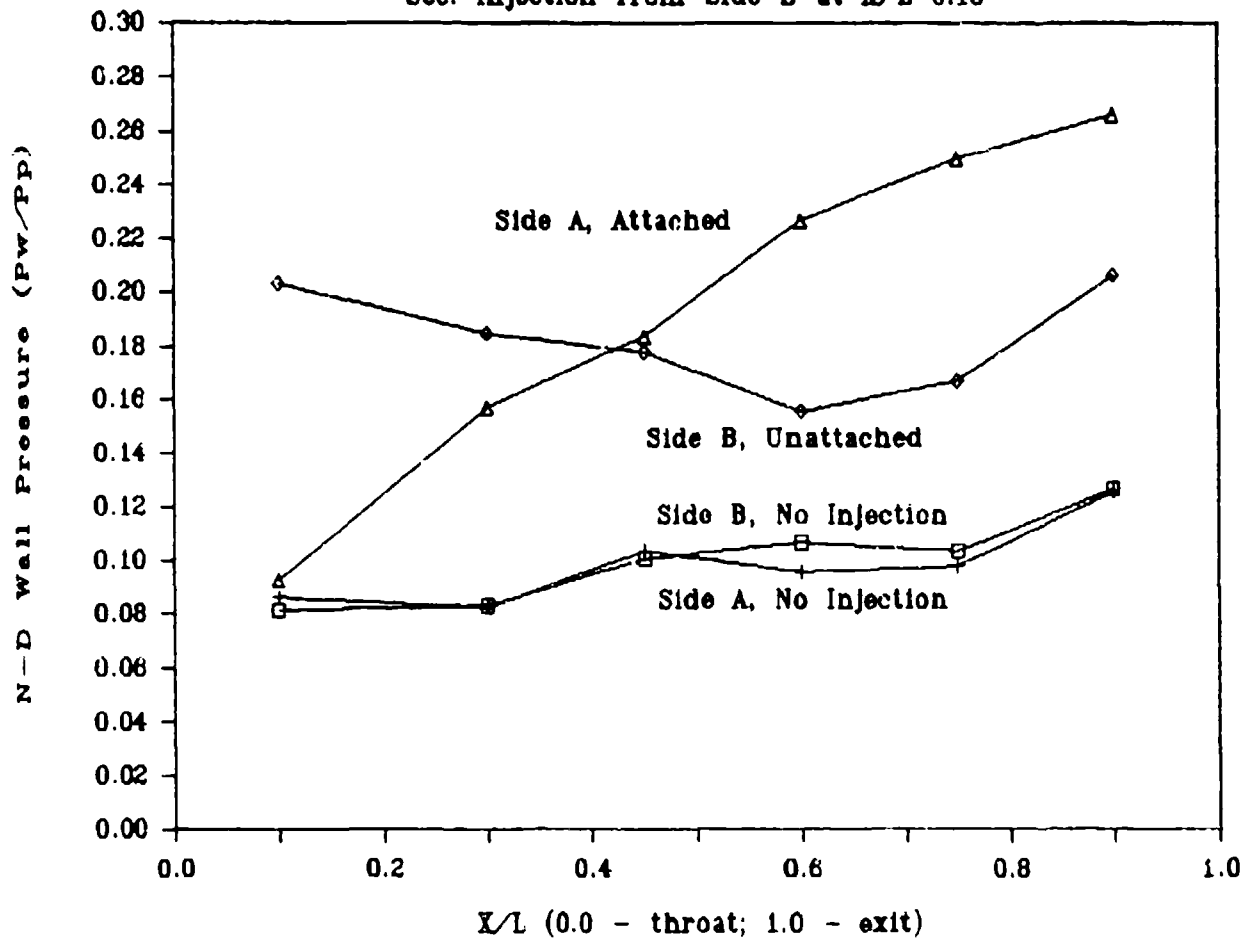
Fig 51. Wall Pressure Distribution of Vectored Condition
LM, As/At = 0.20, Pp = 154.4 psia, Ps/Pp = 0.61

may be due to the relative areas at the secondary injection point. In the two-dimensional nozzle, when the secondary flow is directed into the primary flow, the secondary flow cannot disperse. However, in the axisymmetric nozzle, the secondary flow can not only move the flow toward the opposite wall but fill the volume made vacant by the jet attaching to the wall. It is possible that in a thicker two-dimensional nozzle, the flows would not be so confined, and the decrease in side force with increasing secondary pressure would not be so evident.

Before vectoring then, the increasing secondary pressure moves the flow slightly off center to give some side force, resulting in incomplete vectoring. With just enough pressure, the jet vectors. After vectoring, increases in secondary pressure seem to disrupt the jet until there is no vectoring. Requirement for vectoring then seems to be a "nudge" from the secondary flow, and anything more than the minimum flow will slightly decrease side force.

The combination of side force decreasing after vectoring and axial force increasing after vectoring as secondary pressure increases implies that the thrust angle should be decreasing, as shown by Figs 32, 33, and 34. So for a CJTVC nozzle of this configuration, the desired secondary pressure is the lowest required for vectoring, which gives the largest thrust angle. And, because it is at the lowest pressure necessary, it also means the mass flow is low. Therefore, performance is optimized at the minimum

83

secondary pressure required for vectoring. However, in an actual application, some margin would be used in selecting As or Ps to guarantee vectoring.

Effect of Secondary Area on Vectoring

Increasing the area does tend to reduce the requirement of secondary pressure. In Fig 29, at As/At = 0.15 and Pp = 174.4 psia, the nozzle did not vector for Ps/Pp = 0.25. But in Fig 30, for As/At = 0.17, the nozzle did vector at those pressures. Also, in Fig 31, for As/At = 0.20, the nozzle vectored at the same pressures. So an increase in secondary area reduces the secondary pressure requirement for vectoring, and this may be related to a minimum secondary momentum requirement as discussed earlier.

One aspect of the larger secondary area is the ability to vector under more conditions, and the larger area also affects side force. Figures 29, 30, and 31 show that as the area increases, the side force increases for the vectoring cases. At a Pp = 174.4 psia, Ps/Pp = 0.43, the percentage of force increase between an As/At = 0.15 and As/At = 0.20 is 11%. The equivalent increase in area is 33%, and from Figs 18 and 21, the increase in mass flow is about 17%. Therefore, if the flow vectors with a secondary injection area, and a larger As is used, thrust angle will increase slightly, but the secondary mass flow will increase by a higher percentage.

84

Effect of Extension on Nozzle Performance

As previously stated, the extension to the nozzle bracket extended 50% longer than the length of the nozzle, and this extension affected the performance of the nozzle. Figures 52 through 56 give the comparison between LM and LME, using mass flow ratio, N-D axial force, N-D side force, angle of thrust versus Ps/Pp, and total thrust efficiency, respectively. Non-vectored cases are indicated by a darkened symbol, vectored by an open symbol. For the comparison, the nozzles were tested at the same Pp of 174.4 psia and As/At = 0.20.

From Fig 52, it is noticeable that for most of the cases, the secondary mass flow recorded for the no-extension case is slightly less. But this is most likely due to tests being conducted on different days, and the difference is within 10%, which is within the envelope of the mass flow measuring devices. The interesting point on the graph is at Ps/Pp = 0.26, where the LME nozzle has vectored and the LM nozzle, at the same mass flow ratio and Ps/Pp, has not vectored. Also, at Ps/Pp of 0.32, the mass flows are slightly different, but the nozzle with the extension has vectored and the nozzle without has not. It appears then that the extension reduces the minimum secondary pressure and mass flow requirements.

Figure 53 indicates that the axial force is higher in the LM nozzle than in the LME nozzle, which may be due to frictional effects in the extension. Fig 56 shows the

85
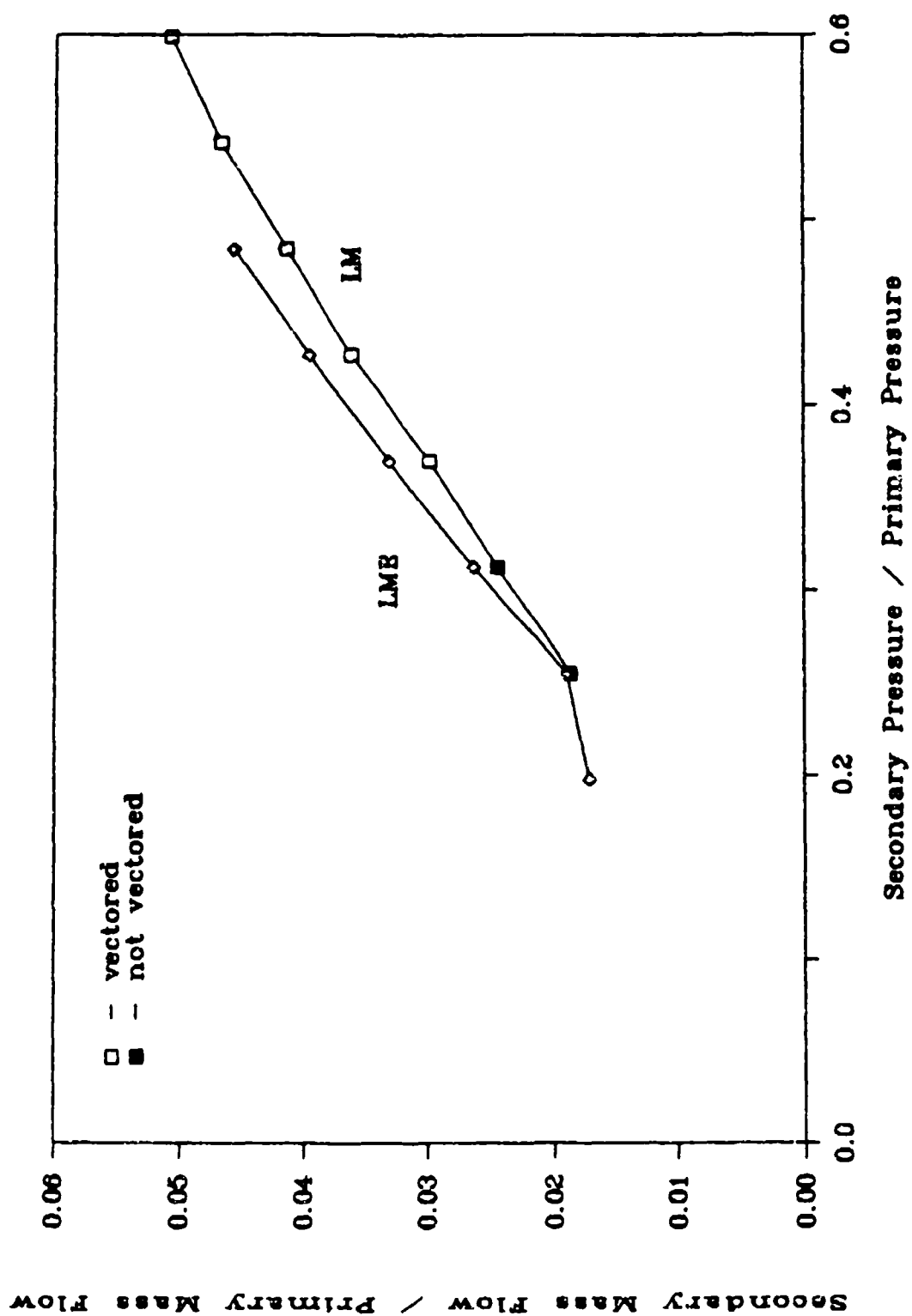
Fig 52. Mass Flow Ratio for Comparison Between LM and LME
As/At = 0.20, Pp = 174.4 psia, $\dot{m}_p$ = 0.85 lbm/sec
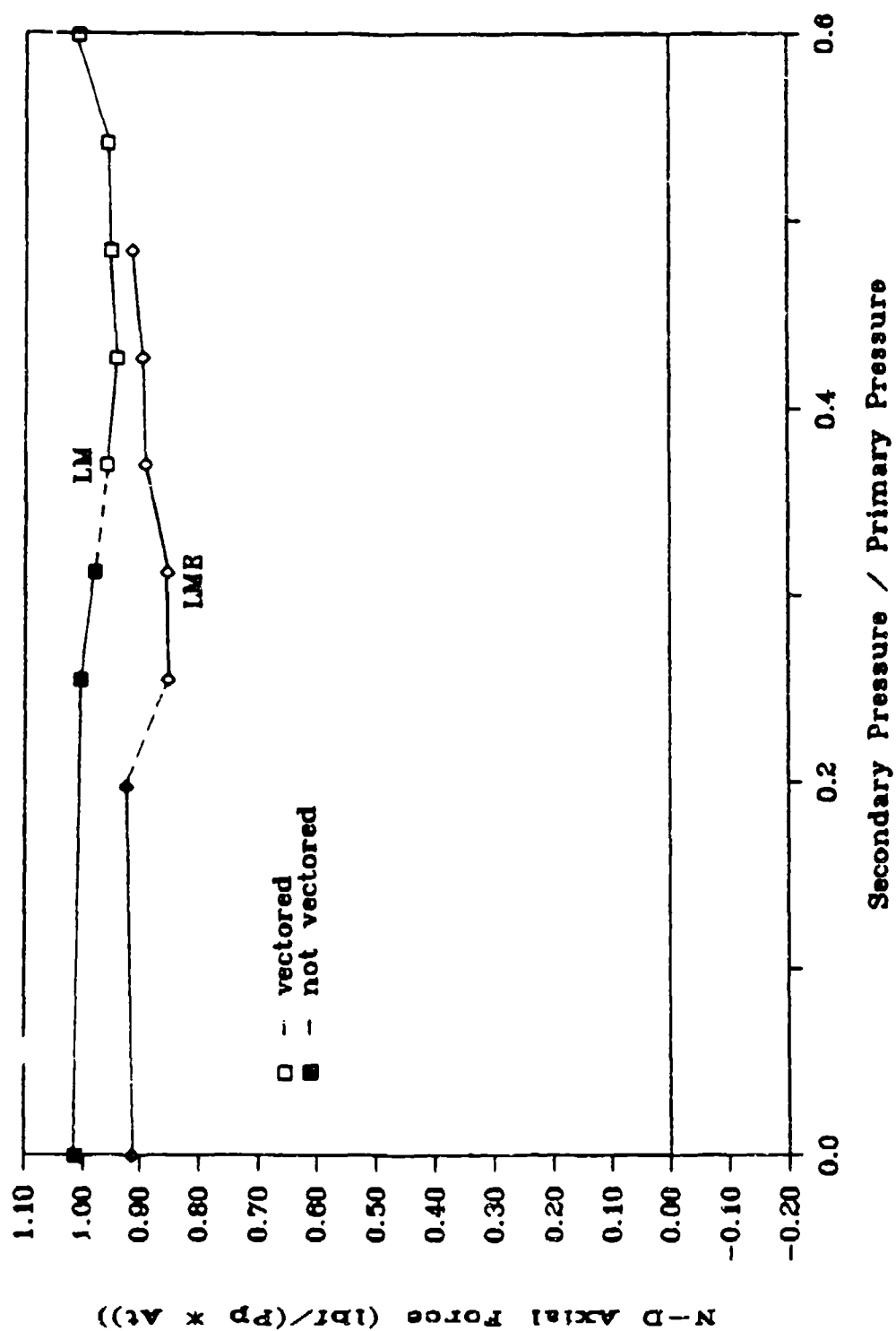
Fig 53. Effect of Extension on Axial Force
As/At = 0.20, Pp = 174.4 psia
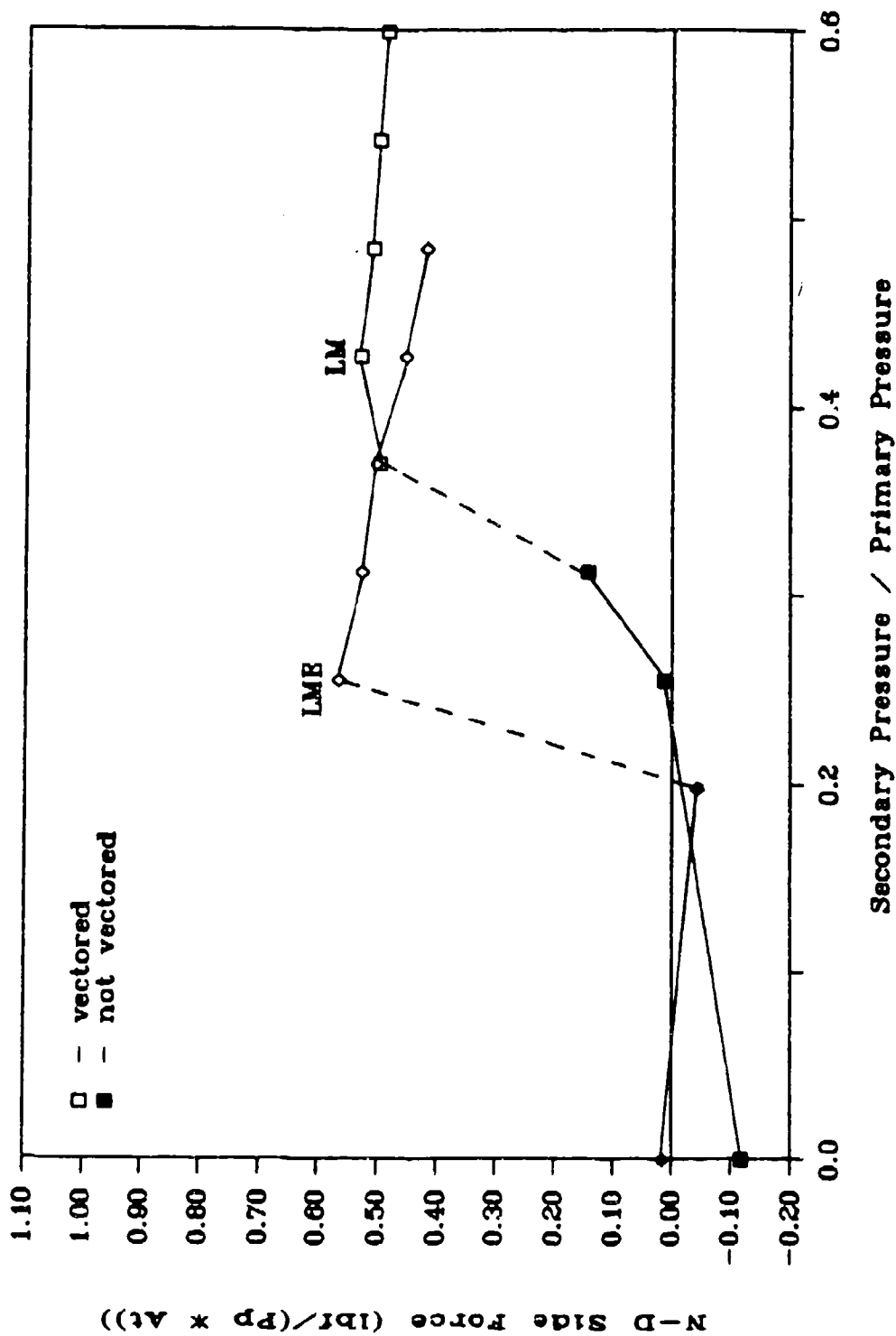
Fig 54. Effect of Extension on Side Force
As/At = 0.20, Pp = 174.4 psia
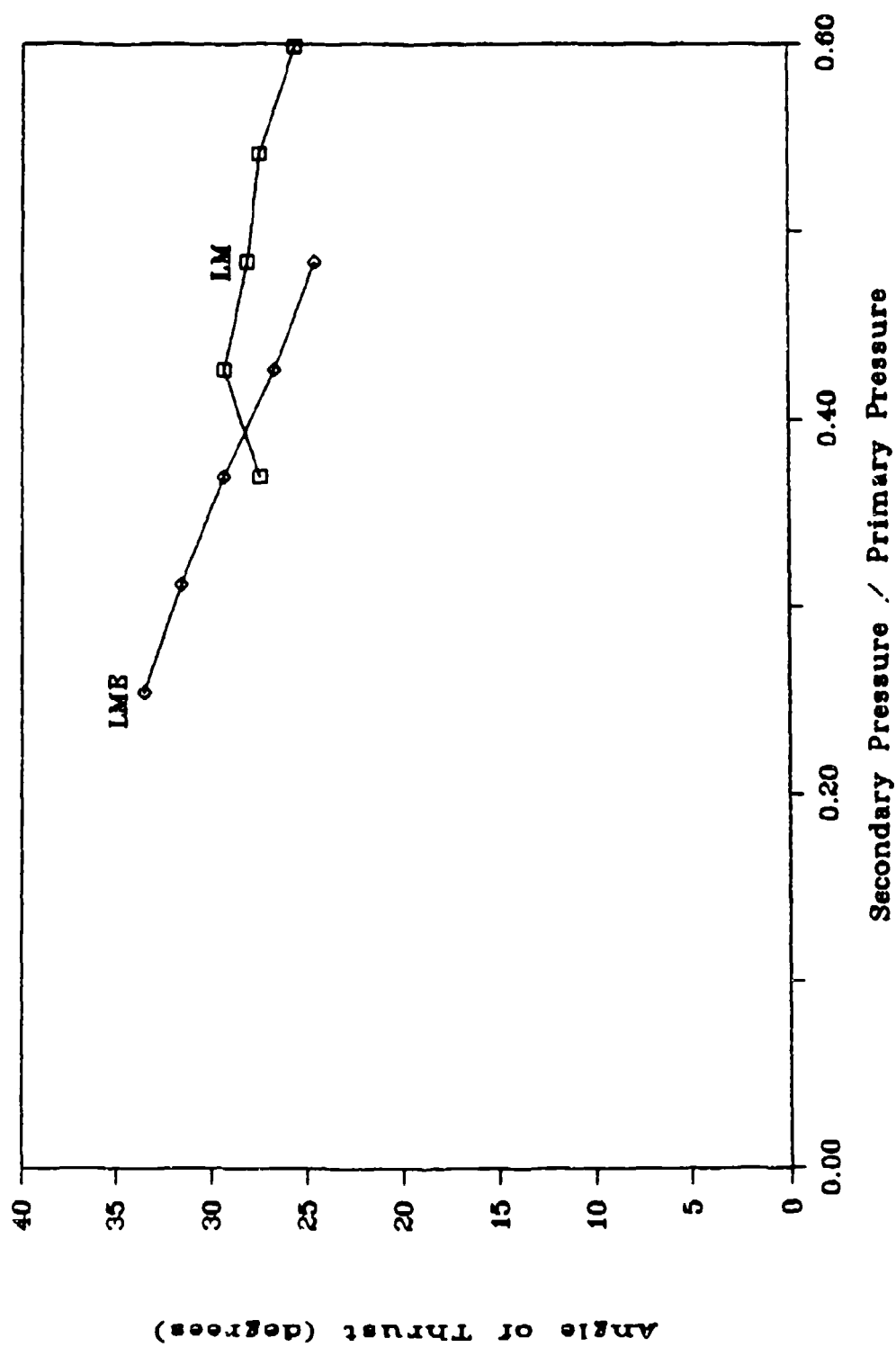
Fig 55. Effect of Extension on Angle of Thrust
As/At = 0.20, Pp = 174.4 psia
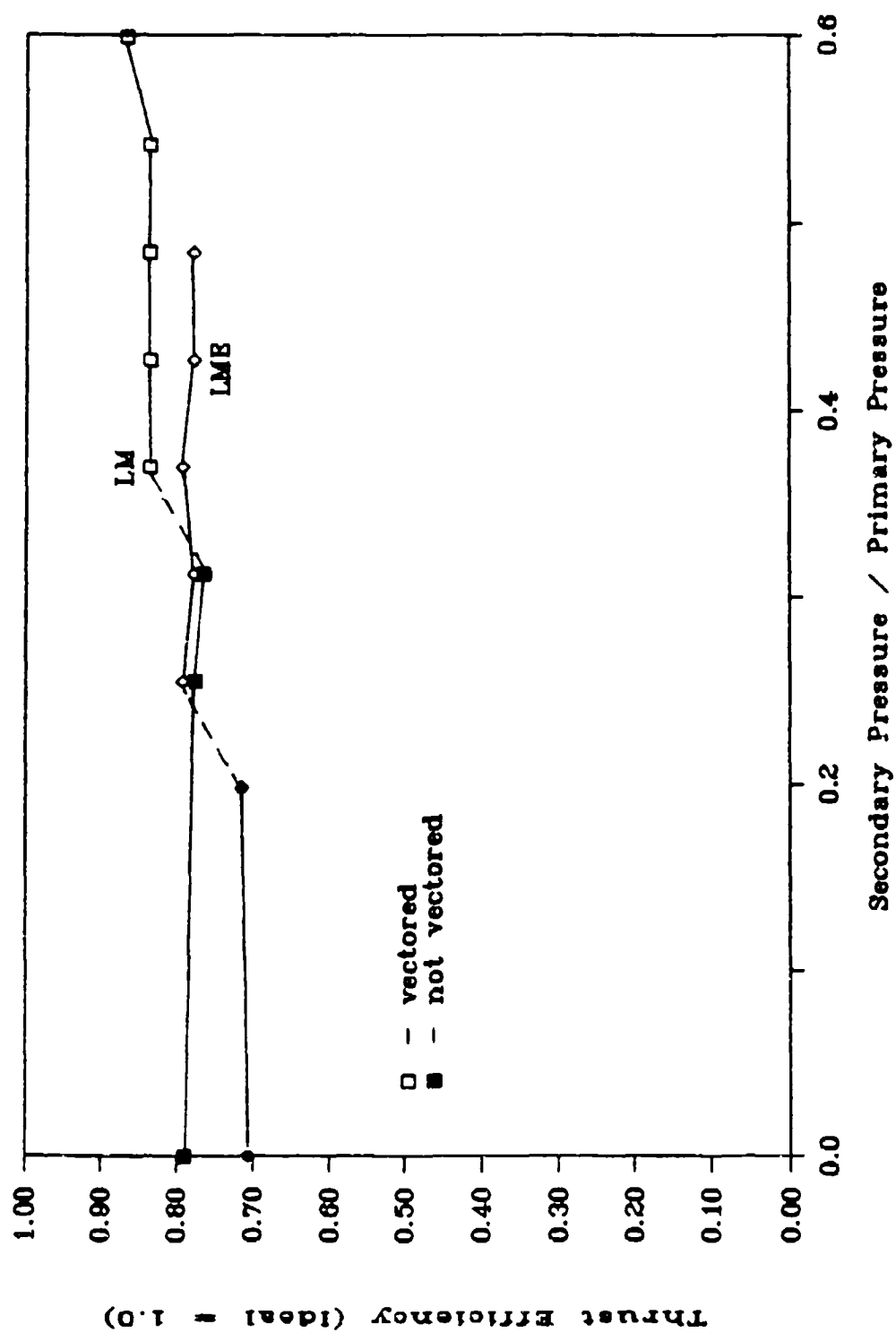
Fig 56. Effect of Extension on Thrust Efficiency
As/At = 0.20, Pp = 174.4 psia

efficiency of both nozzle brackets. As noted previously, the efficiency of the LM nozzle is 5-10% higher than the LME nozzle, both in the vectored and axial cases.

Figure 54 shows the trend of side force using the LME nozzle with incomplete vectoring as discussed previously. As Ps/Pp is increased, side force slightly increases opposite in direction to the side force obtained when the nozzle vectors, until the minimum Ps/Pp for vectoring is reached. But the LM nozzle behaved differently. As the Ps/Pp is increased, side force increases about the same amount as the LME nozzle, but in the same direction as the vectored case. As the minimum Ps/Pp is approached, there is a much more gradual transition to the vectored case. It may be the same effect of incomplete vectoring as displayed in the Fig 44, only that with the bracket, the jet leaves the exit opposite the injection side, giving force in the opposite direction as the vectored case. Therefore, when the nozzle vectors, there is a large gradient of side force because the jet switches directions. Without the bracket, the introduction of secondary flow into the jet causes it to curl and leave the exit plane in the same direction that it vectors, so that the jump in side force is more gradual.

Figure 54 shows the higher Ps/Pp required for the LM nozzle to vector, but it also shows the larger side force that can be obtained at the same Ps/Pp using the LM nozzle. From Fig 55, the angle is larger for the LME case, but that

may be only due to the reduced axial force obtained when using the extension.

Therefore, the extension shifted the domain of vectoring by making the minimum secondary mass flow and Ps requirements slightly lower, but the efficiency of the nozzle decreased as well.

Cross Section of the Secondary Injection

Figures 57 through 61 display graphs comparing the slot, 0.0625 in by 0.50 in, to the circular cross section with the same As/At = 0.17 to determine the effect of secondary cross section. The tests were run at the same Pp of 174.4 psia, and at the same As/At. Figure 57 shows that the slot required a larger Ps/Pp to vector, but Fig 58 shows that when the nozzle with the slot did vector, it did so at a larger angle than the nozzle with the circular cross section. The efficiency of the total thrust produced by the nozzles in either configuration is about the same, in the incomplete and vectored cases, as shown in Fig 61. The smaller axial thrust using the slot, shown in Fig 59, is most probably due to the cosine effect of the larger thrust angle, since the efficiencies were about the same. Figure 60 shows that the side force using the slot injector is much larger after vectoring, by about 20%.

For two-dimensional nozzles, it appears that the slot provides a better performing nozzle when vectoring compared to the circular cross section. However, the vectoring

92
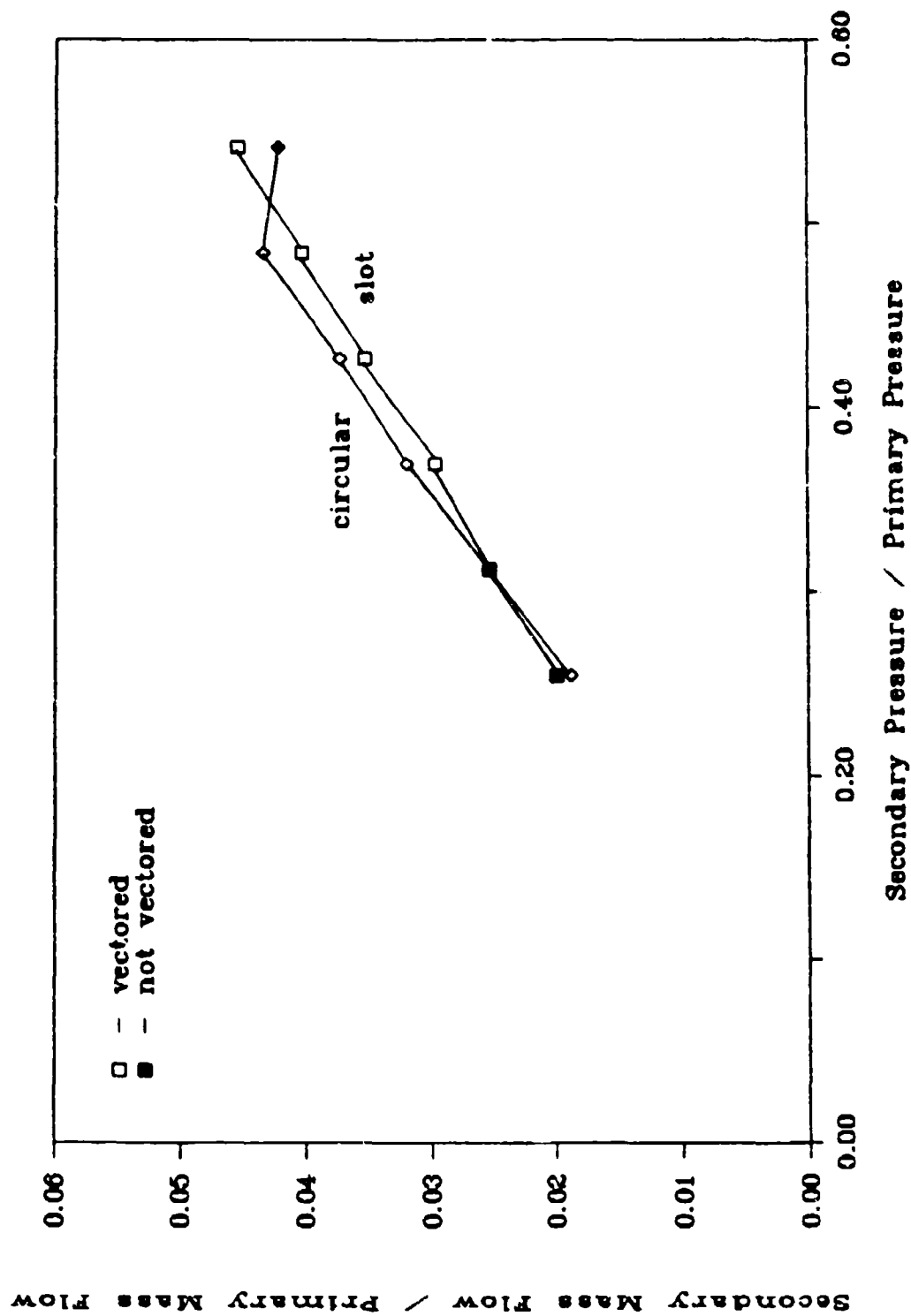
Fig 57.   Mass Flow Ratio for Comparison of Slot and Circular Cross Section
LM, As/At = 0.17, Pp = 174.4 psia, $\dot{m}_p$ = 0.85 lbm/sec
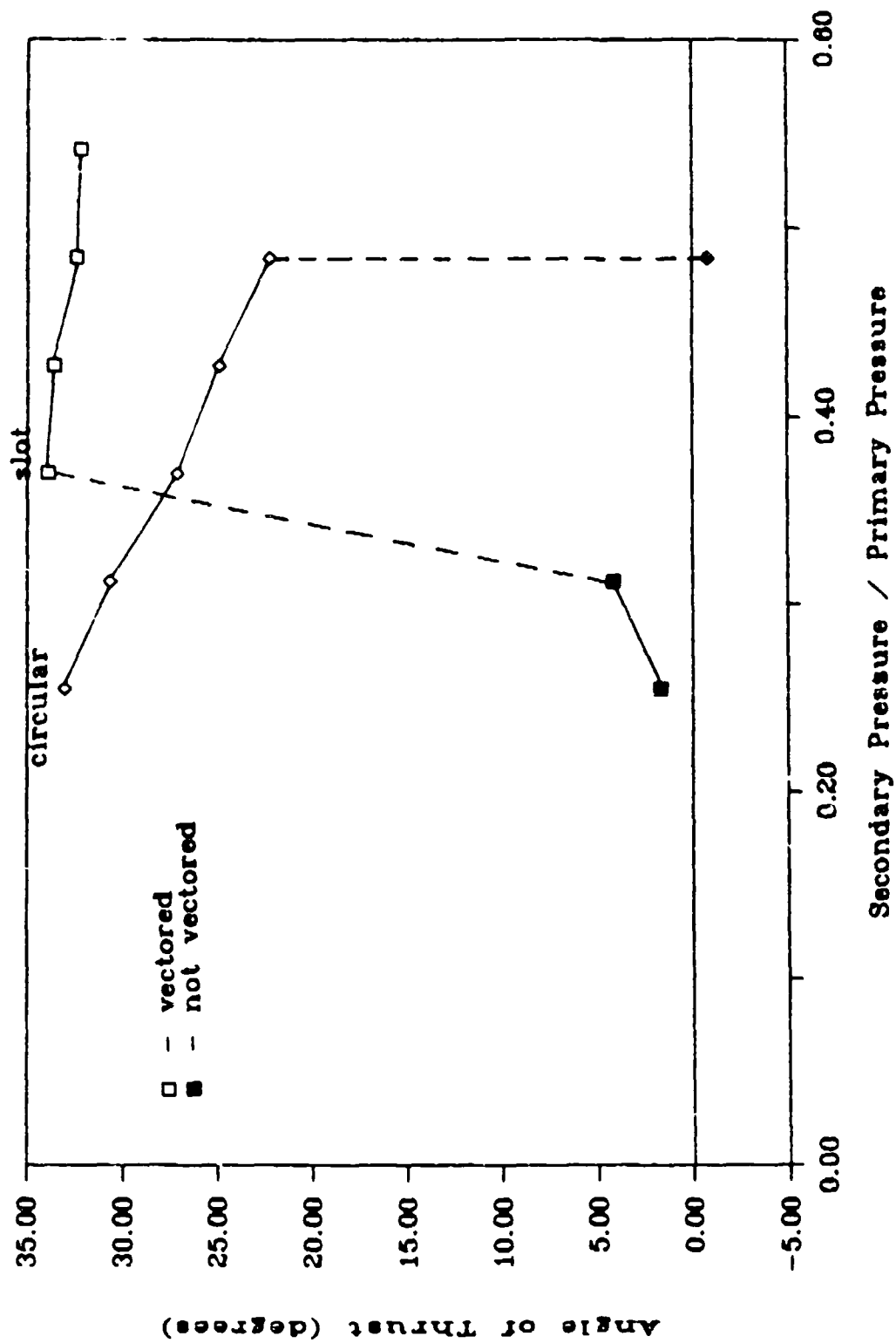
Fig 58. Effect of Secondary Injection Cross Section on Angle of Thrust
LM, As/At = 0.17, Pp = 174.4 psia
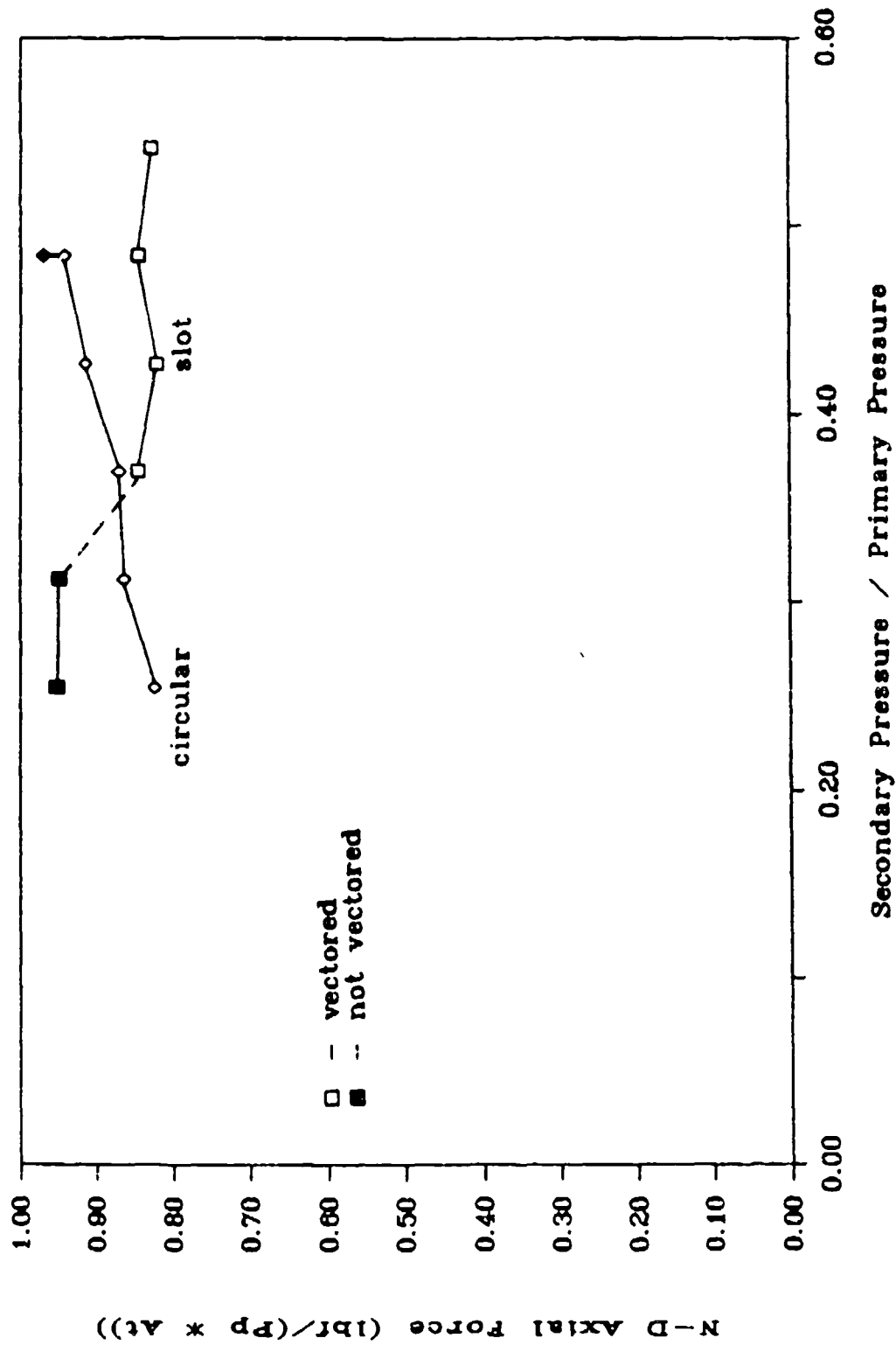
Fig 59. Effect of Secondary Injection Cross Section on Axial Force
LM, As/At = 0.17, Pp = 174.4 psia

95
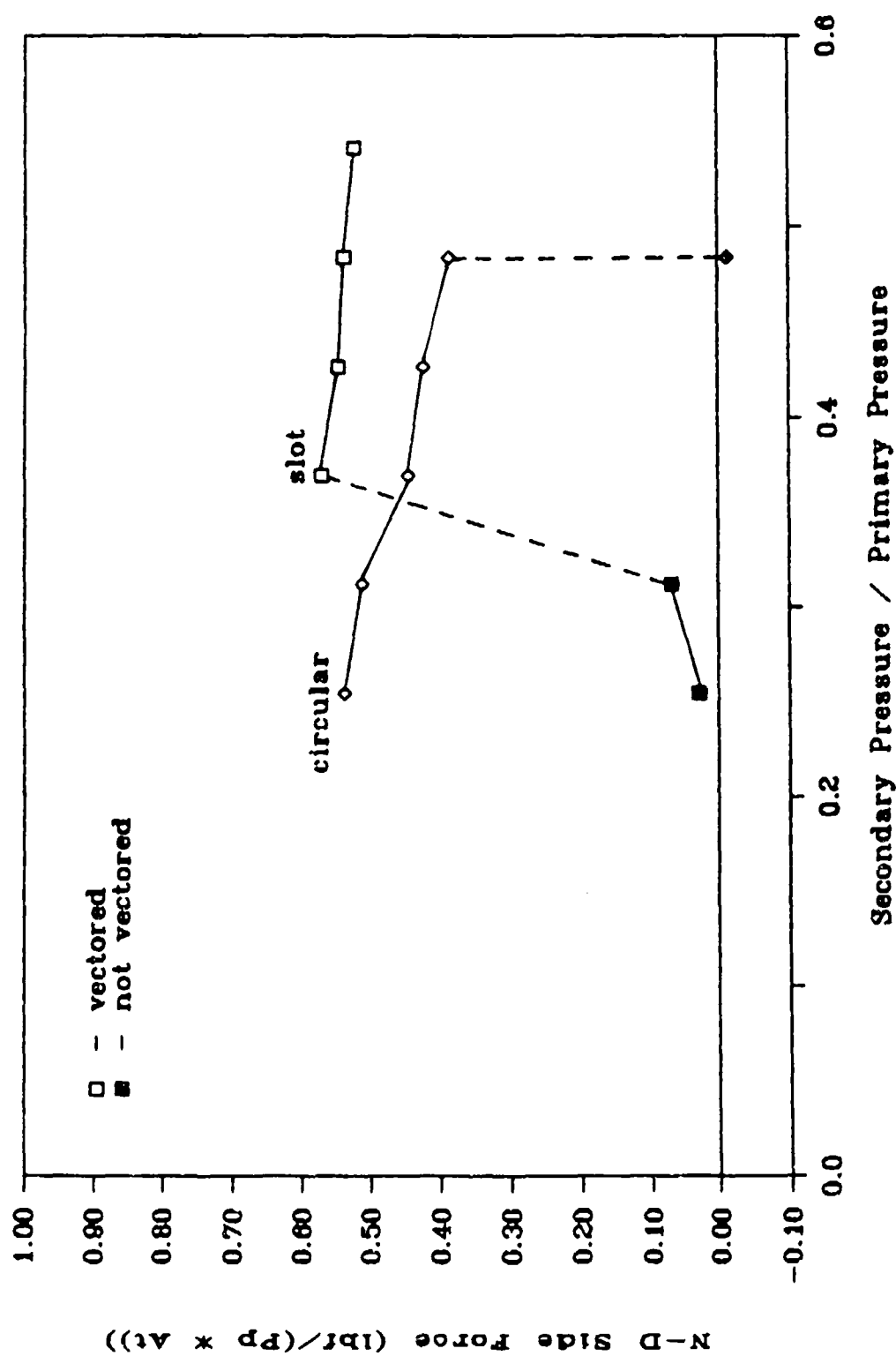
Fig 60. Effect of Secondary Injection Cross Section on Side Force
LM, As/At = 0.17, Pp = 174.4 psia
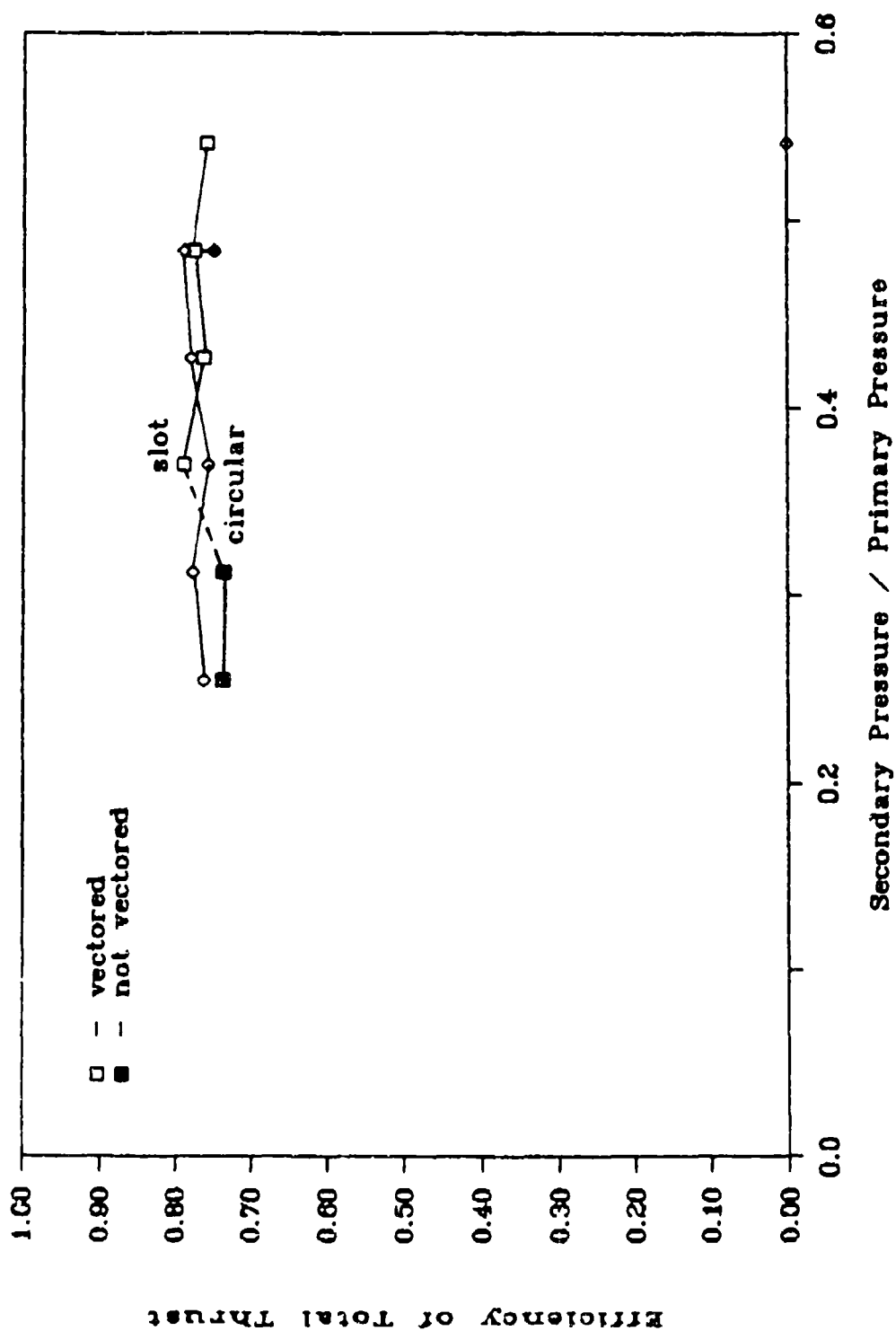
Fig 61. Effect of Secondary Injection Cross Section on Thrust Efficiency
LM, As/At = 0.17, Pp = 174.4 psia

97

requires higher mass flow and Ps/Pp. The efficiency is not
increased, but the thrust angle is larger.

Confirmation of Side Force

Figure 62 is a pressure distribution of the wall cavity
pressure for Pp = 154.4 psia, Ps/Pp = 0.29, As/At = 0.20.
The side force obtained by the test stand was 15.7 lbs, and
by integrating the pressure distribution over the length of
the nozzle, the side force obtained was 15.3 lbs. The
pressure distribution between points was assumed to be
linear, and the pressure between X/L = 0.75 and 0.9 was
linearly extrapolated to give the pressure at X/L =1.0. Also,
the pressure at the throat was found assuming Mach = 1.0 at
the throat, and using the isentropic stagnation to static
pressure relation. The scheme for integration is discussed
in more detail in Appendix D.

Choked or Unchoked Secondary Flow

If the secondary flow choked, it would do so in the
secondary injector because the area of the secondary injector
was much smaller than the manifold, the tubing between the
injector and the solenoid valve, or the throat of the venturi
used to measure secondary mass flow. From the measurements
taken, the Mach number at the venturi throat can be
calculated as shown in Appendix E. Figures 63, 64, and 65
are grap's of the Mach number at the venturi throat versus
Ps/Pp, with darkened symbols indicating the non-vectored
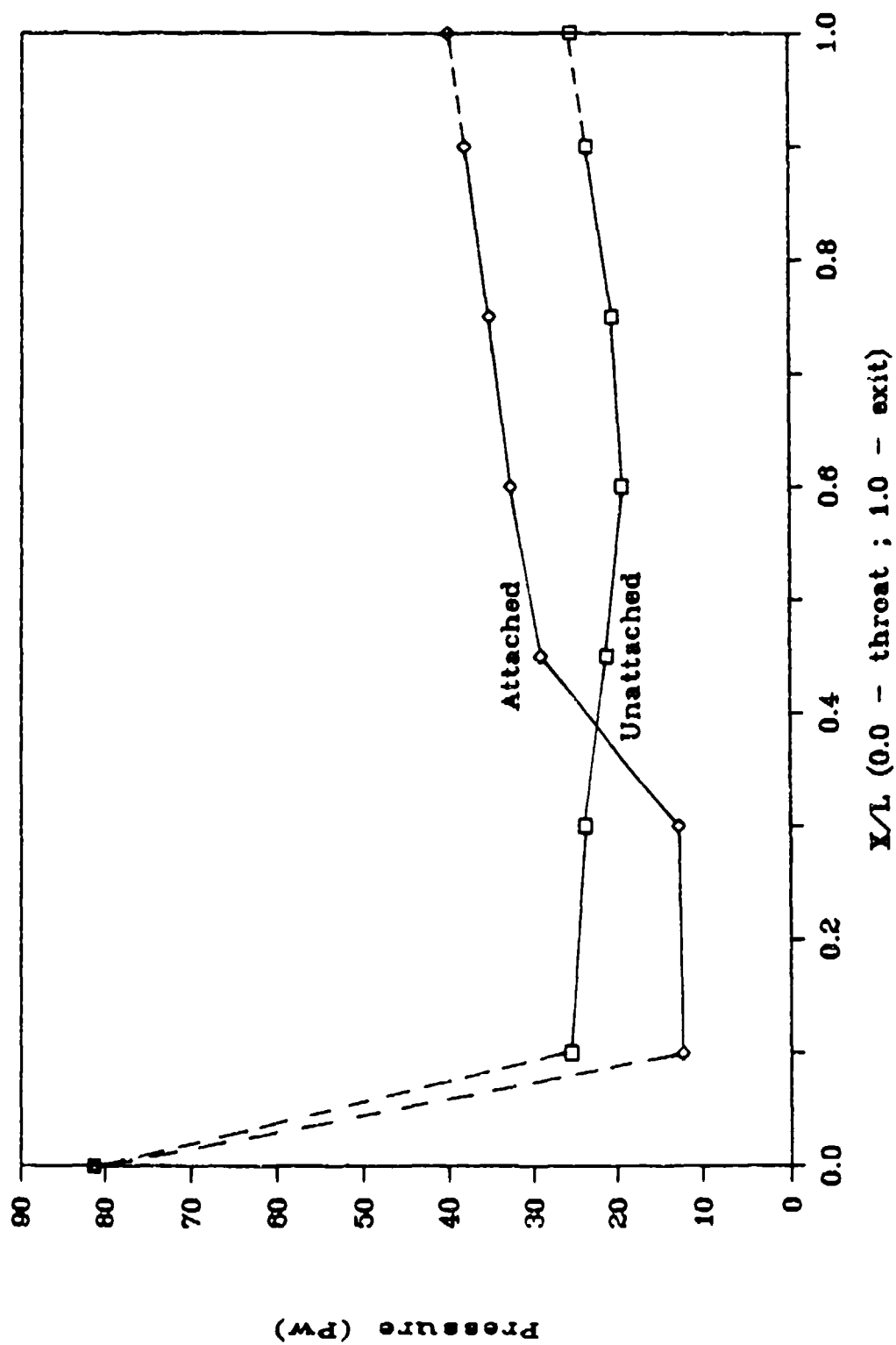
Fig 62. Wall Pressure Distribution for the Calculation of Side Force
LM, As/At=0.20, Pp=154.4 psia, Ps/Pp=0.29
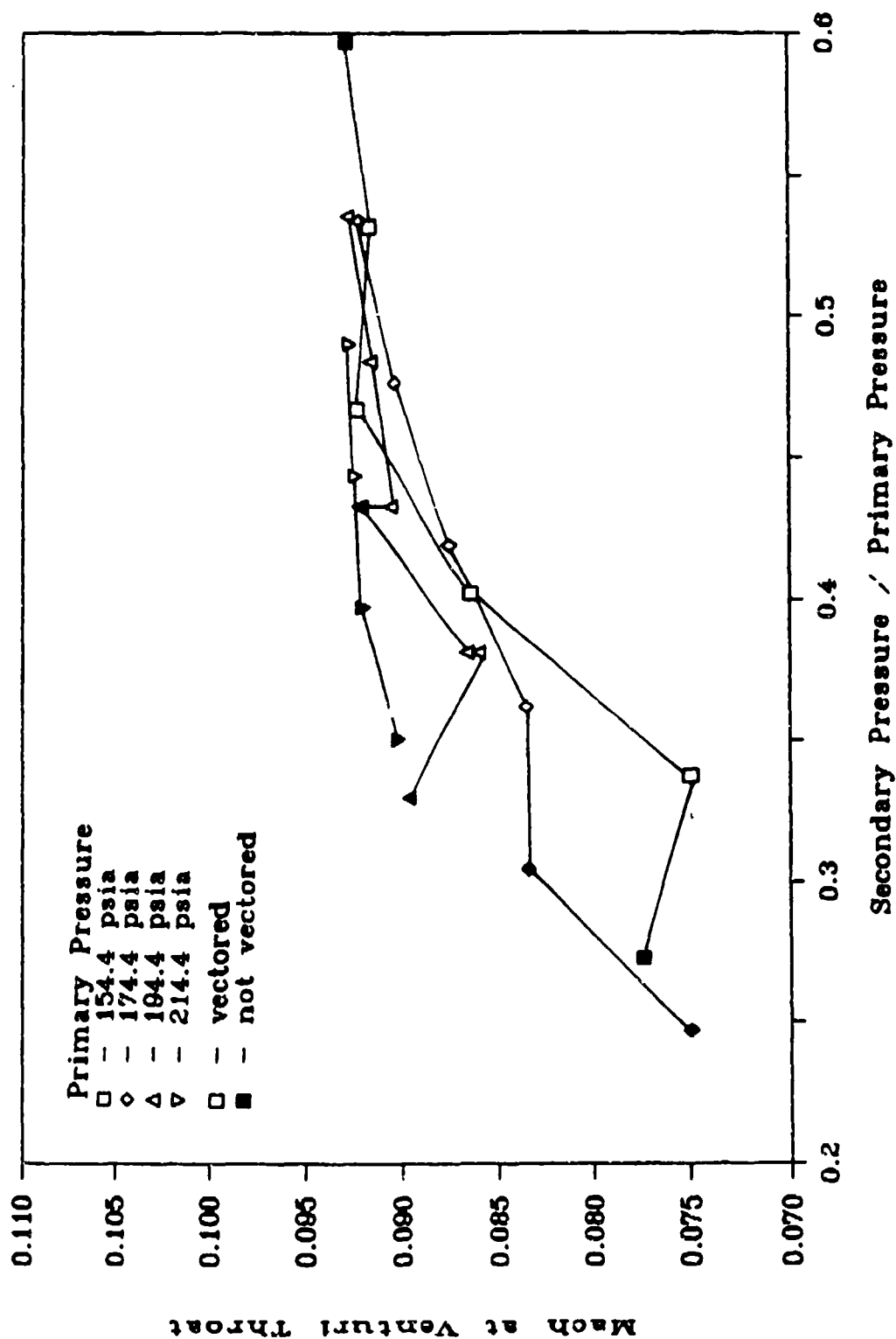
Fig 63. Effect of Ps and Pp on Mach Number at Venturi Throat
LME, As/At = 0.15
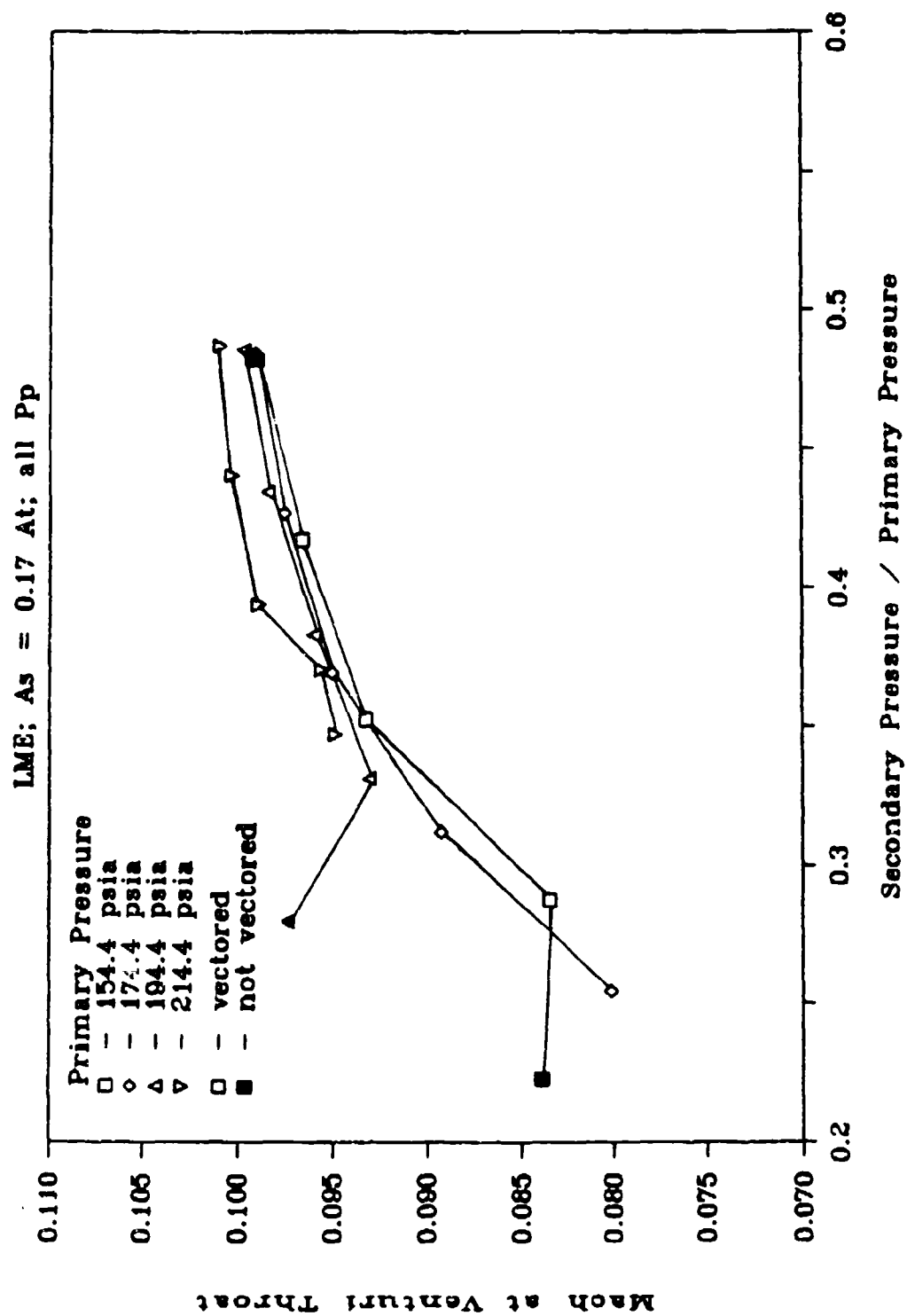
Fig 64. Effect of Ps and Pp on Mach Number at Venturi Throat
LME, As/At = 0.17
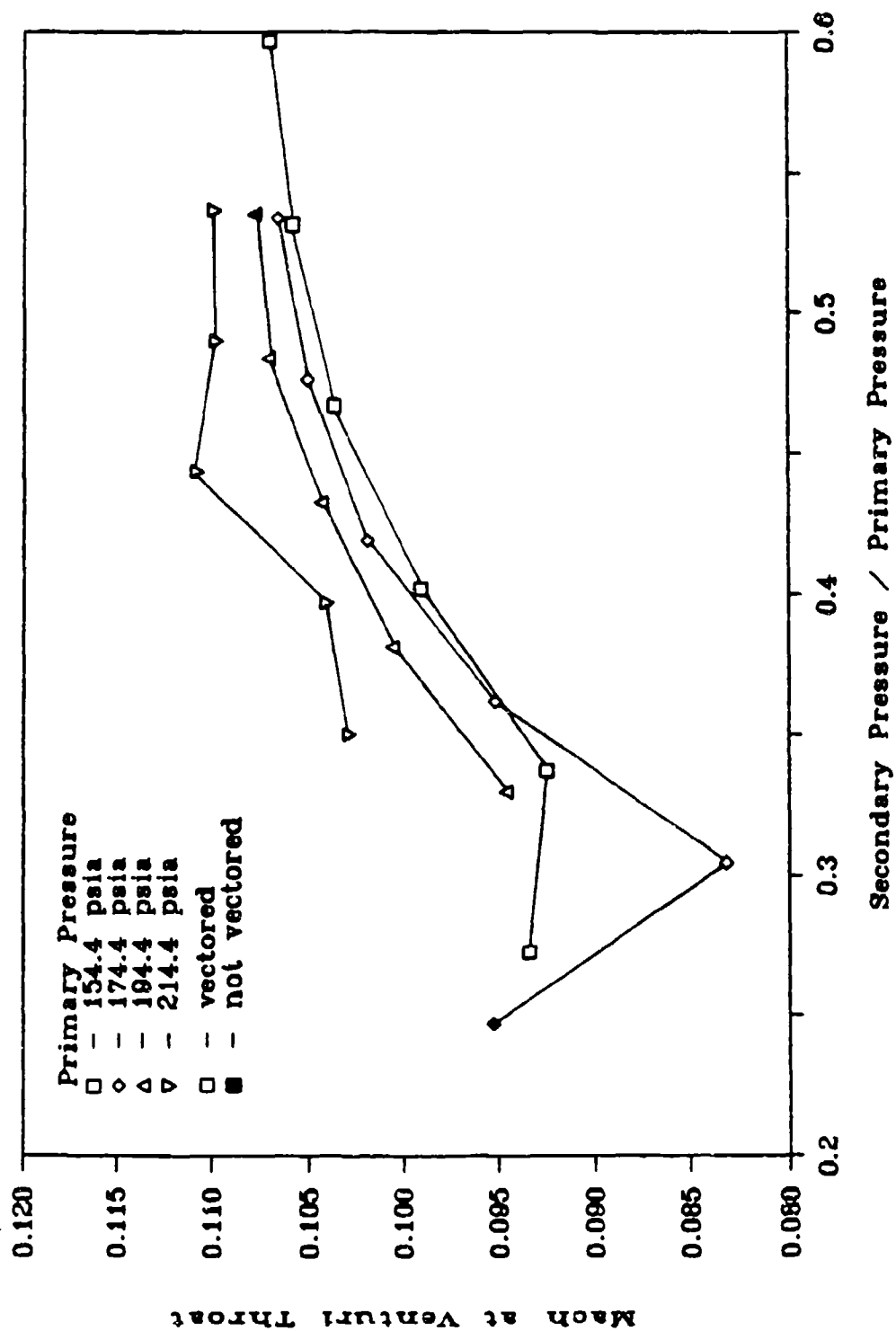
Fig 65. Effect of Ps and Pp on Mach Number at Venturi Throat LME, As/At = 0.20

cases, for the LME nozzle at As/At = 0.15, 0.17, and 0.20.
The graphs show that the Mach number of the venturi reaches
the same maximum value at any of the primary pressures as
Ps/Pp is increased. This would seem to indicate that the
secondary flow was choked at that maximum Mach number that
the venturi reaches. The graphs indicate that the nozzle
will vector whether the secondary flow is choked or not,
because vectoring cases occur where the venturi is not
choked. So secondary Mach number does not seem to affect
vectoring.

VI. Conclusions

1. Successful operation of a two-dimensional CJTVC nozzle is critically dependent geometry, including exit area, length, location of secondary injection port, and secondary injection area. It is also dependent on the primary and secondary pressures.

2. A domain of vectoring exists for a two-dimensional CJTVC nozzle, where too little secondary flow causes incomplete vectoring, and too much can disrupt the jet completely.

3. Mass flow requirements for successful vectoring of a two-dimensional CJTVC nozzle are about 2-3% of the primary mass flow. Secondary pressure between 30 and 50% of the primary pressure is also required, as is a minimum secondary injection area.

4. Thrust angles ±20 and greater are possible from a two-dimensional CJTVC nozzle.

5. Axial thrust drops a maximum of 10% during vectoring from a two-dimensional CJTVC nozzle.

6. Efficiency in the axial condition is about 75%, and in the vectored condition it increases to 80-85%, compared to the thrust from an ideally expanded nozzle at the same primary pressure.

7. Response time for vectoring is less than 50 msec, and might be improved with quicker valves. There is a

tendency for the jet to stay attached to the wall after the secondary flow is shut off.

8. Increasing secondary pressure past that necessary for vectoring slightly reduces side force for a two-dimensional CJTVC nozzle.

9. Increasing secondary area decreases the minimum required secondary pressure. Side force increases at the expense of a larger increase in secondary mass flow.

10. A nozzle with side walls extending past the nozzle exit reduces the secondary pressure and mass flow required for a fixed geometry.

11. A secondary injection port with a cross section of a slot requires more flow and pressure to vector compared to a circular cross section, but the side force is increased at the points it does vector.

12. Choking of the secondary injection does not seem to be require for vectoring.

VII. Recommendations

1. Test an axisymmetric version of this smooth geometry using a cone and a sphere to possibly increase efficiency.

2. Change system to allow force runs and still pictures or video recording from closed circuit TV to be made. This would allow analyst to see what the jet was doing while the forces were being generated.

3. Move the secondary pressure control inside the control room for safety and to pinpoint the pressure required for vectoring.

4. Using the LM nozzle as a basis for length and exit area to throat ratio, test changes to the two-dimensional nozzle in the divergence angle and exit angle. Specifically, determine if either of these are at a design optimum at 20 degrees and 45 degrees, respectively.

5. Test the benefits of an angled secondary injection.

6. Test the same two-dimensional geometry at higher Pp, to see if effects significantly decrease performance.

7. Run a hot test to compare performance with the cold flow test.

8. Obtain a faster and newer computer than the HP-85A to speed data aquisition and analysis.

9. Use higher frequency valves to more accurately determine response of the system.

10.   Test the location of the secondary injection port to see if the optimum location changes with primary pressure.

11.   Check the benefits of a divergent section right outside the nozzle, to which the vectored thrust can attach.

12.   Make shorter side walls to adequately test the smaller length CJTVC (the 16 Wt nozzle). Make a new 16 Wt nozzle, with a length to exit width 5.0, the same as was used for the LM nozzle, and test the nozzle for performance.

13.   Install a static pressure and temperature sensor on the secondary injection port. By using the mass flow rate and the perfect gas law with these measurements, the velocity, Mach number, and momentum of the secondary flow can be calculated.

14.   Dynamically analyze the conditions in the cavity as the nozzle vectors to better understand the mechanism of vectoring.

15.   Determine the effect of the sharp nozzle throat on vectoring. Use smooth throat geometry to analyze the effect.

16.   Determine if the vectorability is affected by a low atmospheric pressure by using a blow down system into a vacuum.

Bibliography

1. Bean, Howard S. <u>Fluid Meters</u>: <u>Their Theory and Application</u>. New York: The American Society of Mechanical Engineers, 1971.

2. Brown, B. G. <u>Experimental Study of Three-Dimensional Confined Jet Thrust Vector Control (CJTVC) Nozzles</u>. MS Thesis, AFIT/GA/AA/85D-3. School of Engineering, Air Force Institute of Technology (AU), Wright-Patterson AFB OH, December, 1985.

3. Cates, J. W. <u>Two-Dimensional Confined Jet Thrust Vector Control With Flow Visualization and Variable Flow Geometry</u>. MS Thesis, AFIT/GAE/AA/85D-2. School of Engineering, Air Force Institute of Technology (AU), Wright-Patterson AFB OH, December, 1985.

4. Fitzgerald, R. K. and R. F. Kampe, "Boundary Layer TVC for Missile Applications," <u>AIAA/SAE/SAME 19th Joint Propulsion Conference</u>, AIAA-83-1153, AIAA, New York, 1983.

5. Fitzgerald, R. K. and R. F. Kampe. <u>Confined Jet Thrust Vector Control (CJTVC) Nozzle Development and Cold Flow Testing Program</u>, NWCTP6126, Naval Weapons Center, China Lake CA, 1980.

6. Fox, R.W. and A.T. McDonald. <u>Introduction to Fluid Mechanics</u>. John Wiley & Sons, New York, 1978.

7. Franke, M.E. and Brown, B.G. "Experimental Study of a Confined Jet Thrust Vector Control Nozzle," <u>Proceedings of the 1986 JANNAF Propulsion Meeting</u>, 1986.

8. Haloulakos, V.E., <u>Fluidic Thrust Vector Control Thruster Development</u>, McDonnell Douglas Astronautics Company, Huntington Beach, CA, 1983.

9. Lambert, P. G. <u>Experimental Study of Axisymmetric Confined Jet Thrust Vector Control Nozzle Performance and Behavior</u>. MS Thesis, AFIT/GAE/AA/86D-8. School of Engineering, Air Force Institute of Technology (AU), Wright-Patterson AFB OH, December, 1986.

10. Lloyd, R., "A Review of Thrust Vector Control Systems for Tactical Missiles," <u>AIAA/SAE 14th Joint Propulsion Conference</u>, AIAA-78-1071, AIAA, New York, 1978.

11. Porzio, A. J. <u>Characteristics of Confined Jet Thrust Vector Control Nozzle</u>. MS Thesis, AFIT/GAE/AA/84D-22. School of Engineering, Air Force Institute of Technology (AU), Wright-Patterson AFB OH, December, 1984.13.

12. Porzio, A.J. and Franke, M.E., "Experimental Study of a Confined Jet Thrust Vector Control Nozzle," <u>AIAA 24th Aerospace Sciences Meeting</u>, AIAA-86-0448, AIAA, New York, 1386.

13. Ryan, R. W. <u>Flow Response of an Axisymmetric Confined Jet Thrust Vector Control</u>. MS Thesis, AFIT/GAE/AA/87D-1. School of Engineering, Air Force Institute of Technology (AU), Wright-Patterson AFB OH, December, 1987.

14. Sutton, G.P. <u>Rocket Propulsion Elements</u>. New York: John Wiley and Sons, 1986.

Appendix A: Calculation of Two Dimensional Nozzle Geometry

The general shape of the nozzle is depicted in Fig 66.
For the line to be tangent to the circle, the slope of the
line must be equal to the slope of the circle at the point of
intersection. With this condition and the equations of a
circle and line, the dimensions of the nozzle can be
calculated with a few boundary conditions. These include the
length, the exit area to throat area ratio, the slope of
divergent section, the exit angle of flow, and the height of
the throat. The unknowns to be solved for are the radius of
the circle, and the x and y coordinates of the point of
intersection and the center of the circle.

The notation used for this analysis:

L = length of nozzle (throat to exit)

AR = exit area to throat area ratio

Wt = width of throat

δ = angle of divergence

θ = exit angle

(x_a, y_a) = intersection between line and circle

(x_c, y_c) = center of circle

R_c = radius of circle

td = tangent δ

s = tangent θ

$\alpha = \dfrac{dt}{2} (AR - 1)$ = y coordinate of endpoint, fixed by
width of throat and exit area to
throat area

The equations used to solve for unknowns are listed on
the page after the figure.
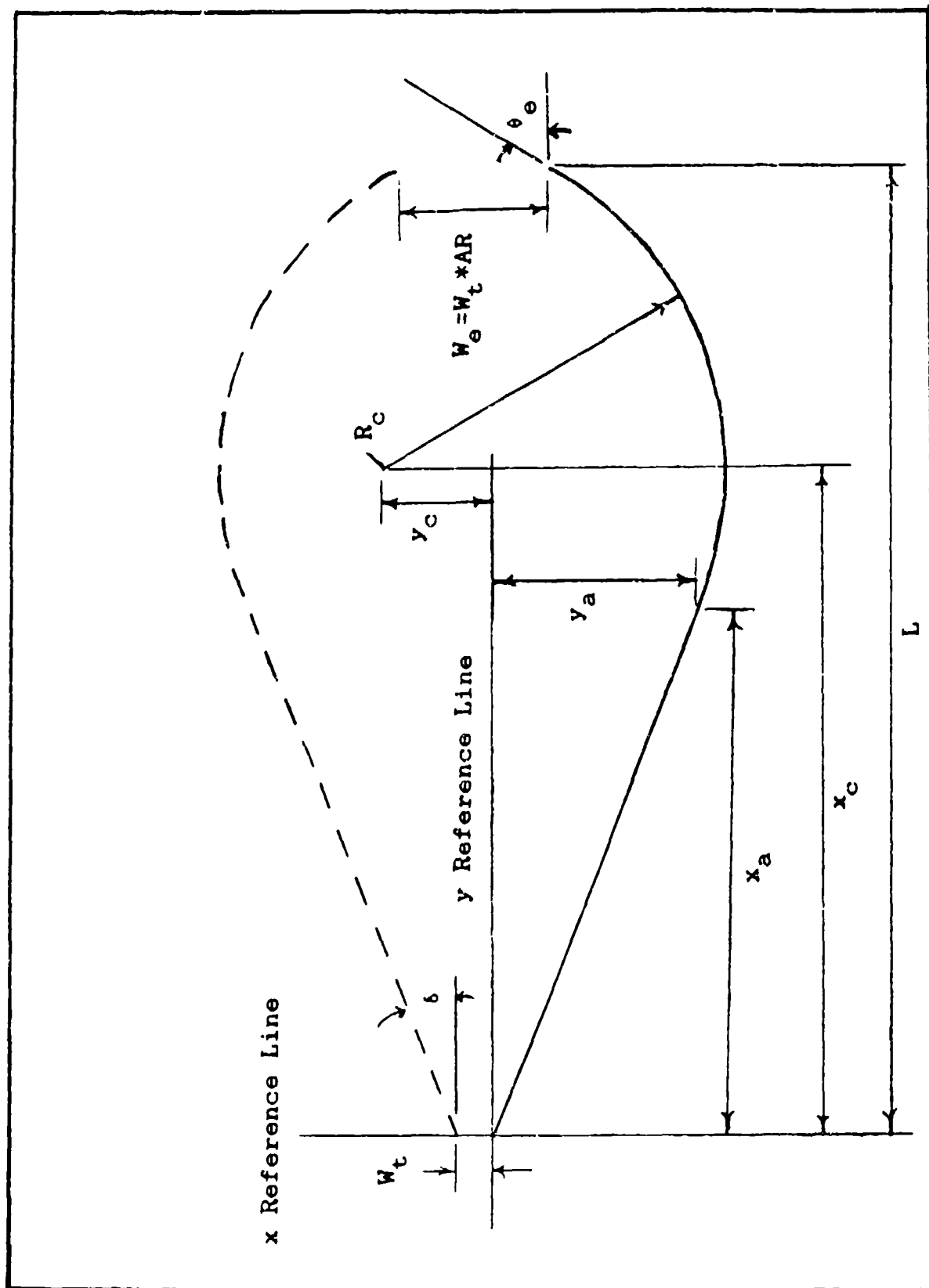
Fig 66. Geometry of Nozzle for Calculation of Design Parameters

111

1) Circle has (x_a, y_a) on it:

$$(x_a - x_c)^2 + (y_a - y_c)^2 = R_c^2$$

2) Circle has (L, α) on it:

$$(L - x_c)^2 + (\alpha - y_c)^2 = R_c^2$$

3) Line has (x_a, y_a) on it:

$$y_a = (td)x_a$$

4) Slope of line at (x_a, y_a) equals slope of circle

$$td = \frac{-(x_a - x_c)}{(y_a - y_c)}$$

5) Slope of circle at (L, α) is $- \tan \theta = -s$

$$-s = \frac{-(L - x_c)}{(\alpha - y_c)}$$

These five equations when solved simultaneously give the x_a, y_a, x_c, y_c, and R_c, which fixes the geometry of the nozzle. The program listed on the next page solves these equations with the inputs listed previously for these five parameters.

```
10 REM   THIS PROGRAM WILL CALCULATE THE DESIGN PARAMETERS FOR A TWO DIMENSIONAL
20 REM   NOZZLE WITH A STRAIGHT LINE AND A CIRCLE, JOINED SMOOTHLY. INPUTS ARE
30 REM   LENGTH "L" (IN INCHES), EXIT AREA/THROAT AREA "AR", THROAT HEIGHT "DT",
40 REM   DIVERGING ANGLE "DELTA", AND EXIT ANGLE "THETAE".
50 REM OUTPUTS ARE: XC-HORIZONTAL DISTANCE TO CENTER OF CIRCLE ; XA-HORIZONTAL
60 REM DISTANCE TO POINT WHERE CIRCLE MEETS THE LINE ; YA-VERTICAL DISTANCE FRO
70 REM REFERENCE LINE TO POINT WHERE CIRCLE MEETS THE LINE ;YC-VERTICAL DISTANC
80 REM TO CENTER OF CIRCLE ; RC - RADIUS OF CIRCLE ; YE - VERTICAL DISTANCE FRO
90 REM REFERENCE LINE TO END OF NOZZLE ; AMAX - MAXIMUM AREA/THROAT AREA
100 PI=4*ATN(1)
110 PRINT "PLEASE INPUT LENGTH OF NOZZLE (IN INCHES) :"
120 INPUT L
130 PRINT "PLEASE INPUT EXIT AREA TO THROAT AREA RATIO :"
140 INPUT AR
150 PRINT "PLEASE INPUT HEIGHT OF NOZZLE THROAT (IN INCHES):"
160 INPUT DT
170 PRINT "PLEASE INPUT ANGLE OF DIVERGENCE (IN DEGREES):"
180 INPUT DELTA
190 PRINT "PLEASE INPUT EXIT ANGLE (IN DEGREES):"
200 INPUT THETAE
210 DELTA=DELTA*PI/180
220 THETAE=THETAE*PI/180
230 S=TAN(THETAE)
240 TD=TAN(DELTA)
250 C=TD*(DT/2-AR*DT/2+L/S)
260 A=(1+(TD*TD))/(1+(TD/S))
270 B=L-(C/(1+(TD/S)))
280 G=1-A
290 H=B-L
300 K=TD-(1+(TD*TD))/(S+TD)
310 M=DT/2-(C/(S+TD))+(L/S)-AR*DT/2
320 A1=((1+S*S)/(S*S))*A*A-G*G-K*K
330 B1=((1+S*S)/(S*S))*2*A*B+2*G*H+2*K*M
340 C1=((1+S*S)/(S*S))*B*B-H*H-M*M
350 XA=(B1-SQR(B1*B1-4*A1*C1))/(2*A1)
360 PRINT "XA =";XA
370 XC=(XA*(1+TD*TD)+C)/(1+TD)
380 PRINT "XC =";XC
390 YC=ABS(XC+AR*DT/2-L)+DT/2
400 PRINT "YC =";YC
410 YA=XA*TD
420 PRINT "YA =";YA
430 YA=YA+DT/2
440 YC1=XC+AR*DT/2-L
450 RC=SQR((XA-XC)*(XA-XC)+(YA-YC1)*(YA-YC1))
460 PRINT "RC =";RC
470 YE=AR*DT/2-DT/2
480 PRINT "YE =";YE
490 AMAX=(2*(RC-YC)+DT)/DT
500 PRINT "AMAX =";AMAX
510 END
```

113

Appendix B: Mass Flow Calculations

Primary Mass Flow

Primary mass flow was measured through an ASME standard orifice flow meter. For this meter, mass flow is governed by the equations (1:63-65):

$$\dot{m} = 0.525 d^2 Y_1 K \sqrt{\rho_1 (\Delta p)} \qquad \text{(B-1)}$$

where

d = inner orifice diameter = 1.125 in

Y_1 = expansion factor = $1 - (0.41 + 0.35\beta)\frac{x}{k}$

$k = 1.4$; $x = \Delta P/P$; $\beta = d/D = 0.60$

D = outer orifice diameter = 1.875 in

ρ_1 = fluid density (lb/ft^3)

p = upstream pressure (lb/in^2)

K = flow coefficient

The flow coefficient, K, can be determined from the expression:

$$K = K_o \frac{(1 + A)}{R_d} \qquad \text{(B-2)}$$

where

$$K_o = K_e \left\{ \frac{(10^6 d)}{(10^6 d + 15 A)} \right\}$$

R_d = Reynolds number based on d

$$K_e = 0.5993 + \frac{0.007}{D} + \left(0.364 + \frac{0.076}{\sqrt{D}} \right) \beta^4$$

$$A = d \left(830 - 5000\beta + 9000\beta^2 - 4200\beta^3 - \frac{530}{\sqrt{D}} \right)$$

114

Using these relationships, and assuming an R_d between 10^6 of 10^7, gives a value for K in Equation (B-2) between 0.6520 and 0.6524. An average of these values were used:

$$Kavg = 0.6522 \qquad (B-3)$$

Substuting (B-3) into (B-1) results in the following expression for primary mass flow:

$$\dot{m}_p = 0.718[1 - 0.3253\left(\frac{\Delta p}{p}\right)]\sqrt{\frac{p\Delta p}{T}} \qquad (B-4)$$

Secondary Mass Flow

A venturi-tube flow meter was used to measure secondary injection flow rates. The equation for secondary mass flow is given by the following for an ideal venturi (6:451):

$$\dot{m}_s = A_t\left(\frac{2P\Delta P}{RT}\right)^{\frac{1}{2}} \qquad (B-5)$$

where

$\dot{m}_s$ = Secondary Mass Flow Rate (lbm/s)

A_t = Area of Throat of Venturi (in^2)

P = Stagnation Secondary Pressure (psia)

ΔP = Pressure Difference across Venturi (psia)

T = Temperature of Secondary Flow (°R)

R = Gas Constant (1.6582 s^{2}lbf^2/lbm^2°R)

Putting these together, with the venturi diameter=0.375 in:

$$\dot{m}_s = 0.12196\left(\frac{P\Delta P}{T}\right)^{\frac{1}{2}} \qquad (B-6)$$

As stated in the text, the temperature of the primary and secondary flows was assumed constant. This could be done because the mass flow rate for both flows is a function of the square root of the absolute temperature, and a difference of even 30 degrees will change the mass flow by only 3%.

Appendix C: <u>Ideal Thrust Calculation</u>

The ideal thrust was calculated using the expression (14:50) :

$$C_T = \sqrt{\frac{2k^2}{k-1}\left(\frac{2}{k+1}\right)^{\frac{k+1}{k-1}} [1 - \frac{P_e^{\frac{k-1}{k}}}{P_o}] + \frac{A_o}{A_t}\left(\frac{P_o}{P_e} - \frac{P_o}{P_o}\right)} \qquad \text{(C-1)}$$

where

C_T = thrust coefficient (thrust/$A_t P_p$)

k = Ratio of specific heats

A_e = Exit area (in^2)

A_t = Throat area (in^2)

P_e = Exit pressure (psia)

P_a = Ambient pressure (psia)

P_p = Primary pressure (psia)

For the ideal nozzle calculation, it was assumed that $k = 1.4$ and $P_e = P_a$. With these assumptions, Equation (C-1) becomes:

$$C_T = \sqrt{3.262[1 - \left(\frac{P_e}{P_o}\right)^{.286}]} \qquad \text{(C-2)}$$

117

Appendix D: Integration of Wall Pressure Distribution to Obtain Side Force

The integration of the wall pressure on both sides of the nozzle to give the measured side force was accomplished as follows. First, since the nozzle was symmetrical, the effect of the wall geometry on the side force was assumed to be the same on both sides, and therefore not considered. The wall pressure distribution on one of the sides was similar to the following:
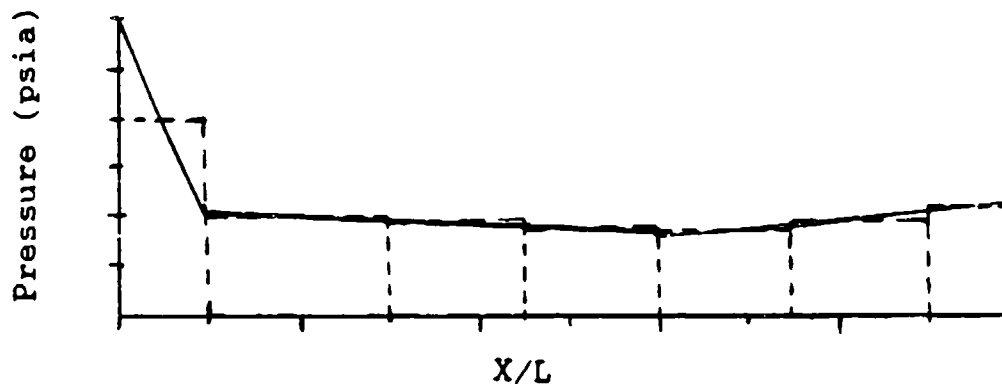
The integration scheme used is illustrated by the dotted lines. In the range between any two points, the pressure distribution was considered linear, and therefore the value of the integration over the range of x was the average value of the two end points of that range multiplied by the range. Summing all the ranges and multiplying by the thickness gave the force on one side. Doing the same procedure on the pressure distribution on the other side gave the force on that side, and the difference between the forces on each side was the side force.

118

Appendix E: Mach Number at Venturi

The Mach number at the secondary mass flow venturi was calculated assuming the secondary pressure set before each run was the stagnation pressure of the flow. Then, the pressure difference measured across the venturi would give the difference between the stagnation pressure and the static pressure in the throat. Once the test was complete, the difference in pressure was subtracted from the stagnation pressure to give the static pressure. Using the static and stagnation pressures and the isentropic Mach number relation gives:

$$M = [5\left(\frac{P_o}{P_o - \Delta P}\right)^{0.286} - 1]^{\frac{1}{2}} \qquad (E-1)$$

where   M = Mach Number at Venturi Throat

P_o = Stagnation Secondary Pressure, set before run

ΔP = Difference in Pressure across Venturi
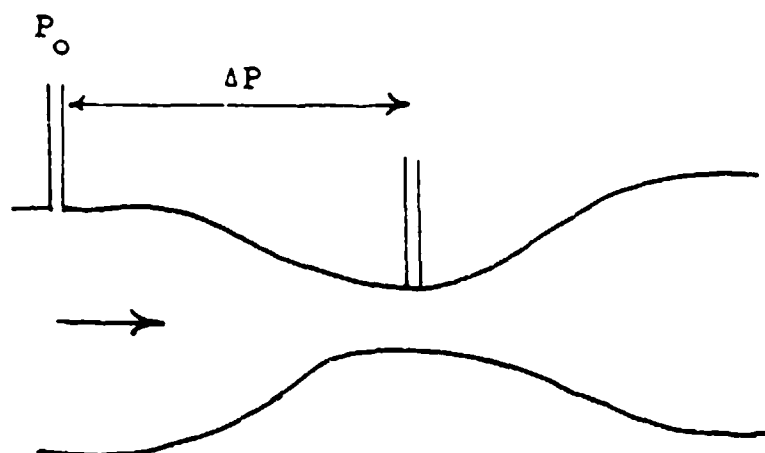
VITA

Second Lieutenant Timothy A. Talda was born on 6 December 1964 in Champaign, Illinois. He graduated from high school in Lower Burrell, PA in 1982, and attended Carngie-Mellon University, from which he received the degree of Bachelor of Science in Mechanical Engineering in May, 1986. Upon graduation, he received a commission in the USAF through the ROTC program, and entered the School of Engineering, Air Force Institute of Technology, in June, 1986.

Permanent Address: 3142 New Hampshire Dr.
Lower Burrell, PA 15068

REPORT DOCUMENTATION PAGE	Form Approved OMB No. 0704-0188

1a. REPORT SECURITY CLASSIFICATION	1b RESTRICTIVE MARKINGS
Unclassified	

2a. SECURITY CLASSIFICATION AUTHORITY	3 DISTRIBUTION/AVAILABILITY OF REPORT
2b. DECLASSIFICATION/DOWNGRADING SCHEDULE	Approved for public release; Distribution unlimited.

4. PERFORMING ORGANIZATION REPORT NUMBER(S)	5. MONITORING ORGANIZATION REPORT NUMBER(S)
AFIT/GAE/AA/87D-22	

6a. NAME OF PERFORMING ORGANIZATION	6b. OFFICE SYMBOL (If applicable)	7a. NAME OF MONITORING ORGANIZATION
School of Engineering	AFIT/ENG	

6c. ADDRESS (City, State, and ZIP Code)	7b ADDRESS (City, State, and ZIP Code)
Air Force Institute of Technology (AU) Wright-Patterson AFB, Ohio 45433-6583	

8a. NAME OF FUNDING/SPONSORING ORGANIZATION	8b. OFFICE SYMBOL (If applicable)	9 PROCUREMENT INSTRUMENT IDENTIFICATION NUMBER

8c. ADDRESS (City, State, and ZIP Code)	10 SOURCE OF FUNDING NUMBERS			
	PROGRAM ELEMENT NO	PROJECT NO	TASK NO	WORK UNIT ACCESSION N

11. TITLE (Include Security Classification)
EXPERIMENTAL INVESTIGATION OF TWO-DIMENSIONAL CONFINED JET THRUST VECTOR CONTROL

12. PERSONAL AUTHOR(S)
Timothy A. Talda, 2Lt, USAF

13a. TYPE OF REPORT	13b. TIME COVERED	14. DATE OF REPORT (Year, Month, Day)	15 PAGE COUNT
MS Thesis	FROM _____ TO _____	December, 1987	134

16. SUPPLEMENTARY NOTATION

17. COSATI CODES			18. SUBJECT TERMS (Continue on reverse if necessary and identify by block number)
FIELD	GROUP	SUB-GROUP	Thrust Control; Secondary Injection; Two Dimensional; Thrust Vector Control Systems; Flow Visualization, Thrust
21	08		

19. ABSTRACT (Continue on reverse if necessary and identify by block number)

Dr. Milton E. Franke

20 DISTRIBUTION/AVAILABILITY OF ABSTRACT	21 ABSTRACT SECURITY CLASSIFICATION
☒ UNCLASSIFIED/UNLIMITED ☐ SAME AS RPT ☐ DTIC USERS	Unclassified

22a NAME OF RESPONSIBLE INDIVIDUAL	22b. TELEPHONE (Include Area Code)	22c. OFFICE SYMBOL
Dr. Milton E. Franke, Professor	513-255-2562	AFIT/ENY

DD Form 1473, JUN 86 — Previous editions are obsolete. — SECURITY CLASSIFICATION OF THIS PAGE

Different types of thrust vector control systems are
described, and a comparison of present systems is presented.
Confined jet thrust vector control is shown to be an effective
alternative. A two-dimensional nozzle that operates as a
confined jet thrust vector control nozzle is experimentally
demonstrated. Effects of changing geometric variables and
inputs on ease of vectoring and performance of vectored thrust
are analyzed. Schlieren photographs and movies show flow
characteristics. Predictions of performance of operable nozzles
are made based on results found in the experiments. Recommendations
for further study are made.